REMOVAL OF THE FERMENTATION INHIBITOR, FURFURAL, USING ACTIVATED CARBON IN CELLULOSIC-ETHANOL PRODUCTION

A Dissertation
Presented to
The Academic Faculty

By

Kuang Zhang

In Partial Fulfillment
Of the Requirements for the Degree
Doctor of Philosophy in the
School of Chemical & Biomolecular Engineering

Georgia Institute of Technology

December 2011

REMOVAL OF THE FERMENTATION INHIBITOR, FURFURAL, USING ACTIVATED CARBON IN CELLULOSIC-ETHANOL PRODUCTION

Approved by:

Dr. William J. Koros, Advisor
School of Chemical & Biomolecular Engineering
Georgia Institute of Technology

Dr. Christopher Jones
School of Chemical & Biomolecular Engineering
Georgia Institute of Technology

Dr. Carson Meredith
School of Chemical & Biomolecular Engineering
Georgia Institute of Technology

Dr. Rachel Chen
School of Chemical & Biomolecular Engineering
Georgia Institute of Technology

Dr. David Bucknall
School of Materials Science & Engineering
Georgia Institute of Technology

Date Approved: October 12, 2011

To Xuan, my wife, and my parents

ACKNOWLEDGEMENTS

The submission of my dissertation marks the culmination of my long and fruitful journey of being a student. I have, through the last four years of my graduate study, been the beneficiary of an amazing amount of support from a large number of people to whom I owe all my success.

I would first like to thank my parents, who have been supportive of me throughout my entire life and encouraged me to succeed in everything I attempt. I am deeply indebted to them for their continued support, love and generosity. I will forever be grateful to my graduate advisor, Dr. Willian Koros, for supporting me through my graduate studies. His passion in research and trust on people set a superb role for me to follow in my future life. My gratitude extends to all my committee members, Dr. Christopher Jones, Dr. Carson Meredith, Dr. David Bucknall, and Dr. Rachel Chen for their valuable time and insightful comments.

My research was conducted as a unique collaboration with Dr. Jones's group and Dr. Chen's group. Special thanks are attributed to Manoj Agrawal who has provided the training on utilizing different equipments for the bio-ethanol fermentation, and answered my questions with great patience. I also acknowledge Teresita Marzialetti for providing biomass-pretreated samples and her constant advices. Without collaboration and help from Dr. Jones's group and Dr. Chen's group, this dissertation would not have been possible. Dr. Steve Miller is appreciated for his helpful advices. The funding support from Chevron Corporation is greatly acknowledged.

I would also like to thank the current and former members of the Koros research group for their help and support throughout my presence here. I owe a large part of my graduate success to the discussions I have had with them. In particular, I would like to thank Dr. Wulin Qiu for starting me off in the research direction that has culminated in this dissertation; Dr. Ryan Adams, Dr. Jason Ward, Dr. Mita Das, Dr. Ryan Lively, Dr. Dhaval Bhandari, Dr. Naoki Bessho, Dr. Cheng Chen, Dr. John Lee, Liren Xu and Chien-Chiang Chen for sharing their data and for providing me with feedback towards my work. JR Johnson and Oguz Karvan were always happy to help me find the solutions to numerous technical problems. I would also like to wish the new members of the team good luck in their research endeavors.

I am grateful to Dhaval Patel and Ying Liu for their support during my initial days in U.S. I will also miss the pleasant time at the trips with Qiong Guo, Ang Li, Yao Li. In addition, Cheng Chen, Liren Xu and Wei-ming Yeh made grocery shopping a lot more fun with their accompany. I want to thank my friends, Canghai Ma & Hongjuan Cui, Xue Ning, Cheng Zhang, Huayu Li, Ying Dai, Lu Liu, and Hongzhi Wang for their continuous help and encouragement during my wife's pregnancy at Atlanta.

Finally, I would like to extend the most sincere sense of gratitude to my wife, Xuan, for being a pillar of support during some really tough times in our lives. I often regard my graduate life as being like a roller-coaster ride. Having supported me throughout the entire ride I owe a special debt of gratitude to Xuan.

TABLE OF CONTENTS

LIST OF TABLES

LIST OF FIGURES

SUMMARY

Ethanol can be produced from lignocellulosic biomass through fermentation; however, some byproducts from lignocellulosics, such as furfural compounds, are highly inhibitory to the fermentation and can substantially reduce the efficiency of bio-ethanol production. The overarching goal of this research was to selectively remove these fermentation inhibitors to enhance the performance of bio-ethanol production.

In an effort to pursue the above-mentioned objective, commercial activated carbon and newly developed polymer-derived carbon were utilized to selectively remove the model fermentation inhibitor, furfural, from water solution. Characterization of the adsorbents was described in detail in terms of morphology, pore structure and surface chemistry. Polymer-derived carbon demonstrated narrow pore size distribution and uniform surface structure.

A key aspect of the present study was inspecting the chemical mechanism involved in the selectivity of adsorbents between furfural and monosaccharides. Polymer-derived carbon with impressive improvement in selectivity between furfural and monosaccharides was demonstrated. The oxygen groups on the carbon surface were believed to have contributed to the decrease on the selectivity of activated carbon between furfural and monosaccharides. Oxidization of activated carbon by nitric acid generated more information which supports the above assumption.

Different adsorption isotherm models and kinetic models were studied to fit commercial activated carbon and polymer-derived carbon individually. Furthermore, the

effect of acetic acid on the adsorption of furfural on activated carbon was investigated, and the negative effect can be eliminated by neutralization with aqueous ammonia.

The toxic effect of furfural on the fermentation of glucose and xylose by *Zymomonas mobilis* was demonstrated. Wild type *Zymomonas mobilis* ZM4 and recombinant stain *Zymomonas mobilis* A3 were used in this study. Bacterial cell growth, sugar consumption and ethanol yield were investigated during the fermentation. When there were 4 g/L furfural in the fermentation broth, cells of ZM4 and A3 stopped growing during the fermentation and zero sugar consumption and ethanol yield occurred correspondingly. The complete elimination of inhibition effect of furfural was observed after polymer-derived carbon treatment of the solution with residual 0.1g/l furfural.

The last part of this thesis focused on regeneration of adsorbents by different methods, including thermal regeneration, pH adjustment and organic solvent stripping. Regeneration efficiency was evaluated by comparing the adsorption capacity of regenerated adsorbent to that of fresh adsorbents. Low ethanol-containing water solution appeared to be an attractive way to regenerate the spent sorbent in the industrial application. A adsorption/desorption cycle was designed in a fixed-bed column system and the adsorbents were successfully regenerated using the standard ethanol-containing water solution. Dynamic mass balance was obtained after running four or five cycles and regeneration results were stable even after twenty cycles. These results paved the way to the potential integration of ethanol production during fermentation into the adsorption/desorption regeneration approach.

CHAPTER 1: INTRODUCTION

1.1 Current State of Ethanol Production

Energy is a vital element in our everyday lives; however, most of the energy we use nowadays comes from fossil fuels. Our dependence on fossil fuels as energy sources has caused natural resource depletion and serious environmental problems. The need for renewable alternatives is becoming ever more urgent. Interest in the use of bio-ethanol worldwide has grown strongly in recent years due to limited oil reserves, concerns about climate change from greenhouse gas emissions and the desire to promote domestic rural economies [1]. Bio-ethanol can be used in fuel mixtures such as E85 (a blended fuel of 85% bio-ethanol and 15% gasoline) in vehicles specially designed for its use. Bio-ethanol could significantly reduce the emissions from the road-transport sector if they were widely adopted.

The U.S. is the world's largest producer and consumer of ethanol, followed by Brazil [2]. Fig. 1.1 illustrates the distribution of global ethanol output by major producing country between 2000 and 2009. Taken together the U.S. and Brazil account for nearly 80% of total world ethanol production. Over the last decade world ethanol production nearly tripled reaching 22.7 billion gallons in 2009 with the most significant growth posted in the U.S.

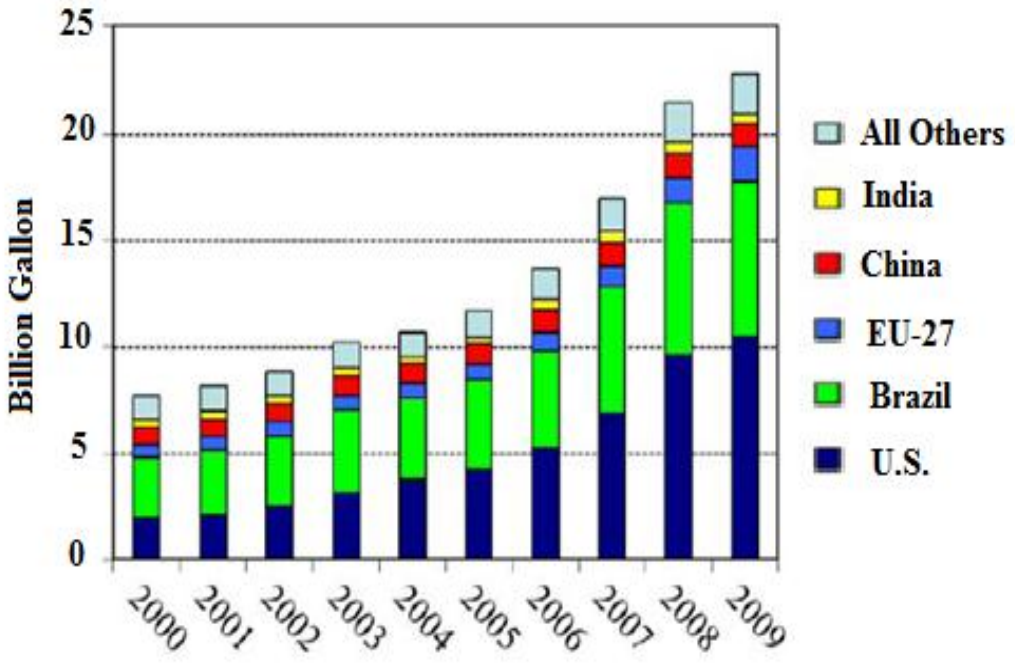

Figure 1.1 World Ethanol Production: 2000-2009 [3].

Ethanol can be produced from diverse feed stocks, including grains such as corn and wheat [4, 5]; and sucrose in the form of cane and beet sugar [6]. Ethanol also can be produced by converting cellulose into its constituent sugars, which then are fermented and distilled into alcohol. Sources of cellulose include biomass such as corn stover, switchgrass, and wood [7, 8].

Currently, ethanol is primarily fermented from the sugar that makes up the starch in grain. Corn is the source of starch for more than 92% of ethanol production in the United States [9]. The starch is converted to dextrose by amylase enzymes, and this sugar is then fermented with yeast, just as in making beer or distilled spirits.

The cost of a bushel of corn is currently hovering around $7.00, and experts link this price increase directly to the growth of the ethanol industry. Fig. 1.2 illustrates the sudden spike in corn prices after the ethanol industry took off. With corn prices surging, corn

ethanol industry experienced supply-demand imbalances at both the local and macro level, with increasing pressure on ethanol producer economics. Meanwhile, the benefits of corn ethanol have come under scrutiny in the popular press for competing with food supplies, contributing to increased commodity prices, high water use and marginal energy balance improvements.

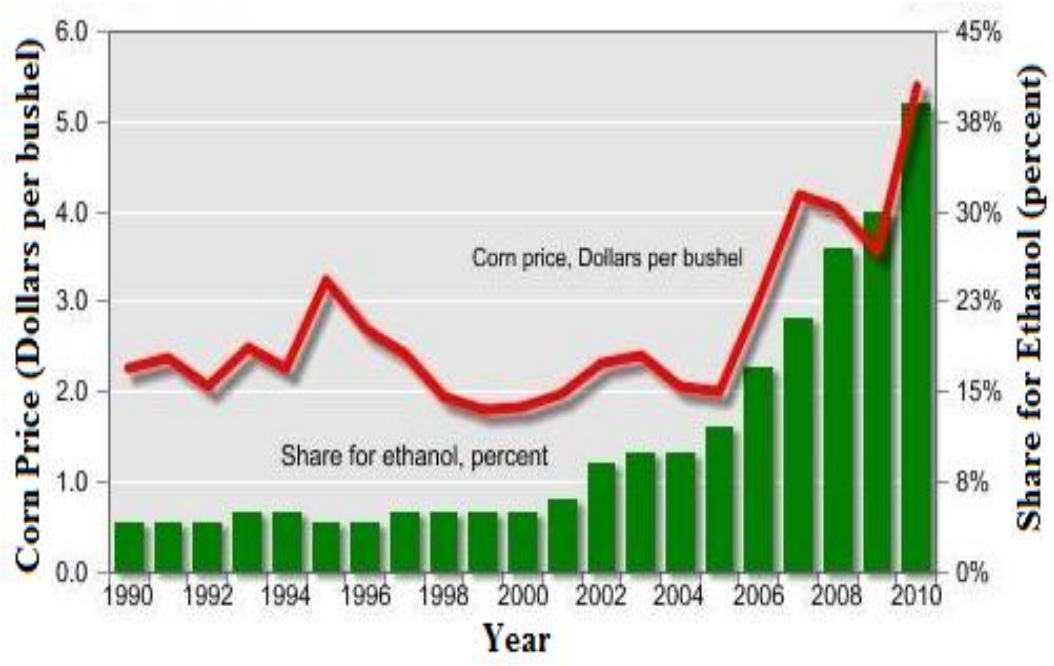

Figure 1.2 Corn price in the world :1990-2010 [3].

Cellulosic biomass is a highly undervalued and underutilized energy asset in the United States and around the world. Cellulose-containing natural products are widely abundant. Cellulose has been estimated to make up half of all the organic carbon on the planet. A 2005 analysis by the Natural Resources Defense Council found that ethanol from cellulose could supply half of U.S. transportation fuel needs by 2050, without decreasing production of food and animal feed [10].

The idea of making fuels from cellulosic biomass is not new. What is new is being able to do it at low cost and on a large scale. Over the past several years, technologies have been in development to address these core issues. Cellulosic conversion technology is coming of age as costs continue to fall and commercial-scale demonstration projects break ground.

National environmental and energy policy plays an important role in determining bio-ethanol demand. The U.S., Brazil, and several European Union **(**EU) member states have the largest programs promoting bio-ethanol in the world. The recent commitment by the United States government to increase bio-energy threefold in ten years has added impetus to the search for viable bio-fuels [10]. In South America, Brazil continued policies that mandate at least 22% bio-ethanol on motor fuels and encourage the use of vehicles that use hydrous bio-ethanol [(96 bio-ethanol + 4 water)/100] to replace gasoline. Future conditions for an international bio-fuel market in Europe will largely be decided by the EU policies on renewable energy and their interplay with national energy policies.

The most significant federal incentives for ethanol in the U.S. are the Renewable Fuels Standard (RFS) [11]. The RFS was expanded under the Energy Independence and Security Act of 2007 (EISA) to require that 36 billion gallons of renewable fuels be used in the nation's motor fuel supply by 2022. EISA caps the use of conventional ethanol produced from corn starch at 15 billion gallons in 2015 and requires the remaining 21 billion gallons to be produced from advanced bio-fuels including at least 16 billion gallons from cellulosic feedstocks. By way of comparison, an estimated 10.6 billion gallons of ethanol were produced and used in 2009, up from 9.2 billion in 2008. The RFS requirement is illustrated in Fig. 1.3.

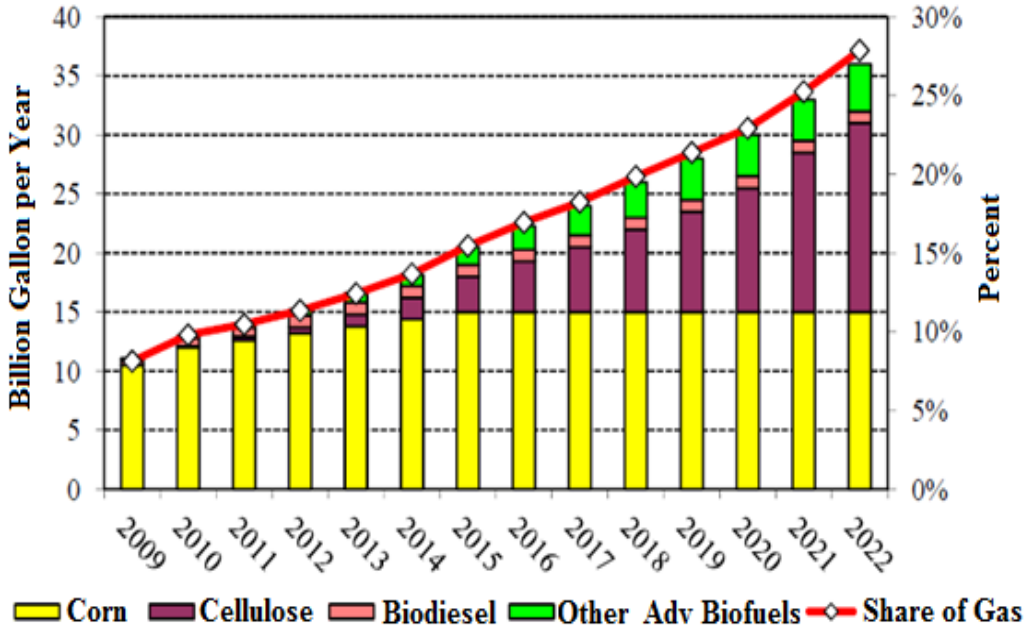

Figure 1.3 Renewable Fuel Standard requirement in the U.S. [11].

1.2 Cellulosic Ethanol Production

Cellulose is the fiber contained in leaves, stems, and stalks of plants and trees. Unlike corn and sugar, cellulose is not used for food, and it can be grown in all parts of the world. Cellulosic ethanol is expected to be less expensive and more energy-efficient than corn ethanol because it can be made from low-cost feedstocks, including wood, waste paper, grasses, and farm residues [12].

Switchgrass, in particular, is considered to be a promising source of cellulosic ethanol [13], because it doesn't have to be replanted each year. Switchgrass, shown at Fig. 1.4, is a prairie grass native to the U.S. known for its hardiness and rapid growth. It was once part of the tall-grass prairie that covered most of the Great Plains and also grew in Alabama and Mississippi. Because it is native, switchgrass is resistant to many pests and plant diseases and is capable of producing high yields with relatively low applications of

fertilizer and other agricultural chemicals. It is also tolerant of poor soils, flooding, and drought. President Bush praised switchgrass in his 2006 State of the Union address for its potential as a bio-fuel source. It can yield 6 to 8 tons per acre, compared to 4 tons per acre for corn, and progressive breeding could double that yield over time.

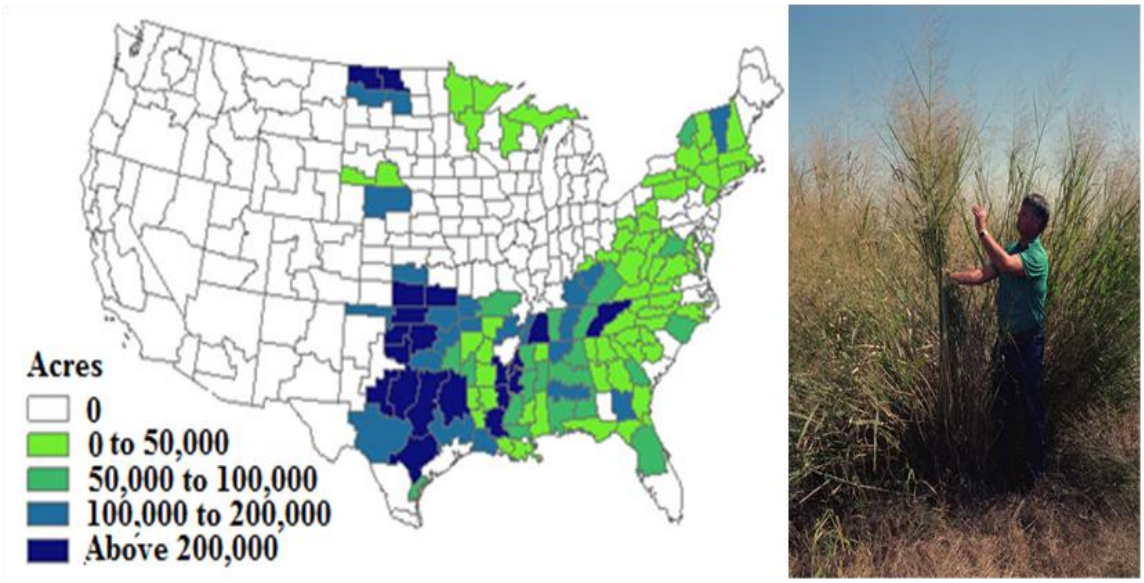

Figure 1.4 The geographic distribution of switchgrass in the U.S. [14].

Production of ethanol from lignocellulosics is more difficult than from sugar cane or starch-rich materials due to its more complex molecular structures [15]. Lignocellulosics mainly consist of three components: cellulose, hemicellulose, and lignin. The source of lignocellulosic biomass is the plant cell wall (Fig.1.5), which has important roles in determining the structural integrity of the plant, and in defence against insects. Plant cell walls contain cellulose consisting of hydrogen-bonded chains of thousands of glucose molecules. Cellulose is surrounded by hemicellulose, a branched polymer composed of pentose and hexose. These cell-wall structures also contain lignin, which provides rigidity and resistance to compression. The crystallinity of cellulose and its association

with hemicellulose and lignin are two key challenges preventing efficient cellulose breakdown into glucose molecules convertible to ethanol.

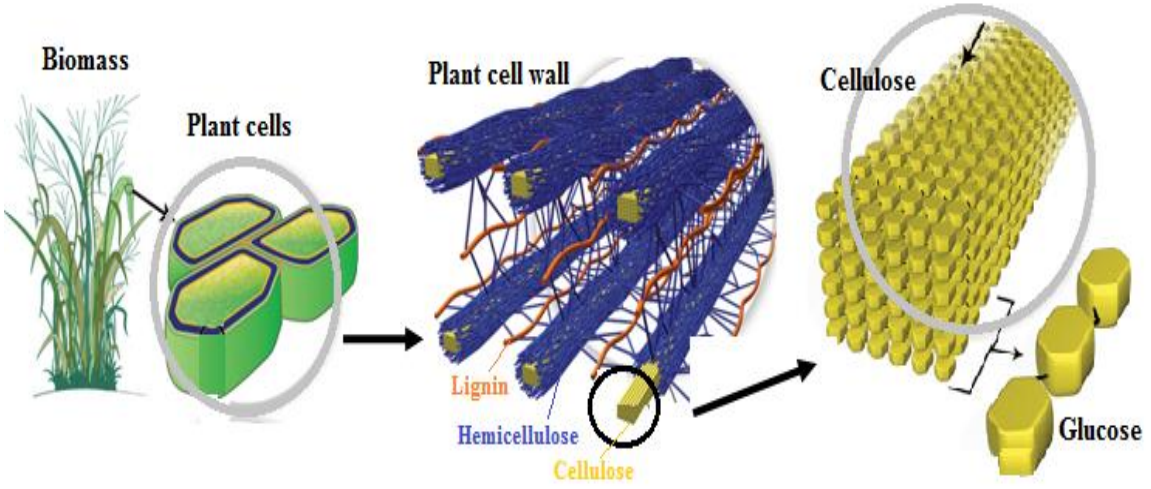

Figure 1.5 Plant cell wall structure: cellulose, hemicellulose, and lignin [16].

Fig. 1.6 highlights some key steps in the cellulosic ethanol production process (1) lignocellulosic biomass is harvested from the feedstock crop, compacted (fresh or dry) and transported to a cellulosic ethanol refinery where it is stored, ready for conversion. (2) Biomass is ground into small, uniform particles. Thermal or chemical pretreatment separates cellulose from other biomass materials and opens up the cellulose surface to enzymatic attack. (3) A mix of enzymes is added to break down cellulose into simple sugars. (4) Microbes produce ethanol by fermenting sugars from glucose and other biomass carbohydrates. (5) Ethanol is separated from water and other components of the fermentation broth and purified through distillation.

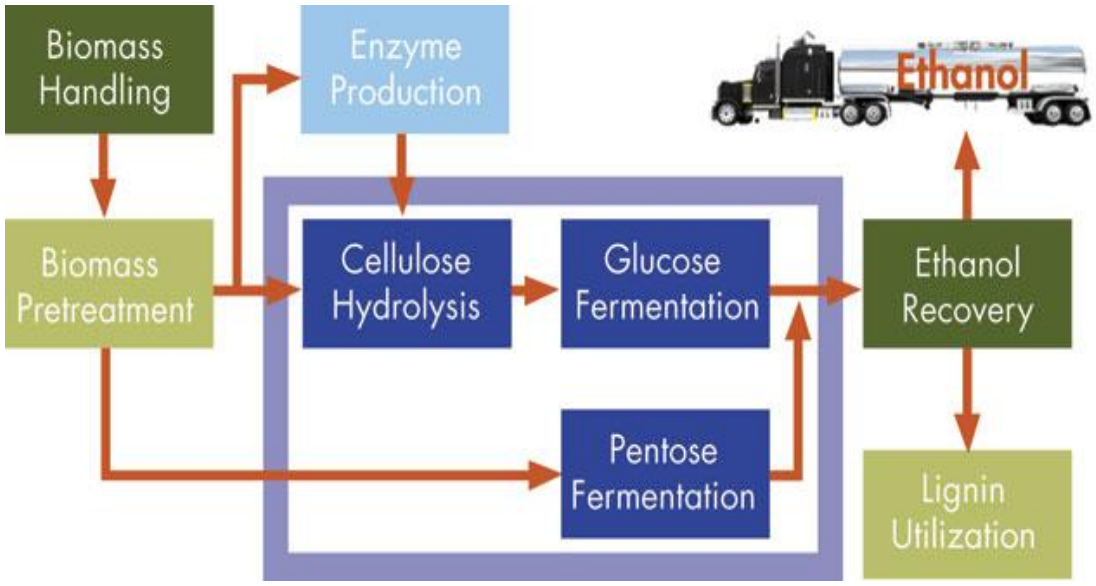

Figure 1.6 Overview of cellulosic ethanol production [17].

1.3 Fermentation Inhibitors

Yeast, such as *Saccharomyces cerevisiae* and bacteria, such as *Zymomonas mobilis* [18, 19], are the common microbes utilized during the ethanol fermentation. The advantages of *Z. mobilis* over *S. cerevisiae* are higher ethanol yield, higher ethanol tolerance, and amenability to genetic manipulations [20]. In addition, the recombinant *Z. mobilis* has the ability to decompose both hexose and pentose, while wild-type *Saccharomyces cerevisiae* is able to utilize only hexose.

Even though the cellulosic ethanol can be produced by fermentation, the fermentation efficiency can be substantially impeded by toxic substances present in pretreated hydrolyzates. Furfural, a pentose degradation product, is highly toxic to *Z. mobilis*. In addition, 5-hydroxymethylfurfural (HMF, a hexose degradation product) and lignin degradation products also have a moderately toxic effect on the organism [21, 22].

Fig. 1.7 shows the growth curve of *Z. mobilis* 8b (a recombinant *Z. mobilis*) as a function of increasing concentrations of furfural and HMF. Growth rates at each

concentration of furfural were plotted against inhibitor concentrations (g/1). Increasing concentrations of furfural caused a reduction in growth rates. The inhibition concentrations of furfural at 0.7, 1.6, 2.6 and 5.0 g/1 caused 25%, 50%, 75% and 100% inhibition of the microbial growth. The inhibition growth rate profile for *Z. mobilis* 8b grown in the presence of HMF is similar to that of furfural. The concentrations of HMF that resulted in 25%, 50% 75% and 100% inhibition of the microbial growth are 1.2, 2.8, 4.7 and 8.0 g/1. Relative final cell densities were reduced at lower concentrations for furfural than HMF, with inhibition first noted at 0.5 g/1 for furfural and 2 g/1 for HMF. In summary, the furfural and HMF present in the aqueous solution during fermentation could significantly affect cell mass yields.

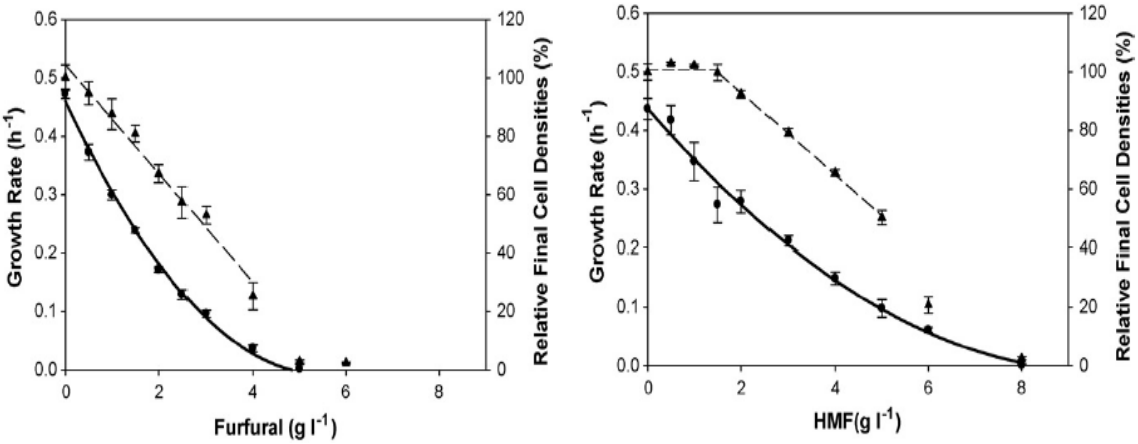

Figure 1.7 Inhibition effect of furfural and HMF on the cell growth of *Zymomonas mobilis* [21].

The mechanism of furfural inhibition has been reported, and direct inhibition of alcohol dehydrogenase (ADH) might have contributed to acetaldehyde excretion. Intracellular acetaldehyde accumulation has been suggested to be the reason for the lag-phase in growth in the presence of furfural [22].

To reduce the inhibitor's toxicity during the fermentation, the development of effective removal strategies for these inhibitors from the biomass-pretreated solution is attractive. Since removing compounds that are inhibitory to microorganisms should improve the overall efficiency of the biomass conversion process, furfural and HMF will be my first target of inhibitors to be removed.

1.4 Previous Research on Removal of Furfural

A number of methods have been employed for removing furfural from aqueous phase. These include distillation, solvent extraction, membrane separation, and sorbents.

Furfural can be separated from aqueous solution by azeotropic distillation at high temperature and pressure (180-200 ^{o}C, 8-10 atm). But a complete recovery of furfural by distillation is not easy since when aqueous solutions of furfural are distilled at atmospheric pressure a minimum-boiling heteroazeotrope is formed, which contains 35% of furfural by weight. Upon condensing, the organic phase contains 84.1% of furfural by weight and 18.4% is contained in the water phase [23].

Recovery of furfural from aqueous effluents was also studied on the extraction of furfural with organic solvents. Croker employed toluene, methyl isobutyl ketone (MIBK) and isobutyl acetate (IBA) as the solvents to extract furfural from the aqueous solution [24]. The solvent loss during extraction process and the cost of toluene is the lowest compared to MIBK and IBA. But toluene is more toxic than the other two solvents. Extraction of furfural by supercritical carbon dioxide was investigated at high pressure and temperature (80-340 bar, 298-333k) [25]. The solubility of furfural increases with decreasing temperature and increasing pressure. Consumption of organic solvent would be considerable if liquid extraction were to be applied in the industrial scale. In addition,

ecological reasons stopped further development of extraction of furfural with organic solvents.

Pervaporative separation of furfural/water mixtures was performed by using prepared flat sheet hydrophobic polyurethaneurea membranes [26]. The overall pervaporation process was observed to be diffusion controlled. The membranes were found to be furfural selective, with separation factor between furfural and water as high as 638 and a permeate flux as high as 44.7 g m^{-2} h^{-1}. The partial flux of furfural increased with an increase in furfural content in the feed and with an increase in feed temperature. The membranes were found to be highly suitable for the separation of furfural from furfural-water mixtures. However, the composition of the aqueous solution is very complex after biomass pretreatment. Dozens of chemicals exist in the solution, thus membrane fouling could easily occur if membrane separation technique were employed in the industrial application.

A number of sorbents have been tested for removing furfural from lignocelluloses hydrolysis liquors. Sorbents reported in the literature include hydrophobic resins, zeolite, and activated carbon.

The removal of furfural from water by adsorption on the Amberlite® polymeric resin XAD-4 (polystyrene-divinylbenzene copolymer bead) was studied [27]. The equilibrium adsorption behavior followed a Langmuir trend at room temperature, where 90 mg of furfural was adsorbed per gram of dry XAD-4 at an equilibrium solution concentration of 2 g/L of furfural. Similar adsorption behavior was also found on XAD-7 (methacrylic ester bead).

Several types of zeolites (MFI, β, faujasite and FER) were investigated as adsorbents of HMF, furfural, and xylose [28]. Adsorption using hydrophobic zeolites has been studied of similar pore size but with different Si/Al ratios. Adsorption isotherms exhibit similar behavior for these zeolites as they preferentially adsorb inhibitors at 298 K. Furthermore, they do not adsorb significant amounts of xylose, possibly because the sugar prefers to partition in the aqueous solution rather than the relatively hydrophobic adsorbent. For zeolite β, there is a decrease in saturation loading of adsorbates with Si/Al ratio decreasing from 100 to 12 or, in other words, increasing hydrophilicity. These results indicate that siliceous or high silica zeolites are desirable for most efficient removal of furfural and HMF.

Coconut-based commercial activated carbon was studied for furfural removal [29]. The equilibrium between furfural in the solution and on the adsorbent surface was practically achieved in 6.0 h. Adsorption kinetics was found to be best represented by pseudo-second order rate expression. The effective diffusion coefficient of furfural was of the order of 10^{-13} m^2/s.

1.5 Research Objectives

Activated carbon is the most widely used and cost-effective sorbent in the industrial application. This research work seeks to utilize activated carbons to remove fermentation inhibitors from the aqueous solution. In the previous research, most adsorbents were tested in the simple furfural-water solution. In this study, the presence of monosaccharides (glucose and xylose) will be considered, and their effect on the competitive adsorption will be investigated.

Our overall goal is to selectively separate enzyme inhibitors from the biomass-pretreated solution and to use the adsorbents efficiently and economically. In order to achieve that, the objectives of the present work are:

(1): Study the adsorption tests of activated carbons to remove the fermentation inhibitors, primarily furfural compounds, from aqueous solution.

(2): Inspect the selectivity of activated carbon between furfural and monosaccharides and explore the underlying mechanism for improvement in adsorbent performances.

(3): Investigate the bacteria cell growth, sugar consumption, and ethanol production during fermentation before and after removing the inhibitors.

(4): Investigate different strategies to regenerate the spent sorbents and identify the most effective and economical approach.

1.6 Dissertation Outline

Chapter two provides background and theory essential to the understanding of adsorption. Chapter three summarized materials and experimental procedures used throughout this work. Chapter four presents the adsorption of furfural from aqueous solution and elucidates the underlying chemical mechanism involved in the selectivity of activated carbon between furfural and monosaccharides. Chapter five features the toxic effect of furfural on cellulosic ethanol fermentation and the elimination of toxic effect after removing furfural. Chapter six is dedicated to the variety of approaches to regenerate the spent adsorbents. Finally, conclusions and recommendations for future research will be made in chapter seven.

1.7 References

[1] Farrell AE, Plevin RJ, Turner BT, Jones AD, O'Hare M, Kammen DM. Ethanol Can Contribute to Energy and Environmental Goals. Science 2006;311:506-508.

[2] Balat M, Balat H. Recent trends in global production and utilization of bio-ethanol fuel. Applied Energy 2009;86:2273-2282.

[3] Cardno Entrix JU. Current State of the U.S. Ethanol Industry. US Department of Energy 2010.

[4] Kaparaju P, Serrano M, Thomsen AB, Kongjan P, Angelidaki I. Bioethanol, biohydrogen and biogas production from wheat straw in a biorefinery concept. Bioresource Technology 2009;100:2562-2568.

[5] Mojovic L, Nikolic S, Rakin M, Vukasinovic M. Production of bioethanol from corn meal hydrolyzates. Fuel 2006;85:1750-1755.

[6] Quintero JA, Montoya MI, Sánchez OJ, Giraldo OH, Cardona CA. Fuel ethanol production from sugarcane and corn: Comparative analysis for a Colombian case. Energy 2008;33:385-399.

[7] Sánchez ÓJ, Cardona CA. Trends in biotechnological production of fuel ethanol from different feedstocks. Bioresource Technology 2008;99:5270-5295.

[8] Varvel GE, Vogel KP, Mitchell RB, Follett RF, Kimble JM. Comparison of corn and switchgrass on marginal soils for bioenergy. Biomass and Bioenergy 2008;32:18-21.

[9] Hettinga WG, Junginger HM, Dekker SC, Hoogwijk M, McAloon AJ, Hicks KB. Understanding the reductions in US corn ethanol production costs: An experience curve approach. Energy Policy 2009;37:190-203.

[10] Demirbas A. Biofuels sources, biofuel policy, biofuel economy and global biofuel projections. Energy Conversion and Management 2008;49:2106-2116.

[11] Hoekman SK. Biofuels in the U.S. - Challenges and Opportunities. Renewable Energy 2009;34:14-22.

[12] Dwivedi P, Alavalapati JRR, Lal P. Cellulosic ethanol production in the United States: Conversion technologies, current production status, economics, and emerging developments. Energy for Sustainable Development 2009;13:174-182.

[13] Felix E, Tilley DR. Integrated energy, environmental and financial analysis of ethanol production from cellulosic switchgrass. Energy 2009;34:410-436.

[14] Stokes RDPaBJ. U.S. Billion-Ton Update: Biomass Supply for a Bioenergy and Bioproducts Industry. US Department of Energy 2011.

[15] Cardona CA, Sánchez ÓJ. Fuel ethanol production: Process design trends and integration opportunities. Bioresource Technology 2007;98:2415-2457.

[16] Thomassen D. U.S. Department of Energy's Genomics: GTL Bioenergy Research Centers White Paper. US Department of Energy 2006.

[17] D. Humbird RD, L. Tao, C. Kinchin,. Process Design and Economics for Biochemical Conversion of Lignocellulosic Biomass to Ethanol. US Department of Energy 2011.

[18] Cazetta ML, Celligoi MAPC, Buzato JB, Scarmino IS. Fermentation of molasses by Zymomonas mobilis: Effects of temperature and sugar concentration on ethanol production. Bioresource Technology 2007;98:2824-2828.

[19] Bai FW, Anderson WA, Moo-Young M. Ethanol fermentation technologies from sugar and starch feedstocks. Biotechnology Advances;26:89-105.

[20] Rogers P, Jeon Y, Lee K, Lawford H. Zymomonas mobilis for Fuel Ethanol and Higher Value Products Biofuels. In: Olsson L, editor: Springer Berlin / Heidelberg; 2007, p. 263-288.

[21] Franden MA, Pienkos PT, Zhang M. Development of a high-throughput method to evaluate the impact of inhibitory compounds from lignocellulosic hydrolysates on the growth of Zymomonas mobilis. Journal of Biotechnology 2009;144:259-267.

[22] Heer D, Sauer U. Identification of furfural as a key toxin in lignocellulosic hydrolysates and evolution of a tolerant yeast strain. Microbial Biotechnology 2008;1:497-506.

[23] Buell CK, Boatright RG. Furfural Extractive Distillation. Industrial & Engineering Chemistry 1947;39:695-705.

[24] Zautsen RRM, Maugeri-Filho F, Vaz-Rossell CE, Straathof AJJ, van der Wielen LAM, de Bont JAM. Liquid–liquid extraction of fermentation inhibiting compounds in lignocellulose hydrolysate. Biotechnology and Bioengineering 2009;102:1354-1360.

[25] Sangarunlert W, Piumsomboon P, Ngamprasertsith S. Furfural production by acid hydrolysis and supercritical carbon dioxide extraction from rice husk. Korean Journal of Chemical Engineering 2007;24:936-941.

[26] Ghosh UK, Pradhan NC, Adhikari B. Separation of furfural from aqueous solution by pervaporation using HTPB-based hydrophobic polyurethaneurea membranes. Desalination 2007;208:146-158.

[27] Weil JR, Dien B, Bothast R, Hendrickson R, Mosier NS, Ladisch MR. Removal of Fermentation Inhibitors Formed during Pretreatment of Biomass by Polymeric Adsorbents. Industrial & Engineering Chemistry Research 2002;41:6132-6138.

[28] Ranjan R, Thust S, Gounaris CE, Woo M, Floudas CA, Keitz Mv, et al. Adsorption of fermentation inhibitors from lignocellulosic biomass hydrolyzates for improved ethanol yield and value-added product recovery. Microporous and Mesoporous Materials 2009;122:143-148.

[29] Sahu AK, Srivastava VC, Mall ID, Lataye DH. Adsorption of Furfural from Aqueous Solution onto Activated Carbon: Kinetic, Equilibrium and Thermodynamic Study. Separation Science and Technology 2008;43:1239-1259.

CHAPTER 2: BACKGROUND AND THEORY

This chapter introduces concepts essential to understanding adsorption process of the adsorbent. The first section briefly reviews two different types of adsorption and the factors affecting adsorption. Subsequent discussion will focus on the pore structure and surface chemical structure of activated carbon, and their effect on the adsorption. Further, different models of adsorption isotherms and kinetics will be introduced. Finally, thermal and chemical regeneration approaches of activated carbon will be reviewed.

2.1 Concept of Adsorption

Adsorption potentials arise as a result of the unsaturated and unbalanced molecular forces that are present on every solid surface [1]. Thus, when a solid surface is brought into contact with a liquid or gas, there is an interaction between the fields of forces of the surface and that of the liquid or the gas. The solid surface tends to satisfy these residual forces by attracting and retaining on its surface the molecules, atoms, or ions of the gas or liquid. This results in a greater concentration of the gas or liquid in the near vicinity of the solid surface than in the bulk gas or vapor phase, despite the nature of the gas or vapor. The process by which this surface excess is caused is called adsorption. The adsorbed molecule is called the adsorbate, and the solid material is the adsorbent.

2.1.1 Physical and Chemical Adsorption

The adsorption involves two types of forces: (1) physical forces that may be dipole moments, polarization forces, dispersive forces and (2) chemical forces that are valence forces arising out of the redistribution of electrons between the solid surface and the adsorbed atoms.

Depending upon the nature of the forces involved, the adsorption is of two types: physical adsorption and chemisorption [2]. In the case of physical adsorption, the adsorbate is bound to the surface by relatively weak van der Walls forces, which are similar to the molecular forces of cohesion. Chemisorption, on the other hand, involves exchange or sharing of electrons between the adsorbate molecules and the surface of the adsorbent. The bond formed between the adsorbate and the adsorbent is essentially a chemical bond and is thus much stronger than in the physisorption. The differences between physisorption and chemisorption are summarized in the below Table 2.1.

Table 2.1 Comparison between Physisorption and Chemisorption [3].

Physisorption	**Chemisorption**
Forces of attraction are van der Waals' forces.	Forces of attraction are chemical bond forces.
Low enthalpy of adsorption (20 - 40 k.J/mole).	High enthapy of adsorption (200 - 400 k.J/mole).
This process is observed under conditions of low temperature.	This process takes place at high temperatures.
It is not specific.	It is highly specific.
Multi-molecular layers may be formed.	Generally, monomolecular layer is formed.
This process is reversible.	This process is irreversible.

The basic mechanism through which activated carbon removes impurities from liquid is referred to as physical adsorption. In an adsorption process (Fig. 2.1), when a solid surface is exposed to liquid, the molecules of the impurities strike the surface of the solid when some of these striking molecules stick to the solid surface and become adsorbed, while some others rebound back. Initially the rate of adsorption is large because the whole surface is bare, but the rate of adsorption continues to decrease as more and more of the solid surface becomes covered by the adsorbate molecules. However, the rate of desorption, which is the rate at which the adsorbed molecules rebound from the surface, increases because desorption takes place from the covered surface. With the passage of time, the rate of adsorption continues to decrease, while the rate of desorption continues to increase, until an equilibrium is reached, where the rate of adsorption is equal to the rate of desorption. It is a dynamic equilibrium because the number of molecules sticking to the surface is equal to the number of molecules rebounding from the surface.

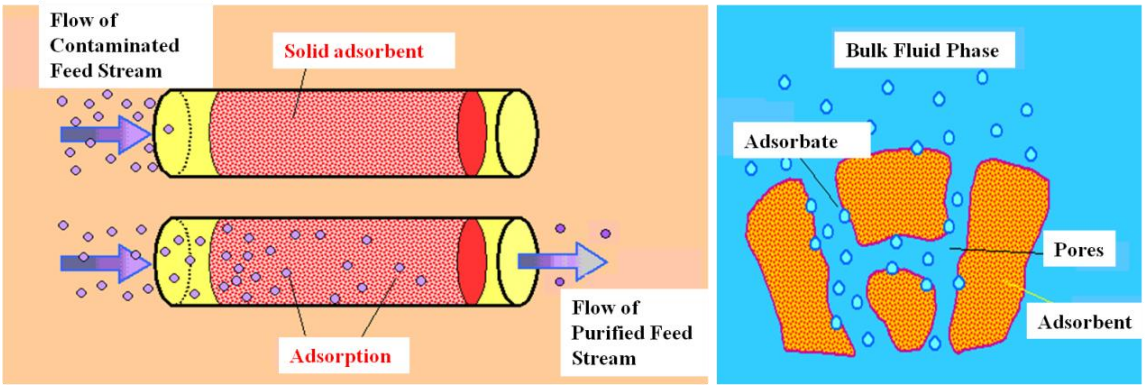

Figure 2.1 Physical adsorption process [2].

2.1.2 Factors Affecting Adsorption

The following parameters have effect on the adsorption of adsorbent [4]:

1. Specific surface area: Larger specific surface area implies a greater adsorption capacity.

2. Pore size: Pore size distribution is necessary to facilitate the adsorption process by providing adsorption sites and the appropriate channels to transport the adsorbate.

3. Chemical structure: The adsorption capacity is determined by the physical or porous structure but is strongly influenced by the chemical structure of adsorbent surface.

4. Particle size: Smaller particles provide quicker rates of adsorption. However, wastewater pressure drop across columns packed with powdered material is too high for use of this material in packed beds.

5. Solubility of solute (adsorbate) in liquid: Substances slightly soluble in water will be more easily removed from water than substances with high solubility. Also, non-polar substances will be more easily removed than polar substances since the latter have a greater affinity for water.

6. Concentration of adsorbate: Adsorption capacity is proportional to concentration of adsorbate.

7. pH: Adsorption capacity may change under pH conditions, which change the solubility of the adsorbate.

8. Contact Time: Sufficient contact time is required to reach adsorption equilibrium and to maximize adsorption efficiency.

2.2 Concept of Activated Carbon Sorbent

Activated carbon is a wide range of amorphous carbonaceous materials that exhibit a high degree of porosity and an extended inter-particulate surface area [4]. Activated

carbons have been used for many centuries. The Egyptians used carbonized wood charcoal about 1500 BC as an adsorbent for medicinal purposes and also as a purifying agent. The first industrial production of active carbon started about 1900 for use of sugar refining industries. Better quality gas-adsorbent carbons received attention during World War I, when they were used in gas masks for protection against hazardous gases and vapors.

Activated carbons are versatile adsorbents. They are used extensively for the removal of undesirable odor, color, taste, and organic and inorganic impurities from domestic and industrial waste water; in air pollution control from industrial and automobile exhausts; in the purification of many chemical, pharmaceutical, and food products. Nearly 80% (~ 300,000 tons/year) of the total activated carbon is consumed for liquid-phase application, and the gas-phase applications consume about 20% of the total production.

Activated carbon can be produced from nearly all carbon-containing organic materials, mainly wood, sawdust, nutsehlls, peat, coal, lignite, petroleum coke, polymer, etc. The use of a suitable precursor is mainly conditioned by its availability and cost, although it also depends on the application.

There are two steps to the manufacturing process, carbonization and activation. Carbonization is the process of heating the carbon in an anaerobic (oxygen-free) environment to break down the complex organic chemicals from which the material is made from, driving off almost everything but carbon and ash.

After carbonization the resulting carbon is then activated by being subjected to exposure to heated gas, most commonly steam, as well as a series of chemical washes. Activation improves the quality of the carbon as an adsorbent by increasing the sizes of

the pores on its surface, maximizing its surface area. Activation also washes away any remaining residues left behind by the carbonization process. There are two main varieties of the activation process, historically referred to as “steam activation” and “chemical activation” [5]. These two processes give fundamentally different pore structures. In the steam activation process, the carbonized material is reacted with steam at temperatures of approximately 1000 ^{o}C. At these conditions, parts of the carbon atoms are removed by ‘gasification’:

$$\mathbf{C\ (solid) + H_2O\ (gas) \text{---}> CO\ (gas) + H_2\ (gas)}$$

During chemical activation, the raw material is impregnated with certain chemicals. The chemical is typically an acid, strong base, or a salt (phosphoric acid, potassium hydroxide, sodium hydroxide, zinc chloride, respectively). A general flow sheet for the manufacture of activated carbon is shown in Fig. 2.2.

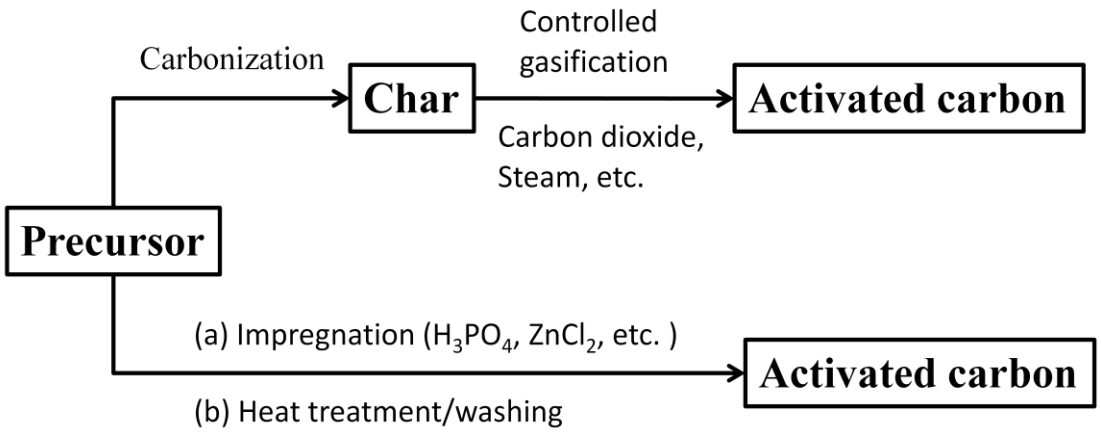

Figure 2.2 Manufacture of activated carbon [5].

2.3 Pore Structure and Chemical Structure of the Activated Carbon

2.3.1 Pore Structure

Activated carbons have a well-developed porous structure. This pore structure formed during the carbonization process is developed further during the activation process.

The structure of the pores and their pore size distribution are largely determined by the nature of the raw material and the history of its carbonization. Activated carbons are usually characterized by a polydisperse capillary structure comprising pores of different sizes and shapes. Several different methods used to determine the shapes of the pores have indicated ink-bottle shape, capillaries open at both ends or with one end closed, regular slit-shape, V-shape, and many other shapes [5].

Activated carbons are associated with pores starting from less than a nanometer to several thousand nanometers. Dubinin proposed a classification of the pores that has now been adopted by the International union of Pure and Applied Chemistry (IUPAC) [5]. This classification is based on their width, which represents the distance between the walls of a slit-shape pore or the radius of a cylindrical pore. The pores are divided into three groups: the micropores, the mesopores, and the marcopores.

Micropores have molecular dimensions, the effective radii being less than 2 nm. They generally have a pore volume of 0.15 to 0.70 cm^3/g. Their specific surface area constitutes about 95% of the total surface area of the activated carbon. Vast numbers of these pores in each particle give the carbon extremely high internal porosity and surface area. Typically, activated carbons contain surface areas in the range of 500-2000 m^2/g.

Mesopores, also called transitional pores, have effective dimensions in the 2 to 50 nm range, and their volume usually varies between 0.1 and 0.2 cm^3/g. The surface area of

these pores does not exceed 5% of the total surface area of the carbon. However, by using special methods, it is possible to prepare activated carbon that have an enhanced mesoporosity, the volume of mesopores attaining a volume of 0.2 to 0.64 cm^3/g and their surface area reaching as high as 200 m^2/g. Besides contributing significantly to the adsorption of the adsorbate, these pores act as conduits leading the adsorbate to the micropore cavity.

Marcopores have effective radii larger than 50 nm, with a pore volume between 0.2 and 0.4 cm^3/g. They are not of considerable importance to the process of adsorption in activated carbon because their contribution to the surface area of the adsorbate is very small and does not exceed 0.5 m^2/g. Macropores act as transport channels for the adsorbate into the mesopores and micropores.

Thus, the porous structure of active carbons is tridisperse, consisting of micro-, meso- and macropores. Each of these groups of pores plays a specific role in the adsorption process. The micropores constitute a large surface area and micropore volume and, therefore, determine to a considerable extent the adsorption capacity of a given activated carbon, provided that the molecular dimensions of the adsorbate are not too large to enter the micropores. Macro- and mesopores can generally be regarded as the highways into the carbon particle, and are crucial for kinetics.

The pore size distribution of a carbon is generally determined indirectly through analysis of nitrogen and argon adsorption isotherms at their respective boiling points. Density functional theory (DFT) is established by considering the intermolecular interactions on the microscopic scale. Several studies using the DFT method succeeded in obtaining the pore size distribution of activated carbon [6, 7].

All pores have walls and show two types of surfaces: the internal or microporous surfaces denoted by S_{mi} and the external surface, S_e. The external surface constitutes the walls of meso- and macropores as well as the edges and the outer facing aromatic sheets. The higher porosity provides a large surface area, which results in exceptional adsorptive properties.

An exact knowledge of the adsorbent surface area is important, since larger specific surface area implies a greater adsorption capacity of the adsorbent. Although the true surface area of microporous materials is difficult to calculate by existing models, the Brunauer–Emmet–Teller (BET) method is widely used to obtain an apparent surface area[8]. The t-plot method was applied to calculate the micropore volume and external surface area (mesoporous surface area). At the low temperature most of the adsorbent does not show any specific interactions, and adsorption of the nitrogen molecules can be approximated by the monolayer model. The level of the plateau on the isotherm corresponds to the amount of the molecules in a dense monolayer. One nitrogen molecule usually occupies 0.162 nm^2 on the polar surface [8]. Thus, if we know the amount of the molecules and the surface area per one molecule, we can calculate the total surface area of the adsorbent.

2.3.2 Chemical Structure of the Carbon Surface

The adsorption capacity of active carbons is determined by their physical or porous structure but is strongly influenced by the chemical structure. The decisive component of adsorption forces on a highly ordered carbon surface is the dispersive component of the van der Walls forces. In graphites that have a highly ordered crystalline surface, the adsorption is determined mainly by the dispersion component due to London forces. In

the case of active carbons, however, disturbances occur in the elementary microcrystalline structure, due to the presence of imperfect or partially burnt graphitic layers in the crystallites. These disturbances cause a variation in the arrangement of electron clouds in the carbon skeleton. This variation, in turn, results in the creation of unpaired electrons and incompletely saturated valences, and this influences the adsorption properties of active carbons, especially for polar and polarizable compounds [9].

Commercial active carbons are almost invariably associated with appreciable amounts of oxygen and hydrogen. In addition, they may be associated with atoms of sulfur, nitrogen, and halogens. These heteroatoms are derived from the starting material and become a part of the chemical structure as a result of imperfect carbonization, or they become chemically bonded to the surface during activation or during subsequent treatments. Studies have shown that these heteroatoms or molecular species are bonded to the edges and corners of the aromatic sheets or to carbon atoms at defect positions and give rise to carbon-oxygen, carbon-hydrogen, carbon-nitrogen, carbon-sulfur, and carbon-halogen surface compounds, also known as surface groups or surface complexes [9]. These heteroatoms can also be incorporated within the carbon layers forming heterocyclic ring systems. Because these edges constitute the main adsorbing surface, the presence of these surface compounds or molecular species modifies the surface characteristics and surface properties of active carbon. All of these heteroatoms influence the properties of the carbons in several ways but the greatest influence comes from the presence of oxygen, in particular edge-bonded-oxygen.

Carbon-oxygen surface groups are by far the most important surface groups that influence the surface characteristics such as wettability, polarity, and acidity, and physico-chemical properties such as catalytic, electrical, and chemical reactivity of these materials [10]. The several types of oxygen groups on the carbon surface, because of the electronegativity of the oxygen atoms, possess dipole moments and their presence has a marked effect on the shapes of adsorption isotherms of polar adsorbates. This influence is of importance for systems suing adsorption from solution, in particular adsorption from aqueous solutions where water molecules are competitively adsorbed at sites of the oxygen surface complexes.

The formation of oxygen groups on the carbon surface can be caused by several methods. Exposure to air produces surface oxygen complexes, a process which can continue for months, more so if there is moisture present. Rates and extents of formation, from molecular oxygen, of these oxygen complexes increase significantly, rising to a maximum with increasing oxidation temperature to 300-350 ^{o}C. Surface oxygen complexes can also be produced by oxidizing agents, such as nitric acid, hydrogen peroxide and ozone O_3. The surface oxygen groups include carboxyl, lactones, quinone, carbonyl, phenol, ether, and pyrone structures. Fig. 2.3 summarizes example of oxygen functional groups found on carbon surfaces.

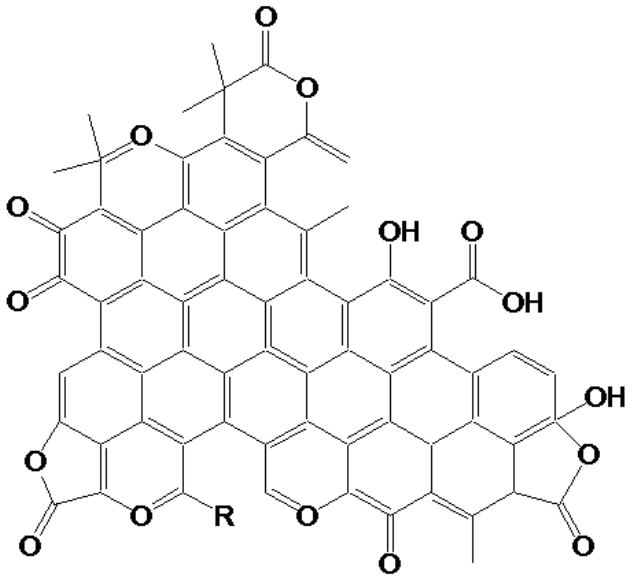

Figure 2.3 Oxygen functional groups on the activated carbon surface [5].

It is therefore of some importance that surfaces of activated carbons be analyzed in terms of amounts of oxygen present. X-ray photoelectron spectroscopy (XPS) is a surface analysis technique and is used for chemical analyses of surface oxygen complexes. XPS will be introduced in detail in Chapter 3.

2.4 Adsorbent Performance: Adsorption Capacity and Selectivity

Adsorption capacity and selectivity are the two important parameters of adsorbent performances. They are calculated by starting with the calculation of mass balance for the adsorbate in the batch experiments as follows:

$$V(C_0 - C_e) = M(q_e - q_0) \qquad (2\text{-}1)$$

Where V is the volume of the solution. C_0 and C_e are the initial and equilibrium concentration of salute in solution (mg/l), respectively. M is the mass of sorbent used (g). q_e is the equilibrium amount of adsorbate per unit mass of adsorbent (mg/g), i.e. the

sorption capacity of the adsorbent. q_0 is initial amount of adsorbate per unit mass of adsorbent (mg/g).

Since, in most cases, virgin carbons are used to determine equilibrium relationship:

$q_0 = 0$

The sorption capacity (q_e) of the furfural was calculated using equation (2-2):

$$q_e = V(C_0 - C_e) / M \qquad (2\text{-}2)$$

The distribution coefficient of adsorbate K_f, i.e., the ratio of the concentration of adsorbate (furfural in this research) in carbon to the equilibrium concentration of salute in the solution, is expressed as equation (2-3):

$$K_f = C_{fc} / C_{fs} \qquad (2\text{-}3)$$

Where and C_{fc} and C_{fs} are the equilibrium concentration of furfural in the carbon and in the solution, respectively. C_{fc} is calculated with equation (2-4):

$$C_{fc} = (C_0 - C_e)V / V_c \qquad (2\text{-}4)$$

Where $V_c = M/\rho$, is the volume of carbon; M is the mass of sorbent, and ρ is the true density of carbon. C_0 and C_e are the initial and equilibrium concentration of furfural in solution.

The distribution coefficient of sugar K_s is calculated with the similar method described above:

$$K_s = C_{sc} / C_{ss} \qquad (2\text{-}5)$$

Where C_{sc} and C_{ss} are the the equilibrium concentration of sugar in the carbon and in the solution, respectively.

Another separation performance of the sorbent is measured by its selectivity. A simple method for determining sorbent selectivity was proposed by Knaebel [11], which involved taking the ratio of Henry law constants. This rough estimate for selectivity can serve as a crude sorbent selection parameter. A more precise estimate can be obtained by comparing the isothermal binary working selectivity of the sorbents as defined by Gaffney [12].

The equilibrium selectivity ($\alpha_{f/s}$) is defined as the ratio of the distribution coefficient of furfural and sugar, as expressed in equation (2-6):

$$\alpha_{f/s} = \frac{K_f}{K_s} = \frac{C_{fc} / C_{fs}}{C_{sc} / C_{ss}} \qquad (2\text{-}6)$$

Where and C_{fc} and C_{fs} are the equilibrium concentration of furfural in the carbon and in the solution, respectively. C_{sc} and C_{ss} are the the equilibrium concentration of sugar in the carbon and in the solution, respectively.

2.5 Adsorption Isotherms

For a given adsorbate-adsorbent system, the adsorption equilibrium can be represented as an adsorption isotherm at constant temperature. The adsorption isotherm is extensively employed for representing the equilibrium states of an adsorption system. The adsorption isotherm gives useful information in the determination of the surface area of the adsorbent, the volume of the pores, and their size distribution. It also provides important information regarding the magnitude of the enthalpy of adsorption.

Adsorption equilibrium is a dynamic concept achieved when the rate at which molecules adsorb onto a surface is equal to the rate at which they desorb. The physical chemistry involved may be complex and no single theory of adsorption has been put forward to explain all the systems. Still now the oldest theories were used to predict the sorption process even though the assumption on which those models lie were found to be not entirely valid in later years. Also most of the adsorption theories have been developed for gas solid systems because the gaseous state is better understood than the liquid. Till now the statistical theories developed for gas – solid systems were applied for liquid solid systems with little confidence for designing of the equipment. The most commonly used equilibrium models to understand the adsorption systems was Langmuir and Freundlich isotherm equation which are explained as follows.

2.5.1 Langmuir Model

In 1916, Irving Langmuir published an isotherm for gases adsorbed on solids, which retained his name. It is an isotherm derived from a proposed kinetic mechanism. It is based on four hypotheses:

1. The surface of the adsorbent is uniform, that is, all the adsorption sites are equal.
2. Adsorbed molecules do not interact.
3. All adsorption occurs through the same mechanism.
4. At the maximum adsorption, only a monolayer is formed.

For adsorbate adsorbed on solids (adsorbent), the Langmuir isotherm [13] can be expressed by:

$$q_e = \frac{q_m K_L C_e}{1 + K_L C_e} \qquad (2\text{-}7)$$

where q_e is the substance amount of adsorbate adsorbed per unit mass of the adsorbent, the unit of q_e is mg/g. q_m is the maximal substance amount of adsorbate per gram of the adsorbent. The unit of q_m is mg/g. K_L is the adsorption constant (l/g); c_e (g/l) is the equilibrium concentration of residual solute in liquid.

Although the Langmuir isotherm equation is of limited significance for the interpretation of the adsorption data because of its idealized character, the equation remains the basic importance for expressing dynamic adsorption equilibrium. Furthermore, it has provided a good basis for the derivation of other more complex models. Many of the equations proposed later and which fit the experimental results over a wide range have been developed using the Langmuir concept. Thus, the Langmuir equation still retains an important position in physisorption as well as chemisorption theories.

2.5.2 Freundlich Model

Herbert Max Finley Freundlich, a German physical chemist, presented an empirical adsorption isotherm [14] for non ideal sorption on heterogeneous surfaces as well as multilayer sorption and is expressed by the equation:

$$q_e = K_F C_e^{\frac{1}{n}} \qquad (2\text{-}8)$$

where q_e (mg/g) is the substance amount of adsorbate adsorbed per gram of the adsorbent. c_e (g/l) is the equilibrium concentration of residual solute in solution after adsorption is complete. K_F, n are constants that must be determined for each solute, carbon type, and temperature.

The equation (2-8) can be written in the linear form as follows:

$$\ln q_e = \ln K_F + \frac{1}{n} \ln C_e \qquad (2\text{-}9)$$

So that a plot of lnq_e against lnC_e gives a straight line with an intercept on the ordinate axis. The values of n and K can be obtained from the slope and the intercept of the linear plot.

The Langmuir isotherm, in fact, has a theoretical justification, while the Freundlich isotherm represents an empirical model. The Langmuir isotherm assumes reversible adsorption and desorption of the adsorbate molecules. The Langmuir isotherm typically represents data well for single components. The Freundlich isotherm can be used also for mixtures of compounds

2.6 Adsorption Kinetics

Because adsorption rate is limited primarily by diffusion, variables that influence diffusion have a significant effect on adsorption rate. For example, a higher concentration gradient across the surface of the carbon particle will increase the rate of adsorption, though a high concentration of solute can eventually have a negative effect on adsorptive capacity. In practice, the primary carbon variable influencing adsorption rate is the size of the carbon particle. Smaller carbon particles have a greater ratio of surface area to volume, making them more accessible to diffusion from solution.

Notably, the size of the particle has little effect on adsorptive capacity as expressed by total surface area. While it is well known that smaller particles of a given mass of carbon would have a greater surface area than larger particles, the huge internal surface area of carbon dominates the calculation so much that the particle size essentially has no effect on capacity.

Of course, the rate of at which sorption occurs can be very important when trying to remove contaminants from water. Perrich defines the rate of adsorption as "the rate at which substances are removed from the liquid phase (adsorbate) to the solid phase (adsorbent) [15]." He describes three main processes which control the adsorption rate: diffusion of the solute through the layer of fluid surrounding the adsorbent particle, diffusion of the solute across the surface of the adsorbent, and adsorption of the solute onto the internal surfaces of the adsorbent pores.

For most purposes, the adsorption of the solute molecule at the site on the internal surface occurs almost instantaneously, so it has little effect on the rate of the overall adsorption. The transfer of solute from the bulk liquid to the surface layer of fluid around a particle can occur rather slowly, but in most treatment systems, this is encouraged by the constant movement of fluid past the surface. On the other hand, the diffusion of the solute through or across the surface of the adsorbent may occur rather slowly, and this diffusion usually limits the rate of the sorption. Because the rate of adsorption is usually limited by diffusion, it is influenced by the same variables which affect diffusion rate. The concentration gradient of the solute across the surface of the adsorbent has a large effect on the rate.

2.6.1 Pseudo-First-Order-Model and Pseudo-Second-Order-Model

The sorption of furfural molecules from liquid phase to a solid phase can be considered as a reversible process with equilibrium being established between the solution and the solid phase. Assuming a non-dissociating molecular adsorption of furfural molecules on ACC particles, the sorption phenomenon can be described as the diffusion controlled process [15].

$$A + S \underset{k_D}{\overset{k_A}{\rightleftharpoons}} A.S$$

where, A is the adsorbate and S is the active site on the adsorbent, and $A.S$ is the activated complex. k_A and k_D are the adsorption and desorption rate constants, respectively. Using first order kinetics it can be shown that with no adsorbate initially present on the adsorbent (i.e. $C_{A.S0} = 0$ at $t = 0$), the uptake of the adsorbate by the adsorbent at any instant t is given as:

$$\ln(q_e - q_t) = \ln q_e - k_1 t \qquad (2\text{-}10)$$

where q_e and q_t are the amounts of furfural adsorbed (mg/g) at equilibrium and at time t, respectively, and k_1 the rate constant adsorption (S^{-1}). Values of k_1 were calculated from the plots of $\ln(q_e - q_t)$ versus t.

The pseudo-second-order model [16] is represented as:

$$\frac{t}{q_t} = \frac{1}{q_e} t + \frac{1}{k_2 q_e^2} \qquad (2\text{-}11)$$

where k_2 (g/mg h) is the rates constant of second-order adsorption. If second-order kinetics is applicable, the plot of t/q versus t should show a linear relationship.

2.6.2 Determination of Diffusivity

Kinetic data could be treated by models given by Boyd et al. [17] which is valid under the experimental conditions used. Applying Vermeulen's approximation to the solution of the simultaneous set of differential and algebric equations [18] leads to calculation of effective particle diffusivity by the following equation:

$$\ln[\frac{1}{(1-F^2(t))}] = \frac{\pi^2 D_e t}{R_a^2} \qquad (2\text{-}12)$$

where $F(t) = q_t/q_e$ is the fractional attainment of equilibrium at time *t*, *De* is the effective diffusion coefficient of adsorbates in the adsorbent phase (m^2/s), *Ra* is radius of the adsorbent particle assumed to be spherical (m), and *t* is the time (min). Thus, the slope of the plot of $ln[1/(1-F^2(t))]$ versus t gives *De*.

2.7 Regeneration of Activated Carbon

2.7.1 Thermal Regeneration

The regeneration of activated carbons involves restoring the adsorptive capacity of saturated activated carbon by desorbing adsorbed contaminants on the activated carbon surface. The most common regeneration technique employed in industrial processes is thermal regeneration. Fig. 2.4 illustrates the thermal regeneration process of activated carbon in industry. The thermal regeneration process generally follows three steps [19]:
(1) Adsorbent drying at approximately 105 ℃. (2) High temperature desorption and decomposition (500–900 ℃) under an inert atmosphere. (3) Residual organic gasification by an oxidising gas (steam or carbon dioxide) at elevated temperatures (800 ℃).

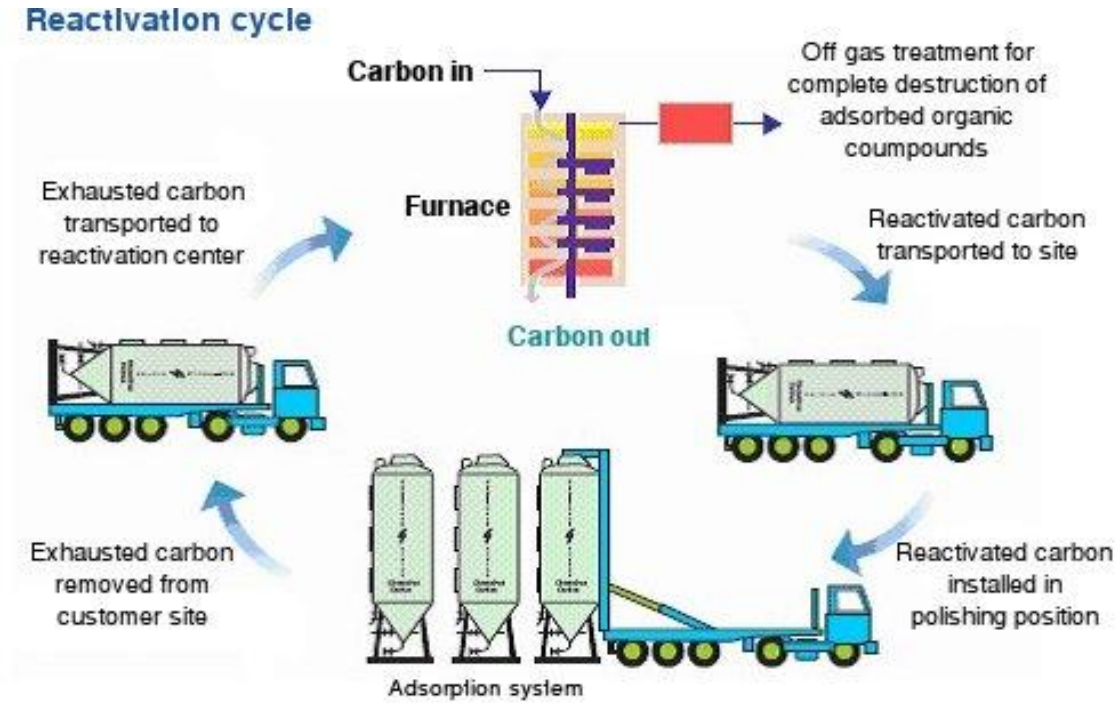

Figure 2.4 Thermal regeneration process of activated carbon in industry [19].

The heat treatment stage utilizes the exothermic nature of adsorption and results in desorption, and in some cases partial cracking and polymerization of the adsorbed organics. The final step aims to remove charred organic residue formed in the porous structure in the previous stage and re-expose the porous carbon structure regenerating its original surface characteristics. After treatment the adsorption column can be reused. In each adsorption-thermal regeneration cycle, between 5–15 wt% of the carbon bed is typically burnt off resulting in a loss of adsorptive capacity [20].

Thermal regeneration is a high energy-consuming process due to the high required temperatures making it both an energetically and commercially expensive process. Plants that rely on thermal regeneration of activated carbon have to be of a certain size before it is economically viable to have regeneration facilities onsite. As a result it is common for

smaller waste treatment sites to ship their activated carbon cores to a specialized facility for regeneration, increasing the process already significant carbon footprint.

2.7.2 Chemical Regeneration

Current concerns with the high energy/cost nature of thermal regeneration of activated carbon have encouraged research into alternative regeneration methods to reduce the environmental impact of such processes. Solvent regeneration is an alternative to thermal regeneration[21, 22]. The desorption of adsorbate from the carbon surface by solvent extraction is a partitioning process. When the solubility of adsorbate is higher in a solvent than in the water, the presence of the solvent in the sorption system can reduce the solid-to-liquid equilibrium concentration ratio of the adsorbate; thus desorption takes place as the solvent is displacing or mixing with the water. In the case of the spent carbon with a large quantity of adsorbate, regeneration with solvent extraction is economically attractive and offers several advantages[23]:

(1) It can be done relatively rapidly in situ; thus it minimizes downtime for the absorbers and completely eliminates unloading, transporting and repacking of the carbon.

(2) No carbon attrition occurs; thus the cost of replacing attrited carbon is avoided.

(3) No degradation of the carbon surface or pore structure due to repetitive pyrolysis and re-oxidation can occur. Hence, the carbon can last almost indefinitely.

(4) Recovery of valuable adsorbents is possible; or, if they are not valuable, they can be easily disposed of by combusting them along with residual solvent.

(5) With properly chosen solvents, solvent removal from the columns and subsequent recovery by distillation can be done easily.

The regeneration of activated carbon will be exploited in depth in Chapter 6.

2. 8 References

[1] Yang RT. Adsorbents: Fundamentals and Applications. Wiley Interscience 2003.

[2] Salis A, Meloni D, Ligas S, Casula MF, Monduzzi M, Solinas V, et al. Physical and Chemical Adsorption of Mucor javanicus Lipase on SBA-15 Mesoporous Silica. Synthesis, Structural Characterization, and Activity Performance. Langmuir 2005;21:5511-5516.

[3] Oura K. Surface Science, An Introduction. Berlin: Springer 2003.

[4] Marsh H. Activated Carbon. Elsevier 2006.

[5] Roop Chand Bansal MG. Activated carbon adsorption. Taylor Francis 2005.

[6] El-Merraoui M, Aoshima M, Kaneko K. Micropore Size Distribution of Activated Carbon Fiber Using the Density Functional Theory and Other Methods. Langmuir 2000;16:4300-4304.

[7] Ustinov EA, Do DD, Fenelonov VB. Pore size distribution analysis of activated carbons: Application of density functional theory using nongraphitized carbon black as a reference system. Carbon 2006;44:653-663.

[8] Hu Z, Srinivasan MP. Preparation of high-surface-area activated carbons from coconut shell. Microporous and Mesoporous Materials 1999;27:11-18.

[9] Chingombe P, Saha B, Wakeman RJ. Surface modification and characterisation of a coal-based activated carbon. Carbon 2005;43:3132-3143.

[10] Li L, Quinlivan PA, Knappe DRU. Effects of activated carbon surface chemistry and pore structure on the adsorption of organic contaminants from aqueous solution. Carbon 2002;40:2085-2100.

[11] Knaebel KS. For your next separation consider adsorption. Journal Name: Chemical Engineering; Journal Volume: 102; Journal Issue: 11; Other Information: PBD: Nov 1995 1995:Medium: X; Size: pp. 92-102.

[12] Gaffney TR, Kirner, J.F. W.P. O2 VSF process with low O2 capacity adsorbents. US Patent 1993.

[13] Langmuir I. The adsorption of gases on plane surfaces of glass, mica and platinum. J Am Chem Soc 1918:1361–1403.

[14] Freundlich H. Over the adsorption in solution. J Phys Chem 1906:385-471.

[15] Srivastava VC, Swamy MM, Mall ID, Prasad B, Mishra IM. Adsorptive removal of phenol by bagasse fly ash and activated carbon: Equilibrium, kinetics and thermodynamics. Colloids and Surfaces A: Physicochemical and Engineering Aspects 2006;272:89-104.

[16] Ho YS, McKay G. Pseudo-second order model for sorption processes. Process Biochemistry 1999;34:451-465.

[17] Boyd GE, Adamson AW, Myers LS. The Exchange Adsorption of Ions from Aqueous Solutions by Organic Zeolites. II. Kinetics1. Journal of the American Chemical Society 1947;69:2836-2848.

[18] Skelland AHP. Diffusional Mass Transfer. Wiley: NY 1974.

[19] Sabio E, González E, González JF, González-García CM, Ramiro A, Gañan J. Thermal regeneration of activated carbon saturated with p-nitrophenol. Carbon 2004;42:2285-2293.

[20] Bagreev A, Rahman H, Bandosz TJ. Thermal regeneration of a spent activated carbon previously used as hydrogen sulfide adsorbent. Carbon 2001;39:1319-1326.

[21] Cooney DO, Nagerl A, Hines AL. Solvent regeneration of activated carbon. Water Research 1983;17:403-410.

[22] Sutikno T, Himmelstein KJ. Desorption of phenol from activated carbon by solvent regeneration. Industrial & Engineering Chemistry Fundamentals 1983;22:420-425.

[23] Grant TM, King CJ. Mechanism of irreversible adsorption of phenolic compounds by activated carbons. Industrial & Engineering Chemistry Research 1990;29:264-271.

CHAPTER 3: MATERIALS AND EXPERIMENTAL METHODS

This chapter will first introduce all the materials used in this study, followed by the experimental procedures used to test the activated carbons. The methods to regenerate the spent carbons will be shown subsequently. Moreover, the experimental protocols utilized to perform bio-ethanol fermentation will be presented. A summary of the complementary techniques employed to characterize the morphological, elemental and structure information of the materials will be provided in this chapter. Other techniques employed to characterize the concentration of furfural, monosaccharides and ethanol will be shown at the end of this chapter.

3.1 Materials

3.1.1 Adsorbates

The model inhibitors investigated in this work are furfural (99% purity, Sigma-Aldrich, St.Louis, MO), and HMF (99% purity, Sigma-Aldrich, St.Louis, MO). In the adsorption tests, furfural and HMF were added into the solution at concentration of 3.6 g/L and 0.36 g/L, respectively. Concentrations of furfural and HMF were chosen so as to be close to those found in switch grass hydrolyzate[1]. Fig. 3.1 shows the chemical structure of furfural and HMF. Table 3.1 shows the properties of furfural and HMF.

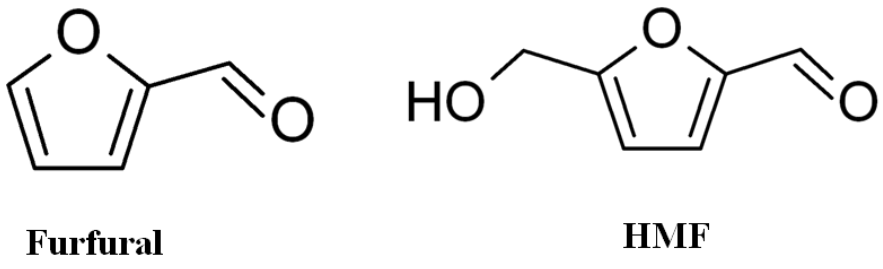

Figure 3.1 Chemical structure of furfural and HMF.

Table 3.1 Physical and chemical properties of furfural and HMF.

	Furfural	**HMF**
Molecular formula	$C_5H_4O_2$	$C_6H_6O_3$
Density	1.16 g/cm^3 [2]	1.29 g/cm^3 [2]
Melting point (1 atm)	-37 ℃ [2]	32 ℃ [2]
Boiling point (1 atm)	162 ℃ [2]	291 ℃ [2]
Solubility in water (25 ℃)	83 g/L [2]	364g/L [2]

3.1.2 Adsorbents

Two types of activated carbon were studied as adsorbents. The first type is commercial activated carbon. Norit_1240 (Norit Americas Incorporated, Marshall, TX) is coal-based and steam activated. The commercial activated carbon was granular with size of 8×20 U.S. Standard Mesh. Before the adsorption tests, the commercial activated carbon was ground into powder form by using mortar. The selected carbon fractions were dried at 105 ℃ for 48 h, allowed to cool in a desiccator and stored in clean glass jars.

The second type of activated carbon is polymer-derived carbon. Poly-furfural was synthesized by the following process [3-5]. Predetermined amounts of furfural were dissolved in an appropriate amount of ethanol at room temperature. The mixture was decanted into a pressure resistant glass bottle after adding a certain amount of concentrated sulfuric acid (98 wt %) as the catalyst. As soon as the bottle was sealed, the mixture was heated to 80 ^{o}C in a water bath and the reaction was allowed to continue for 6 h. Subsequently, the organic gels (poly-furfural) were washed with water, and dried at

130 ^{o}C under vacuum for 2 days. Finally, poly-furfural was carbonized in a quartz tube furnace at 800 ^{o}C with a heating rate of 10 ^{o}C /min for 3 h under an argon atmosphere (argon flow rate 200 ml/min). Here, poly-furfural and pyrolyzed poly-furfural were denoted as PF and PF800, respectively.

To investigate the impact of carbon surface oxygen groups on the sorption process, a known amount of commercial carbon (Norit-1240) and polymer-derived carbon (PF800) were oxidized using 60 wt% nitric acid [6]. The reactions were heated to 78 ^{o}C and the reactions were allowed to continue for 6 h with continued stirring. The oxidized carbons were then washed with distilled water until no further change in pH could be detected. The modified carbon samples are represented by Norit_1240_HNO_3 and PF800_HNO_3, respectively.

3.2 Batch Adsorption Tests

Batch adsorption tests were performed to study the adsorption behavior of the adsorbents in the inhibitor-containing water solution. Commercial activated carbon and polymer-derived carbon were investigated under the same conditions and their comparative results were studied.

3.2.1 Determination of Equilibrium Time

Laboratory tests for measuring adsorptive capacity are designed to be rapid screening methods for determining the performance of activated carbon. Results from laboratory batch tests conducted at equilibrium will correlate directly with full scale plant process performance. The laboratory tests can accurately measure adsorptive capacity of different types of activated carbon and identify the carbon type with the best cost performance. To

achieve accurate results, the adsorption measurements were performed under equilibrium conditions. Therefore, the first step in the laboratory tests is to determine the minimum contact time required to establish equilibrium conditions. Fig. 3.2 shows the condition of the batch tests. The adsorption batch tests were performed in the sealed glass vials at room temperature (25 ^{o}C). The glass vials were put in the shaker to agitate the samples.

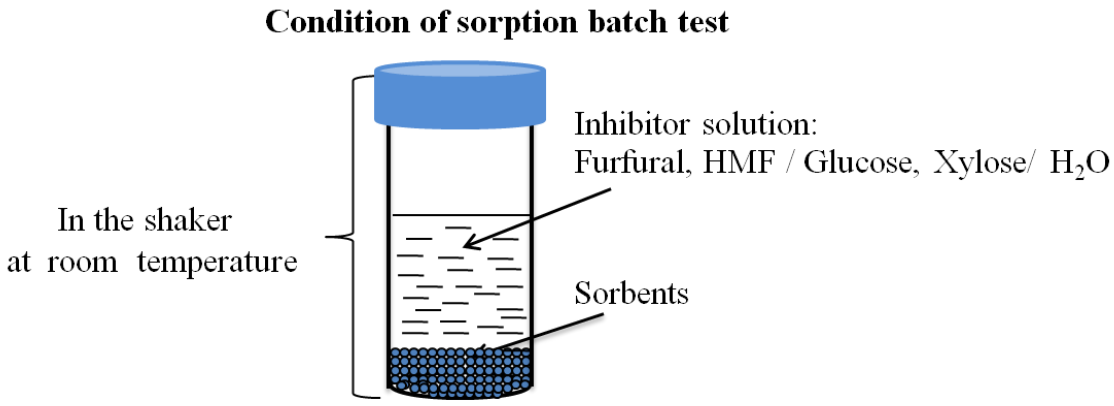

Figure 3.2 Condition of adsorption batch tests.

The experimental procedures used to determine the equilibrium time are shown as follows:

1. A predetermined weight of carbon is added to a glass bottle. The amount of carbon is 1 wt% of the process liquid, which contains 3.6 g/l furfural, 0.4 g/l HMF, 10 g/l glucose, and 2 g/l xylose.
2. Transfer 50 ml of the process liquid to the bottle and seal the bottle.
3. Agitate the sample in the shaker at room temperature for different time periods. Samples were withdrawn at appropriate time intervals.
4. After mixing the carbon and liquid for the specified contact time, immediately filter each sample to separate the process liquid from the carbon. Analyze the filtrate to

determine the inhibitor (furfural and HMF) remaining in the solution.

5. Prepare a graph with the inhibitor removed on the Y-axis vs. the carbon contact time on the X-axis. The test results will produce a plot as shown in Fig. 3.3. There is usually a sharp break in the curve at the optimum contact time. Contact times in excess of this value have a very limited effect on removal of additional inhibitor or increases in carbon adsorptive capacity.

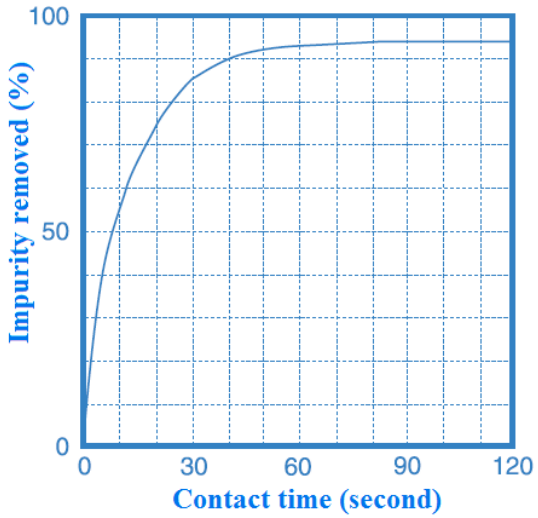

Figure 3.3 Determination of equilibrium time in the adsorption batch tests.

3.2.2 Determination of Adsorption Capacity

Once the optimum contact time is determined, the next step is to measure the total adsorptive capacity of the activated carbon.

1. A known amount of carbon was added to six bottles. At least one of the bottles should contain sufficient carbon to remove impurities to a concentration level that is below the desired treatment goal.
2. Add 10 mL of inhibitor solution (with different concentration of inhibitors) to each

bottle, and seal the bottles.

3. Agitate the samples in the shaker at room temperature for the optimum contact time determined earlier.
4. Immediately filter the sample to remove the carbon from the solution.
5. Analyze the filtrate to determine the inhibitor (furfural and HMF) remaining in the solution. Calculate the adsorptive capacity as follows:

$$\textbf{Adsorptive Capacity} = \frac{\textbf{Weight of Inhibitor Adsorbed}}{\textbf{Carbon Weight}}$$

With known initial inhibitor concentration and carbon weight used, inhibitor uptake can be calculated by determining the remaining inhibitor concentration. Accordingly, adsorption parameters, such as adsorptive capacity and equilibrium selectivity, can be achieved.

3.3 Regeneration of Activated Carbon

3.3.1 Thermal Regeneration

For regeneration, the spent activated carbons were air dried at room temperature. Then, the spent activated carbons were put in a quartz cylinder (35 cm long and 5 cm I.D.) which was externally heated by a furnace. The quartz cylinder was purged with N_2 gas for 10 min to ensure no air remained in the cylinder and both ends of the cylinder were sealed before the furnace was turned on. Heating under an N_2 environment prevented oxidation of activated carbons, which could happen under atmospheric conditions at elevated temperature, and rendered the regenerated carbons useless. Regeneration temperatures were tested at 300 ^{o}C and 800 ^{o}C for 2 h, repectively, with heating rate 15

^{o}C/min. The regenerated activated carbons were then used for furfrual adsorption tests, and their adsorption capacity was compared with that of the fresh adsorbents.

3.3.2 pH Adjustment

The condition of desorption batch tests by pH adjustment or organic solvent stripping is similar to that in adsorption tests, except that the virgin adsorbents were replaced by the spent adsorbents and that the inhibitor-containing solution was substituted by the eluent, shown in Fig. 3.4. Spent activated carbons with 0.2 g of furfural adsorbed per gram of carbon was mixed with a certain amount of eluents or organic solent. The mass ratio of eluent to spent activated carbon is 100. The mixture was incubated at room temperature (25 ^{o}C) for 30 min with agitation.

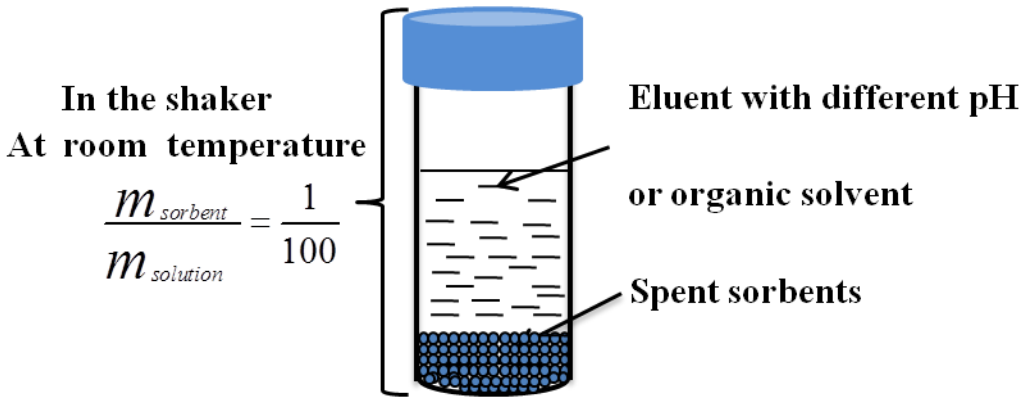

Figure 3.4 Condition of desorption batch tests.

To restore the adsorption capacity of the spent adsorbents, spent adsorbents were contacted with eluents with different pH: (a) deionized water (DI water), (b) 5 wt% H_2SO_4/H_2O, and (c) 5 wt% $NaOH/H_2O$, respectively. The content of furfural in the eluent, desorbed from the spent adsorbents, was analyzed by UV after the desorption tests.

3.3.3 Organic Solvent Extraction

Five different organic solvents were evaluated for their ability to desorb inhibitors from the spent adsorbents. The solvents tested were DMSO (Dimethyl sulfoxide), DCM (Dichloromethane), TFH (Tetrahydrofuran), ethanol and butanol. The content of furfural in the organic solvent, desorbed from the spent adsorbents, was analyzed by UV after the desorption tests. The regeneration efficiency of each organic solvent was calculated and compared with each other.

3.4 Column Tests of Adsorption/desorption Cycle

Based on the results in batch tests, adsorption tests in column system were also investigated. An adsorption-desorption regeneration cycle was proposed as shown in Fig. 3.5. After biomass pretreatment, a furfural-rich feed goes to an adsorption column for furfural removal, followed by the flow of low furfural-containing feed from adsorption column to fermentation for ethanol production. After fermentation, the ethanol-containing liquid flows back into the column to desorb the furfural from sorbent. Furfural enriched liquid then goes to distillation to purify ethanol from the solution. After desorption, the regenerated sorbent is ready for the next cycle of adsorption-desorption. The efficiency of adsorbent use could be greatly improved by this regeneration method. Additionally, the presence of furfural in the liquid has no effect on the purification of ethanol by distillation, due to the high boiling point of furfural (162 ℃).

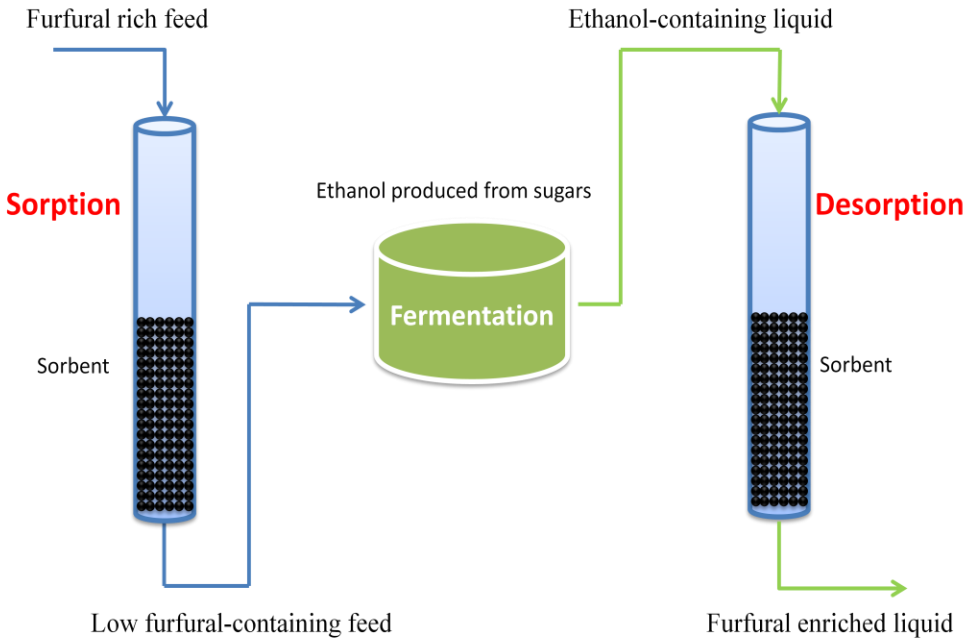

Figure.3.5 Adsorption-desorption regeneration cycle in the column system.

Norit_1240 was studied in the column system, because it is granular (8×20 mesh), which is suitable in the column system. The step of fermentation between adsorption and desorption in Fig. 3.5 was simulated by adding a certain amount of ethanol into the liquid after sorption process to simulate 7.5wt% ethanol was produced in the fermentation. The biomass-pretreated liquid, used in the adsorption test, was simulated by the water solution with 4 g/L furfural, 10 g/l glucose and 2 g/l xylose. 100 g of Norit-1240 was placed in the column, while 2 liters water solution was pumped into the column. The flow rate was controlled at 50 ml/min.

3.5 Fermentation Experiments

The toxic effect of furfural and HMF on the fermentation of *Zymomonas mobilis* on glucose and xylose were studied. Microbial cell growth, sugar consumption and ethanol production were investigated during the fermentation. The results were compared with

those of the fermentation after inhibitors were selectively removed from the broth by adsorbents.

3.5.1 Microorganism

Wild type *Zymomonas mobilis* ZM4 (ATCC31821) was obtained from ATCC (American Type Culture Collection). *Zymomonas mobilis* A3, a mutant from wild-type *Zymomonas mobilis* ZM4, was also used in this study. A3 was engineered to decompose both glucose and xylose, while ZM4 is able to utilize only glucose [7].

For long-term storage, all strains were kept at -80 ^{o}C in 30% (v/v) glycerol solution by mixing 500μl sterile medium with culture (overnight cultured) with 500μl 60% (v/v) glycerol solution in a 1ml vial. Glycerol solution was prepared by mixing glycerol and deionized water. The 60% glycerol solution was autoclaved at 120 ^{o}C for 20 minutes.

3.5.2 Pre-seed Culture

Pre-seed culture for *Zymomonas mobilis* ZM4 and A3 was prepared by inoculating a single colony (from agar plate) into 9 ml of RM (rich medium) culture medium supplemented with 5 g/l glucose and 1 g/l xylose. RM medium contained 1 wt% yeast extract, 0.2 wt% KH_2PO_4. Autoclave stock solutions for glucose, xylose and RM medium separately. Cooled them and then mixed appropriately to get desired solution. 1 M H_3PO_4 or NH_4OH was used to adjust the pH of liquid medium to make sure the pH is between 5.5 and 6. Pre-seed culture was performed at 30 ℃ in a 15-ml screw-cap centrifuge tube statically for 24 hours. Measure the optical density (OD) of the pre-seed culture against RM media as blank. Pre-seed culture was grown to the stationary phase.

3.5.3 Seed Culture

Inoculate 25 ml of RM media supplemented with 10 g/l glucose and 2 g/l xylose in a 50 ml centrifuge tube with the pre-seed cultures such that the starting OD for the seed culture is 0.1. Seed culture was performed at 30℃ in shaker at 250 rpm for 24 hours**.** **S**amples of the seed culture were taken after 12 hours to analyze the concentration of glucose and xylose by HPLC. Appropriate amount of cells were harvested from seed culture at exponential phase. Ideally, main fermentation should be started with seed cultures when the seed cultures for both ZM4 and A3 are near glucose exhaustion i.e. about 0.5 g/l of glucose out of 10 g/l glucose remains.

3.5.4 Main Fermentation

The seed culture was centrifuged at 16,000×g at 4^{o}C for 10 min and supernatant was poured out. The cells were gently resuspended by pipetting in 10 ml of RM media. Gentle resuspension is important since vigorous pipetting can kill cells. Resuspended cells of ZM4 and A3 were put in their appropriate tubes such that the starting OD of main fermentation was 0.05. The solutions in different tubes contained different amounts of furfural and HMF (with and without adsorption by activated carbon). The main fermentation was performed at 30℃ in shaker at 250 rpm. 200µl samples were withdrawn for HPLC analysis at regular intervals. The OD measurement should be timed properly so as to give a good growth profile.

3.6 Characterization

3.6.1 Scanning Electron Microscopy (SEM)

SEM images were obtained with SEM machines LEO 1530, equipped with a thermally assisted field emission gun operating at 3.5 kV for activated carbons. The electron conductivity of the carbon was high so that metal sputtering was not necessary. Furthermore, in order to see the fine structures on carbon surfaces, no metal sputtering was applied to carbons to avoid the formation of nm scale metal particles. Lower voltage is preferred to dim the electron beam and observe the fine structures. The samples were dried at 100^{o}C for 24 hours before the analysis.

3.6.2 Thermo Gravimetric Analysis (TGA)

In the thermal regeneration, the weight the spent adsorbents was monitored by TGA (Q5000IR, TA Instruments, New Castle, DE). In a typical TGA experiment, samples are heated to a desired temperature and the sample weight (or weight loss) is monitored simultaneously.

3.6.3 Ultraviolet-visible Spectroscopy (UV-Vis)

The impurities (furfural and HMF) in the aqueous solution were analyzed by using UV-spectrophotometer. A standard solution of the furfural and HMF was scanned to determine the wavelength (λ_{max}) corresponding to maximum absorbance. By using this wavelength a standard graph of absorbance versus concentration of furfural and HMF was prepared, respectively. This graph showed a linear variation up to 10 mg/l concentration. Therefore, the samples with higher concentration of furfural and HMF (>10 mg/l) were diluted with distilled water, whenever necessary, to make the

concentration less than 10 mg/l, for the accurate determination of the furfural and HMF concentration.

3.6.4 X-ray Photoelectron Spectroscopy (XPS)

The surface chemical composition of the samples was determined by X-ray photoelectron spectroscopy (XPS). The analysis was performed on a Thermo K-Alpha under 5×10^{-10} Pa. The survey scans were collected from 200 to 600 eV with a pass energy of 50 eV. For calibration purposes, the carbon 1s electron bond energy corresponding to graphitic carbon was referenced to 284.5 eV. The samples were dried at 100^{o}C for 24 hours before the analysis.

3.6.5 High-Performance Anion-Exchange Chromatography (HPAEC)

The concentration of glucose and xylose in the adsorption tests were analyzed by HPAEC. Glucose and xylose standards were prepared by mixing 1 ml DI water with various amounts of sugars. The corresponding sugar concentrations were 0, 5, 25, 50, 75, and 100 g/l, respectively. 100 µl were transferred to the HPAEC vial for HPAEC analysis. Sugars were measured by Dionex LC20 HPAEC equipped with PA10 column. The calibration line was then plotted. Concentrations of glucose and xylose were calculated from calibration curves.

3.6.6 BET Surface Area and Pore Structure

BET surface area, micropore volumes and pore size distributions were determined from calculated from nitrogen physisorption measurements performed on a Micromeritics ASAP 2020. Prior to analysis, samples were outgassed overnight at 100 ^{o}C. BET surface areas [8, 9] were determined from adsorption isotherms that were completed with a 0.1 g

sample. The density functional theory (DFT) [10, 11]was used to calculated micropore volumes, and micropore size distributions from the N_2 adsorption data.

3.6.7 Analytical Methods in Fermentation

3.6.7.1 Optical Density (OD)

OD value of the sample was measured by Beckman spectrophotometer DU530 at 600 nm. Samples were diluted as needed to allow the absorbance reading to fall between 0.05 and 0.4 where Beer's law was a linear function of biomass concentration. Because optical density was directly proportional to the dry cell mass concentration (*c*) and easy to measure, it was routinely used to follow cell growth [12]. Conversion from one dimension to the other was accomplished by applying the equation $OD = kc$, where ***k*** is the constant. The corresponding biomass concentration is then multiplied by the dilution factor to obtain the actual biomass concentration in the culture.

Specific growth rate was determined from the plots of optical density (OD) vs. time. The behavior of cells in exponential growing phase as a function of time could be described with the following equations [13]:

$$Y = ae^{\mu t} \qquad (3\text{-}1)$$

where a is the original OD value 0.05. μ is defined as the specific growth rate (h^{-1}). Y is the OD value and t is time (h). The equation can be written as:

$$\ln(Y / 0.05) = \mu t \qquad (3\text{-}2)$$

When ln (Y/0.05) is plotted with growth time, a linear line should result, and the slope is μ.

3.6.7.2 Ethanol, Glucose and Xylose Measurement

The concentration of ethanol, glucose and xylose in the fermentation experiments was analyzed by High-performance liquid chromatography (HPLC). Ethanol standards were prepared by mixing 1 ml DI water with various amounts of 100% ethanol (HPLC grade). The amounts of 100% ethanol were 0, 6, 13, 20, 26, 32, 40, and 47 µl, respectively. The corresponding ethanol concentrations were 0, 0.47, 1.01, 1.54, 2.00, 2.45, 3.03, and 3.54 % (w/v), respectively. 100 µl were transferred to the HPLC vial for HPLC analysis. Ethanol was measured by Agilent 1100 HPLC equipped with an Aminex HPX-87H column (Bio-Rad) with 5 mM H_2SO_4 at 0.4 ml/min as mobile phase. The calibration line was then plotted. Calibration line is a relationship between ethanol concentration and the area (nRIU*s).

Samples from the fermentation medium were prepared as follows. After OD measurement, 200µl of sample was taken in eppendroff tubes and then was centrifuged for 10 minutes at 13000 rpm at 4ºC. 150µl of supernatant was collected and poured in a 1 ml syringe which has a 0.22 µm filter attached at its mouth. 50 ul of the filtrate was taken and diluted 10 times by adding 450ul water. 100 ul of the diluted sample was taken and put into a HPLC vial. No air bubbles should be remained in the solution. Area (nRIU*s) of each sample was obtained. Ethanol concentration was then calculated from the calibration line.

HPLC analysis allows simultaneous measurement for ethanol, glucose, and xylose. Calibration lines for glucose and xylose were prepared similar with ethanol. Concentrations of glucose and xylose in fermentation samples were calculated from calibration curves.

3.7 References

[1] Franden MA, Pienkos PT, Zhang M. Development of a high-throughput method to evaluate the impact of inhibitory compounds from lignocellulosic hydrolysates on the growth of Zymomonas mobilis. Journal of Biotechnology 2009;144:259-267.

[2] Record of CAS RN 98-01-1 in the GESTIS Substance Database from the IFA

[3] Shindo A, Izumino K. Structural variation during pyrolysis of furfuryl alcohol and furfural-furfuryl alcohol resins. Carbon 1994;32:1233-1243.

[4] Wang YX, Tan SH, Jiang DL, Zhang XY. Preparation of porous carbon derived from mixtures of furfuryl resin and glycol with controlled pore size distribution. Carbon 2003;41:2065-2072.

[5] Zarbin AJG, Bertholdo R, Oliveira MAFC. Preparation, characterization and pyrolysis of poly(furfuryl alcohol)/porous silica glass nanocomposites: novel route to carbon template. Carbon 2002;40:2413-2422.

[6] Li L, Quinlivan PA, Knappe DRU. Effects of activated carbon surface chemistry and pore structure on the adsorption of organic contaminants from aqueous solution. Carbon 2002;40:2085-2100.

[7] Sáez-Miranda JC, Saliceti-Piazza L, McMillan JD. Measurement and Analysis of Intracellular ATP Levels in Metabolically Engineered Zymomonas mobilis Fermenting Glucose and Xylose Mixtures. Biotechnology Progress 2006;22:359-368.

[8] Hu Z, Srinivasan MP. Preparation of high-surface-area activated carbons from coconut shell. Microporous and Mesoporous Materials 1999;27:11-18.

[9] Lastoskie C, Gubbins KE, Quirke N. Pore size distribution analysis of microporous carbons: a density functional theory approach. The Journal of Physical Chemistry 1993;97:4786-4796.

[10] El-Merraoui M, Aoshima M, Kaneko K. Micropore Size Distribution of Activated Carbon Fiber Using the Density Functional Theory and Other Methods. Langmuir 2000;16:4300-4304.

[11] Ustinov EA, Do DD, Fenelonov VB. Pore size distribution analysis of activated carbons: Application of density functional theory using nongraphitized carbon black as a reference system. Carbon 2006;44:653-663.

[12] Lee C, Lim H. New device for continuously monitoring the optical density of concentrated microbial cultures. Biotechnology and Bioengineering 1980;22:639-642.

[13] Rebroš M, Rosenberg M, Grosová Z, Krištofíková Lu, Paluch M, Šipöcz M. Ethanol Production from Starch Hydrolyzates using <i>Zymomonas mobilis and Glucoamylase Entrapped in Polyvinylalcohol Hydrogel. Applied Biochemistry and Biotechnology 2009;158:561-570.

CHAPTER 4: SELECTIVE ADSORPTION OF FURFURAL

4.1 Overview

This chapter presents the characterization results of commercial activated carbon and polymer-derived carbon. SEM images reveal the homogenous structure of polymer-derived carbon and heterogeneous structure of commercial carbon. XPS reveals the existence of oxygen functional groups on the commercial carbon surface, while polymer-derived carbon only contains trivial oxygen groups. The oxygen groups on the carbon surface are believed to have contributed to the decrease on the selectivity of activated carbon between furfural and sugars. Oxidization of activated carbon by nitric acid generated more information which supports the above assumption. Different adsorption isotherm models and kinetic models were studied to fit commercial activated carbon and polymer-derived carbon individually. Furthermore, the effect of acetic acid on the separation of furfural was investigated, and the negative effect can be eliminated by neutralization with aqueous ammonia. In addition, adsorption tests were performed by utilizing the true biomass hydrolytes.

4.2 Characterization of Adsorbents

4.2.1 Morphology of Activated Carbon

SEM micrographs of activated carbons are shown in Fig. 4.1. The size of Norit_1240 powder is about 200-400 micrometers in diameter and the surface of Norit_1240 is heterogeneous. The frameworks of PF800 are composed of aggregates of homogeneous spherical particles, shown in micrograph C. The size of PF800 particles is about 40 micrometers.

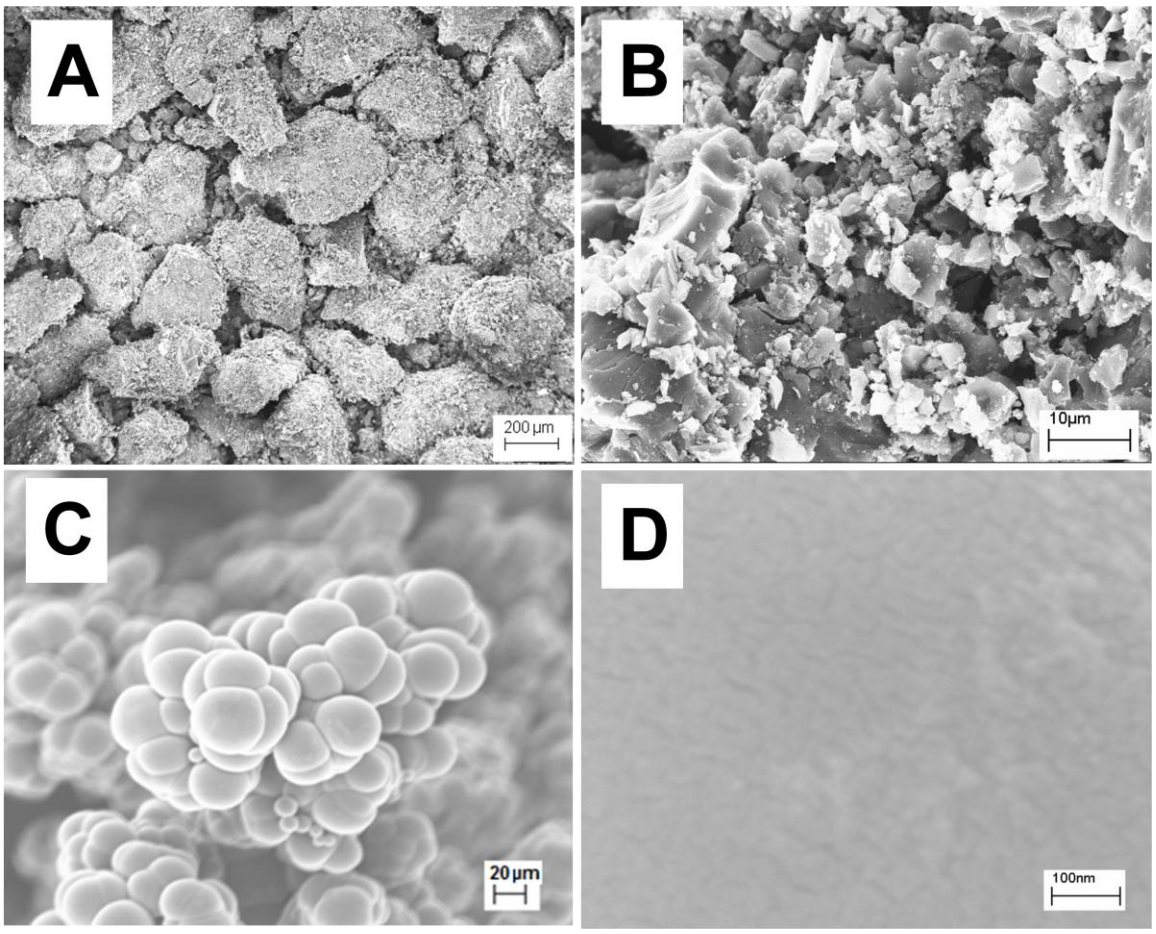

Figure 4.1 SEM of commercial activated carbon Norit_1240 (A, B), and polymer-derived carbon PF800 (C, D).

4.2.2 Porosity and Surface Area of Activated Carbon

Fig.4.2 shows the nitrogen adsorption-desorption isotherms on Norit_1240. The isotherms take up a shape resembling a combination of type I and type II isotherm, according to the classification by International Union of Pure and Applied Chemistry (IUPAC). Adsorption at low relative pressure increases steeply, suggesting the presence of a large amount of micropores. Isotherms show an inflection in the region of $p/p^o > 0.1$, and at high relative pressure, $p/p^o > 0.8$, where extents of adsorption rise very rapidly. Such isotherms are characteristic of adsorption on open surfaces with multilayer formation (condensation) occurring in the final stages of the process. Also, type II isotherms describe adsorption in mixed situations of micropores and exteranl surfaces. Additionally, the hysteresis loop of desorption became pronounced. These observations suggest the mesopore content of the adsorbent. In addition to the isotherms shown in Fig. 4.2a, the representation in a logarithmic scale of the relative pressures in Fig.4.2b allows a clear understanding of the adsorption occurring at low relative pressures.

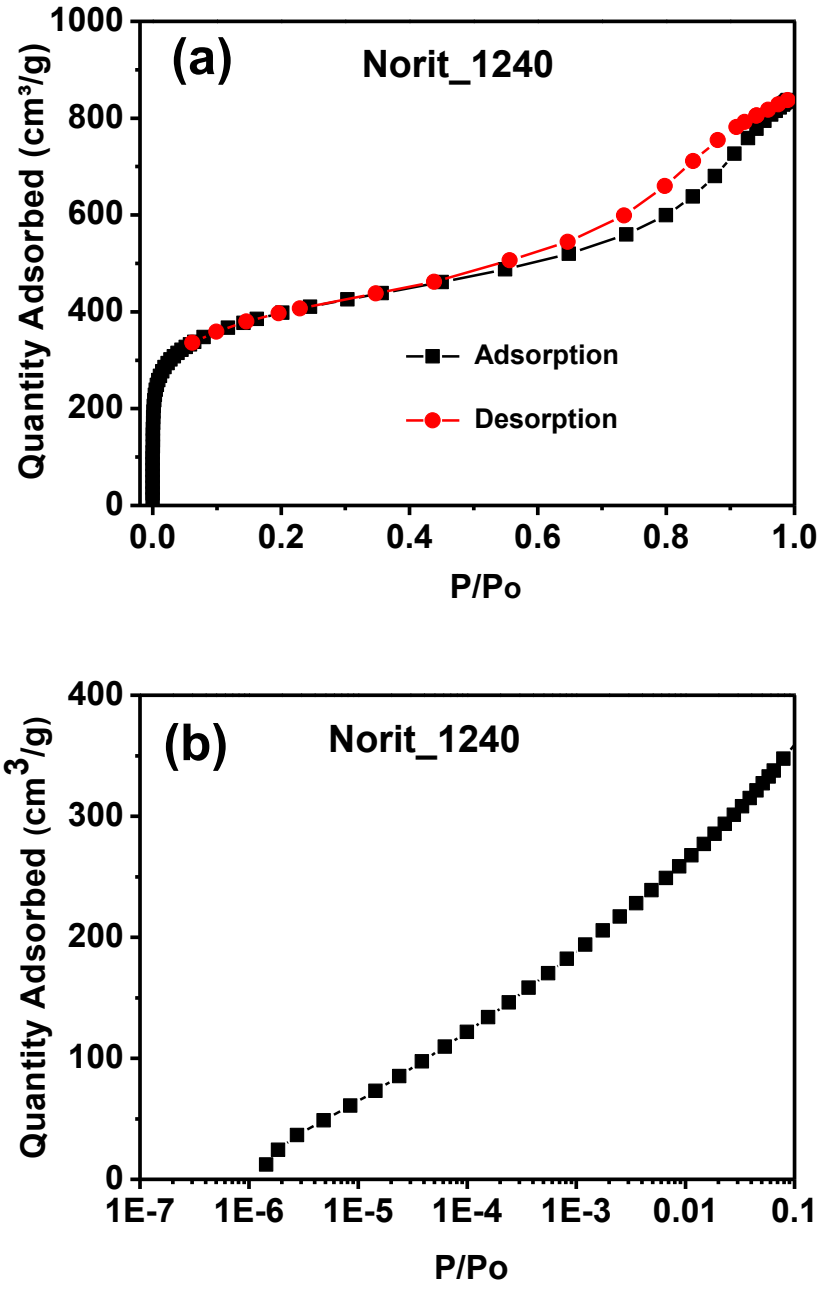

Figure 4.2 Nitrogen adsorption isotherm on Norit_1240 at 77 K: (a) linear scale; (b) logarithmic scale.

Fig. 4.3 presents experimental adsorption isotherms of nitrogen on the samples of PF800 at 77 K. The shape of the isotherms is of type I with a plateau that is almost horizontal and parallel to the pressure axis. The major uptake occurs at low relative pressures (less than 0.1), and the adsorption at higher relative pressures is small. The fact that the adsorption does not increase continuously but attains a limiting value shown by the plateau is due to the pores being so narrow that they cannot accommodate more that a single molecular layer. This is indicative of highly microporous materials with a narrow pore size distribution (pore diameters are relatively uniform).The sharp uptake indicates the presence of the stronger interaction of a nitrogen molecule with the pore wall. The desorption hysteresis loops due to capillary condensation in mesopores are not very obvious, indicating that the samples hardly possess mesopores.

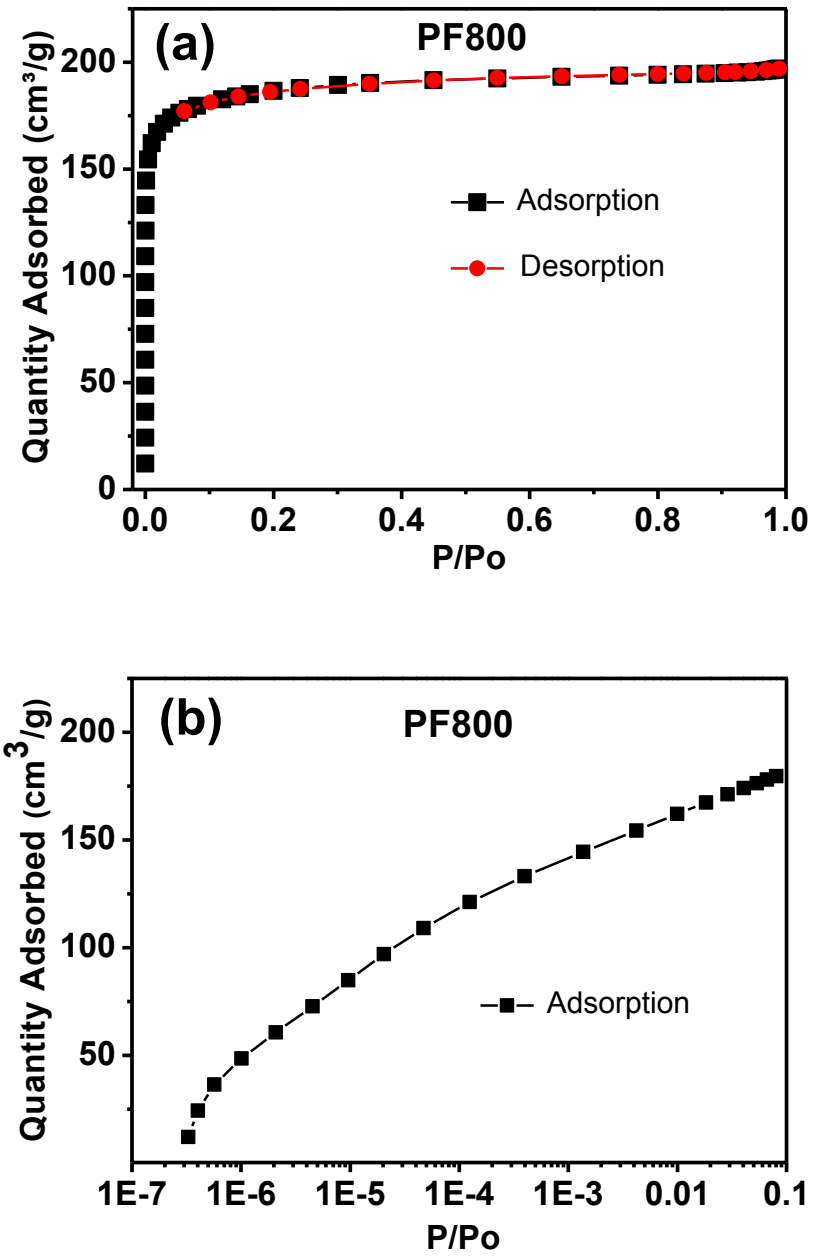

Figure 4.3 Nitrogen adsorption isotherm on PF800 at 77 K: (a) linear scale; (b) logarithmic scale.

The pore size distribution of activated carbons was determined by using Density functional theory (DFT). Fig. 4.4 depicts micropore size distributions for carbon samples. Micropores of PF800 were concentrated in the 0.8 to 1 nm width range. For the commercial Norit_1240, the pore size distributions were broader and less uniform than those of PF800. Micropores of Norit_1240 were concentrated in the 1.5 to 1.7 nm width range. However, Norit_1240 exhibits small peaks at pore width larger than 2 nm, indicating incipient mesoporosity.

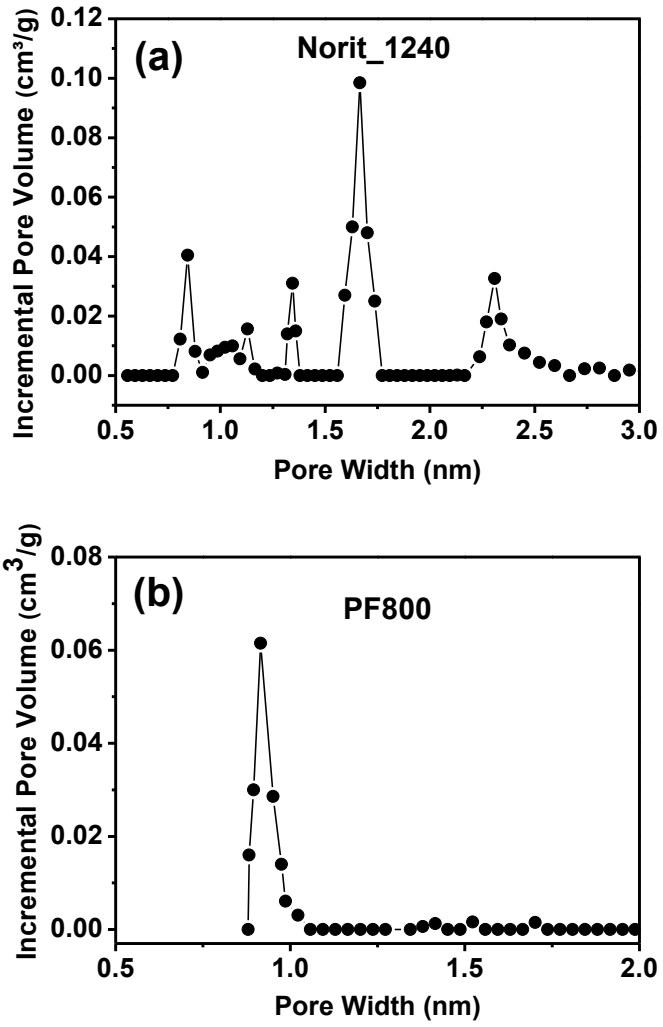

Figure 4.4 Pore size distribution of activated carbon by density functional theory (DFT) [1]: (a) Norit_1240; (b) PF800

Table 4.1 Porosity parameters of activated carbons calculated from nitrogen adsorption isotherms. S_{BET}: BET surface area; S_{me}: mesopore surface area; V_{mi}: micropore volume; V_{tot}: total volume; V_{me}: mesopore volume; d: average pore diameter.

Sample ID	S_{BET} (m^2/g)	S_{me} (m^2/g)	V_{mi} (cm^3/g)	V_{tot} (cm^3/g)	V_{me} (cm^3/g)	V_{me}/V_{tot} (%)	d (nm)
PF800	735	75	0.283	0.294	0.011	3.7	0.92
Norit_1240	1556	435	0.551	0.81	0.259	31.9	1.76

Table 4.1 lists the porosity parameters of the carbon samples calculated according to the BET equation, the t-plot, and the BJH method from the nitrogen adsorption and desorption isotherms at 77 K [2]. Both carbon samples exhibit high BET surface area. The mesopore surface area and mesopore volume of PF800 are very small. As a result, the mesoporosity (the percentage of mesopore to total pore volume, V_{me}/V_{tot}) of PF800 is only 3.7%. For the commercial carbon, the mesopore surface area and mesopore volume are much larger, and the mesoporosity is 31.9%. The average pore diameter of Norit_1240 is 1.76 nm, almost two times higher than that of PF800.

4.2.3 Chemical Structure of Activated Carbon Surface

The XPS survey spectra of the investigated carbons indicate the presence of two distinct peaks due to carbon and oxygen (Fig. 4.5). The O1s spectra (530-538ev) reveal the presence of oxygen functionalities, such as carbonyl and carboxyl groups, on the carbon samples [3, 4]. The intensity of the oxygen peak indicates the entire amount of associated oxygen on the carbon surface. The oxygen content of sample PF800 is 0.5%, i.e., much lower than 5% as in the sample Norit_1240. Pure carbon is hydrophobic in character. The hydrophobicity decreases, and the carbon becomes more hydrophilic, as

the amount of oxygen associated with the carbon surface increases. Therefore, the carbon samples with various oxygen content could perform differently in the adsorption tests.

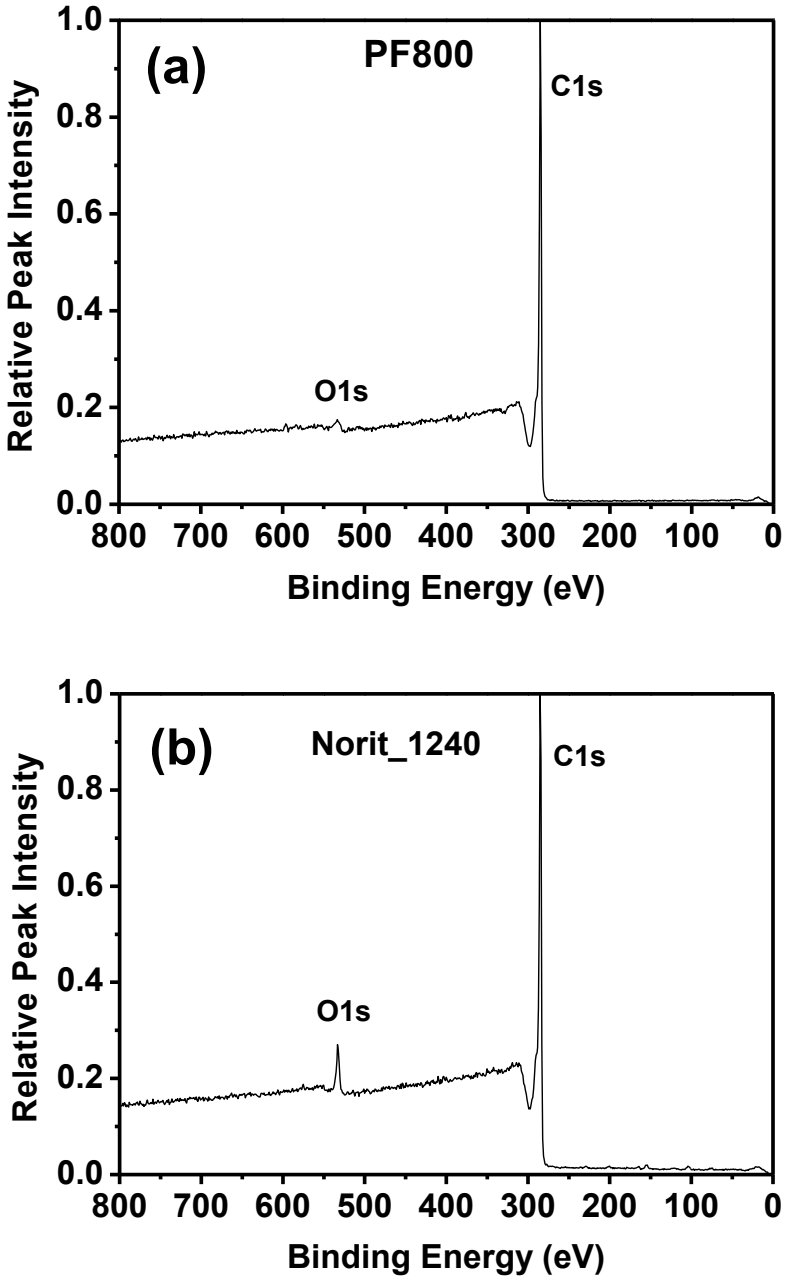

Figure 4.5 Chemical composition of activated carbon surface by XPS: (a) PF800; (b) Norit_1240.

4.3 Analytical Methods for Furfural Compounds and Monosaccharides

4.3.1 Calibration Curves for Furfural and HMF

The furfural and HMF in the aqueous solution were analyzed by using UV-spectrophotometer. A standard solution of the furfural was scanned to determine the wavelength (λ_{max}) corresponding to maximum absorbance. The wavelength corresponding to maximum absorbance was 278 nm, as shown in Fig. 4.6a. By using this wavelength a standard graph of absorbance versus concentration of furfural was prepared in Fig. 4.6b. This graph showed a linear variation up to 10 ppm. Therefore, the samples with higher concentration of furfural (10 ppm) were diluted with distilled water, whenever necessary, to make the concentration less than 10 ppm, for the accurate determination of the furfural concentration. It was observed that both glucose and xylose had no influence on UV spectra of the furfural solution, i.e., the wavelength and absorbance of furfural did not change with the addition of glucose and xylose.

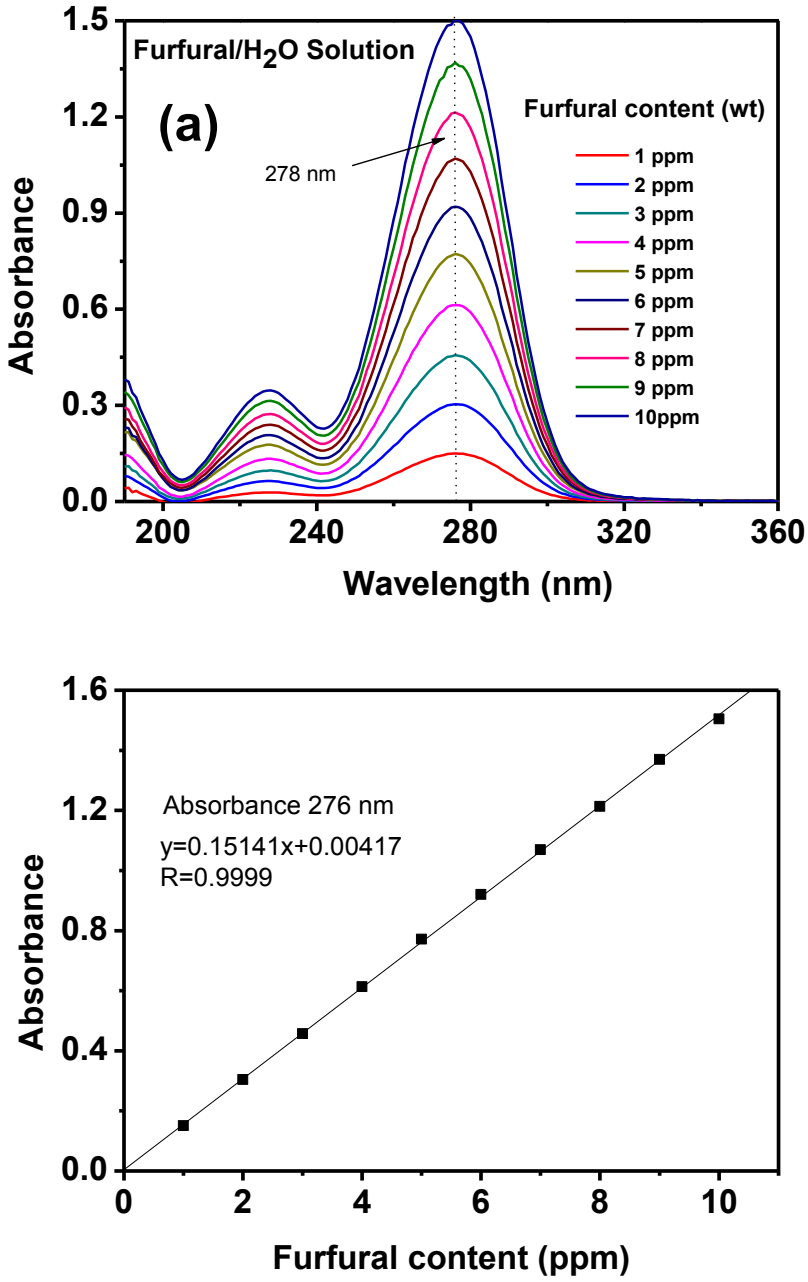

Figure 4.6 UV-spectrum analysis of furfural in water solution: (a) UV absorption; (b) calibration curve.

Similarly, HMF has a maximum absorption at 284 nm in UV-spectrum, as shown in Fig. 4.7a. Good linearity was also observed between the absorbance and HMF

concentration up to a HMF concentration of 10 ppm. The calibration curve was used to calculate the concentration of HMF before and after adsorption tests.

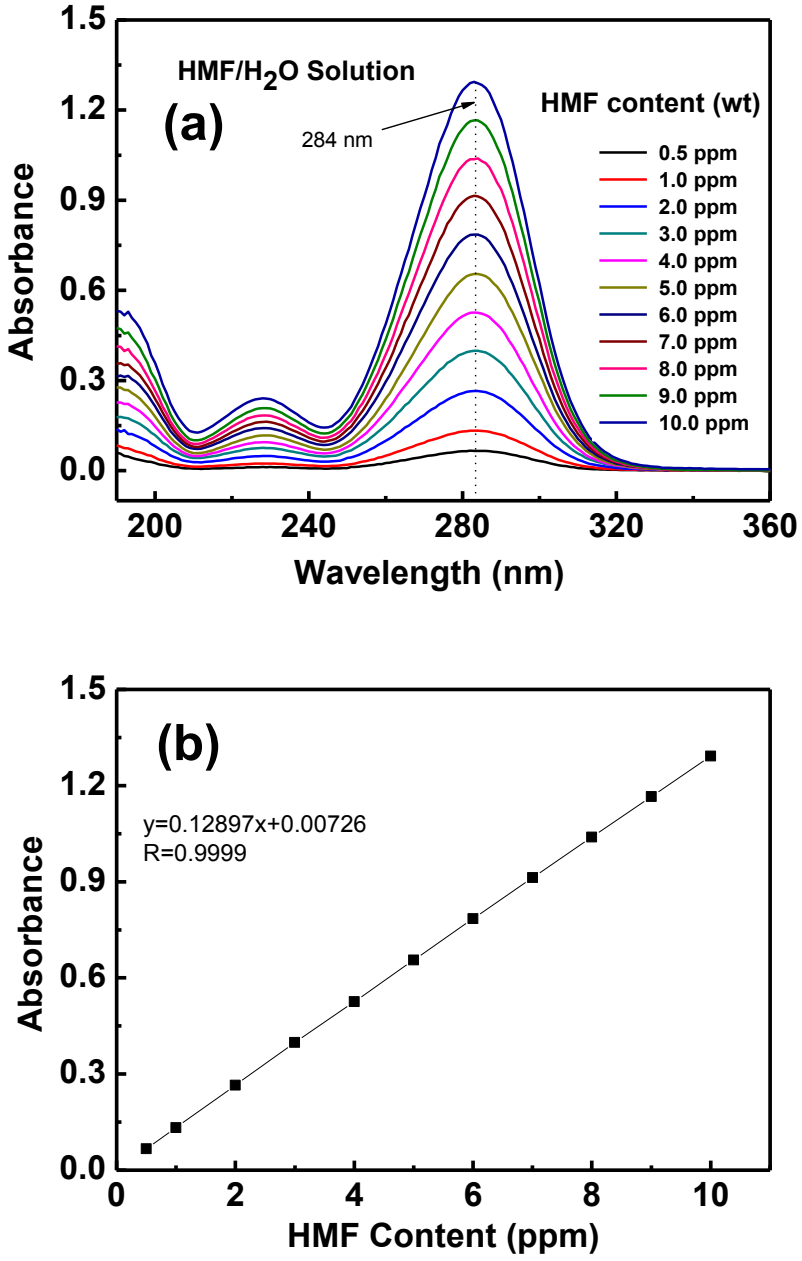

Figure 4.7 UV-spectrum analysis of HMF in water solution: (a) UV absorption; (b) calibration curve.

4.3.2 Calibration Curves for Monosaccharides

In the adsorption tests, glucose and xylose were analyzed by High-performance anion exchange chromatography (HPAEC**)**. The calibration curves between sugar concentration and the area (nRIU*s) were then plotted. Calibration curves with good linearity are shown in Fig.4.8. Concentrations of glucose and xylose were calculated from calibration curves.

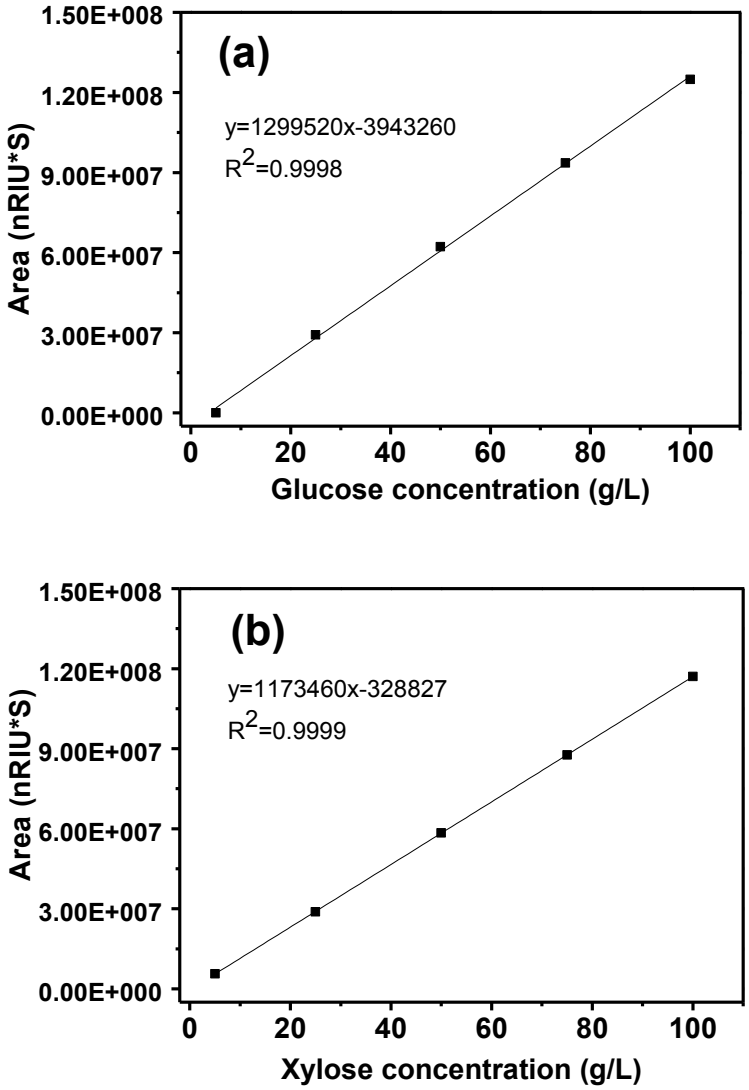

Figure 4.8 Calibration curves of monosaccharide in water solution by HPAEC analysis: (a) glucose; (b) xylose.

4.4 Batch Adsorption Tests

4.4.1 Equilibrium Time

During the adsorption batch tests for determining equilibrium time, the aqueous samples were taken at preset time intervals, and the concentration of furfural was measured. The amount of adsorption at time *t*, q_t (mg/g), was calculated by:

$$q_t = \frac{(C_o - C_t)V}{M} \qquad (4\text{-}1)$$

where C_o is the initial concentration of furfural in solution (mg/L). C_t (mg/L) is the liquid-phase concentrations of furfural at any time *t*. *V* is the volume of the solution, and *M* is the mass of dry adsorbent used (g).

As can be seen from Fig. 4.9, the amount of the adsorbed furfural onto activated carbons increases with time and, at some point in time, reaches a constant value beyond which no more is removed from solution. At this point, the amount of the furfural desorbing from the activated carbons is in a state of dynamic equilibrium with the amount of the furfural being adsorbed onto the activated carbons. The time required to attain this state of equilibrium is termed the equilibrium time, and the amount of furfural adsorbed at the equilibrium time reflects the maximum adsorption capacity of the adsorbent under those operating conditions. The equilibrium time of adsorption of furfural on PF800 is 40 s. For Norit_1240, the equilibrium time is 120 s.

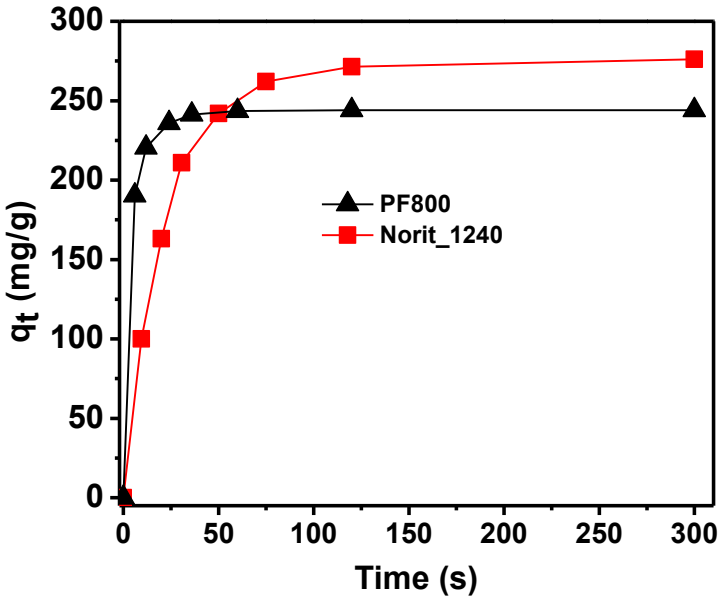

Figure 4.9 Equilibrium time of activated carbons in the adsorption batch tests. (at 25 ^{o}C)

4.4.2 Adsorption Isotherms

PF800 and Norit_1240 were tested for adsorption isotherms for furfural in batch tests. The amount of adsorption at equilibrium, q_e (mg/g), was calculated using the following equation:

$$q_e = \frac{(C_o - C_e)V}{M} \qquad (4\text{-}2)$$

where C_o and C_e are initial and equilibrium concentration of furfural in solution (mg/L). V is the volume of the solution, and M is the mass of dry adsorbent used (g).

Under equilibrium conditions, the furfural content in adsorbent and in residual solution is shown in Fig. 4.10. Both PF800 and Norit_1240 demonstrate large sorption capacity of furfural. But PF800 shows large sorption capacity even at low furfural concentration. This indicates good affinity between PF800 and furfural.

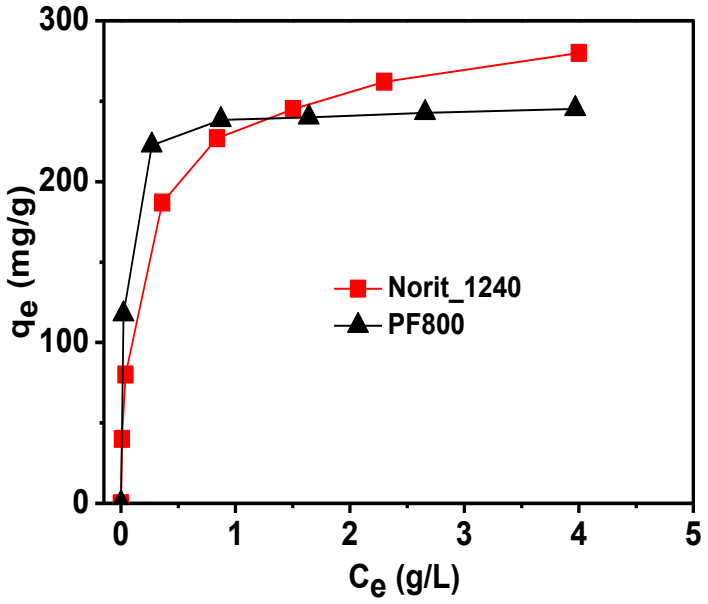

Figure 4.10 Adsorption isotherms of activated carbons for furfural in the adsorption batch tests.

The adsorption isotherm indicates how the adsorption molecules distribute between the liquid phase and the solid phase when the adsorption process reaches an equilibrium state. Adsorption isotherm is basically important to describe how solutes interact with adsorbents, and is critical in optimizing the use of adsorbents.

Adsorption isotherms of activated carbons were fitted to two well-known isotherms, Langmuir and Freundlich [5, 6]. Langmuir isotherm assumes monolayer adsorption onto a surface containing a finite number of adsorption sites of uniform strategies of adsorption with no transmigration of adsorbate in the plane of surface. Freundlich isotherm model assumes heterogeneous surface. We tried to use the two isotherm equations given by Freundlich and Langmuir to fit the experimental data for furfural on carbon.

The form of Langmuir's isotherm model is given by the following equation:

$$q_e = \frac{q_m K_L C_e}{1 + K_L C_e} \qquad (4\text{-}3)$$

where q_e is the amount adsorbed at equilibrium (mg/g), C_e is the equilibrium concentration of the adsorbate (furfural)(mg/l). q_m and K_L are Langmuir constants related to adsorption capacity and rate of adsorption, respectively.

Freundlich model is given by the following equation:

$$q_e = K_F C_e^{\frac{1}{n}} \qquad (4\text{-}4)$$

where q_e is the amount adsorbed at equilibrium (mg/g), C_e is the equilibrium concentration of the adsorbate. K_F and n are Freundlich constants, n giving an indication of how favorable the adsorption process and K_F ((mg/g)/(L/mg)$^{1/n}$) is related to the adsorption capacity of the adsorbent. The slope $1/n$ is a measure of adsorption intensity or surface heterogeneity, becoming more heterogeneous as its value gets closer to zero [7].

The isotherm constants and the correlation coefficient (R^2) with the experimental data are listed in Table 4.2. The correlation coefficient (R^2) was employed in this study to find out the suitable isotherm model to represent the experimental data [8]. For PF800, the R^2 value for Langmuir isotherm is closer to unity in comparison to the value obtained for Freudlich isotherm. Therefore, Langmuir isotherm is the suitable isotherm equation for the adsorption of furfural on PF800. The results demonstrate the formation of monolayer coverage of furfural molecule on the surface of PF800. For Norit_1240, Freudlich isotherm is the suitable isotherm equation for the adsorption of furfural, since the R^2 value for Freudlich isotherm is closer to unity than Langmuir. This indicates the

heterogeneous surfaces of Norit_1240. Fig. 4.11 and Fig. 4.12 present how well the individual isotherm fit the data for PF800 and Norit_1240, respectively.

Table 4.2 Isotherm parameters for the removal of furfural by PF800 and Norit_1240 (at 25 ℃).

Langmuir $q_e = \frac{q_m K_L C_e}{1 + K_L C_e}$			
	K_L(L/mg)	**q_m (mg/g)**	**R^2**
PF800	**41.6**	**245**	**0.9997**
Norit_1240	**20.6**	**272**	**0.9272**
Freundlich $q_e = K_F C_e^{1/n}$			
	K_F ((mg/g)/(L/mg)$^{1/n}$)	**1/n**	**R^2**
PF800	**189**	**0.307**	**0.9476**
Norit_1240	**224**	**0.113**	**0.9985**

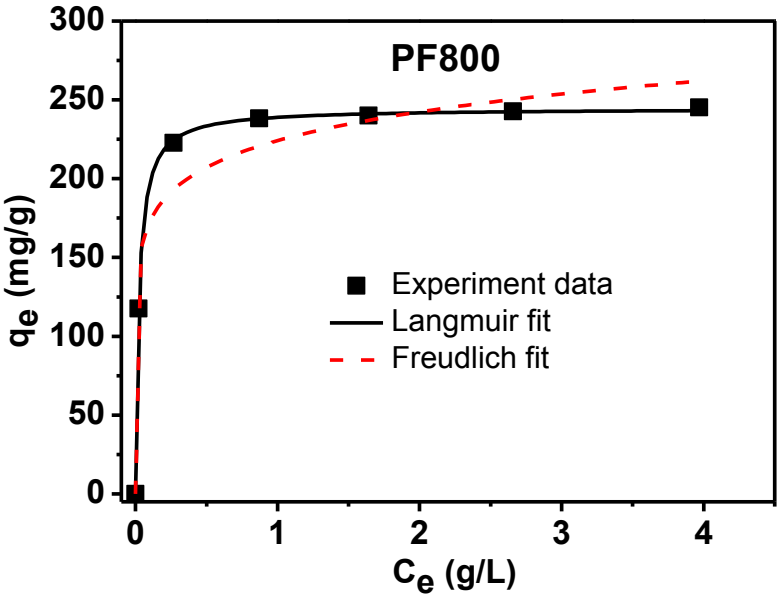

Figure 4.11 Equilibrium adsorption isotherm of furfural on PF800 (at 25 ℃).

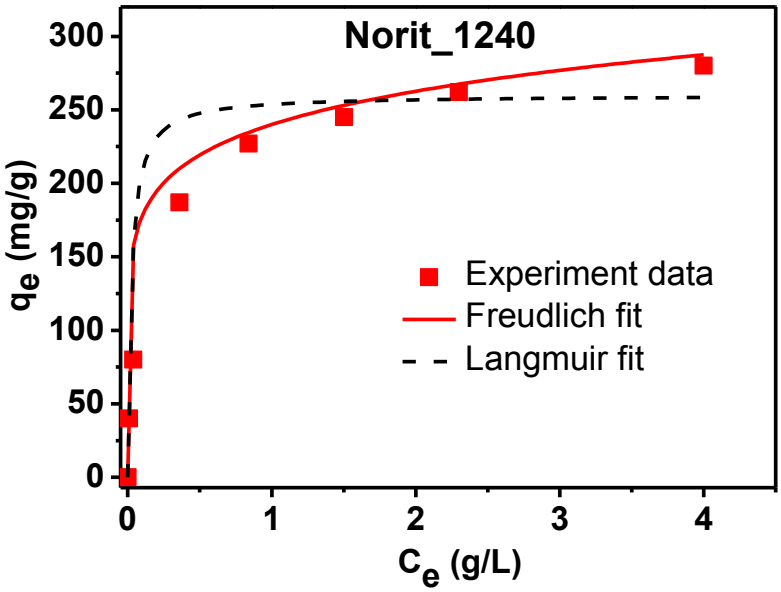

Figure 4.12 Equilibrium adsorption isotherm of furfural on Norit_1240 (at 25 ℃).

4.4.3 Adsorption Kinetics

Two kinetic models, pseudo-first-order and pseudo-second-order models, were used to investigate the adsorption process of furfural on activated carbons. The procedures of kinetic experiments were basically identical to those of equilibrium tests. The rate constant of adsorption was determined from the pseudo first-order equation given by Langergren and Svenska [9]:

$$\ln(q_e - q_t) = \ln q_e - k_1 t \qquad (4\text{-}5)$$

where q_e and q_t are the amounts of furfural adsorbed (mg/g) at equilibrium and at time t, respectively, and k_1 the rate constant adsorption (S^{-1}). Values of k_1 were calculated from the plots of $\ln(q_e - q_t)$ versus t (Fig. 4.13). The experimental q_e values do not agree with the linear fit. This shows that the adsorption of furfural onto activated carbon is not a first-order kinetic.

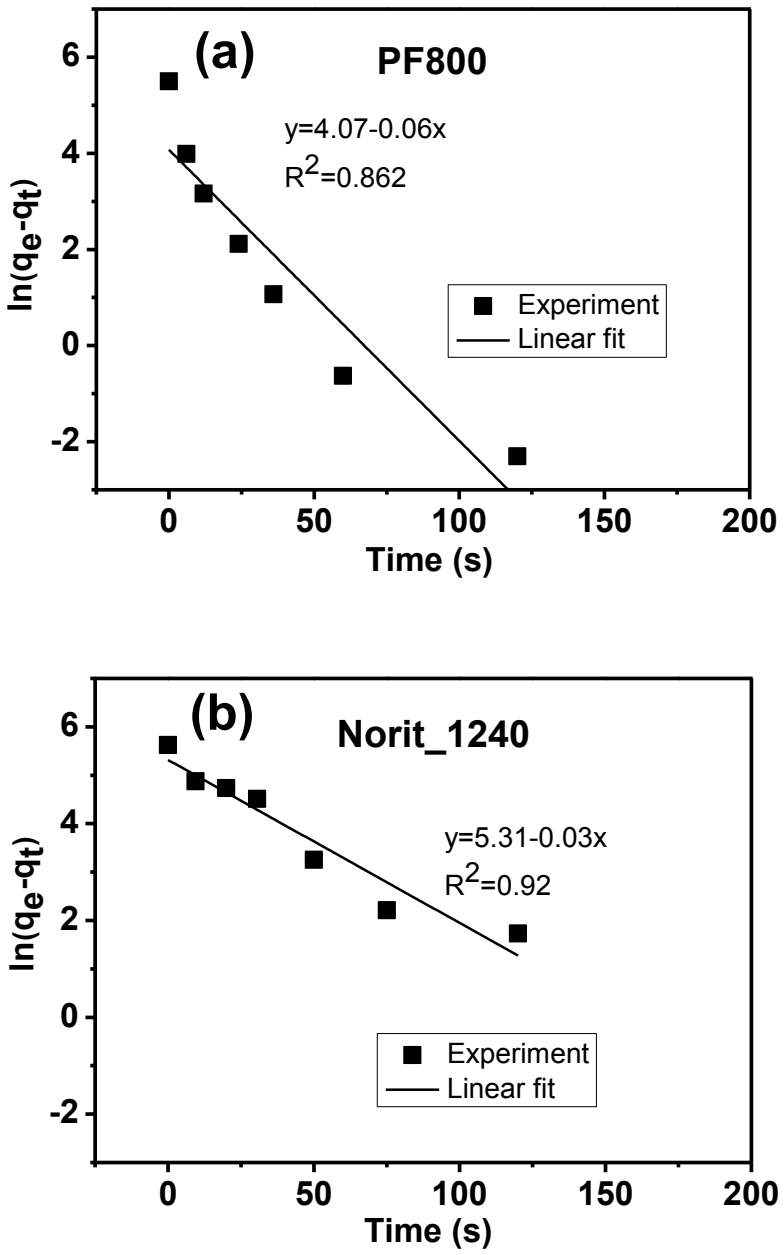

Figure 4.13 Pseudo-first-order kinetics for adsorption of furfural by activated carbons: (a) PF800; (b) Norit_1240 (at 25 ℃).

On the other hand, a pseudo second-order equation based on equilibrium adsorption [10] is expressed as:

$$\frac{t}{q_t} = \frac{1}{q_e} t + \frac{1}{k_2 q_e^2} \qquad (4\text{-}6)$$

where k_2 (g/mg h) is the rates constant of second-order adsorption. If second-order kinetics is applicable, the plot of t/q versus t should show a linear relationship. The linear plots of t/q versus t show a good agreement between experimental and the linear fit. The correlation coefficients for the second-order kinetic model are greater than 0.99 indicating the applicability of this kinetic equation and the second-order nature of the adsorption process of furfural on activated carbon.

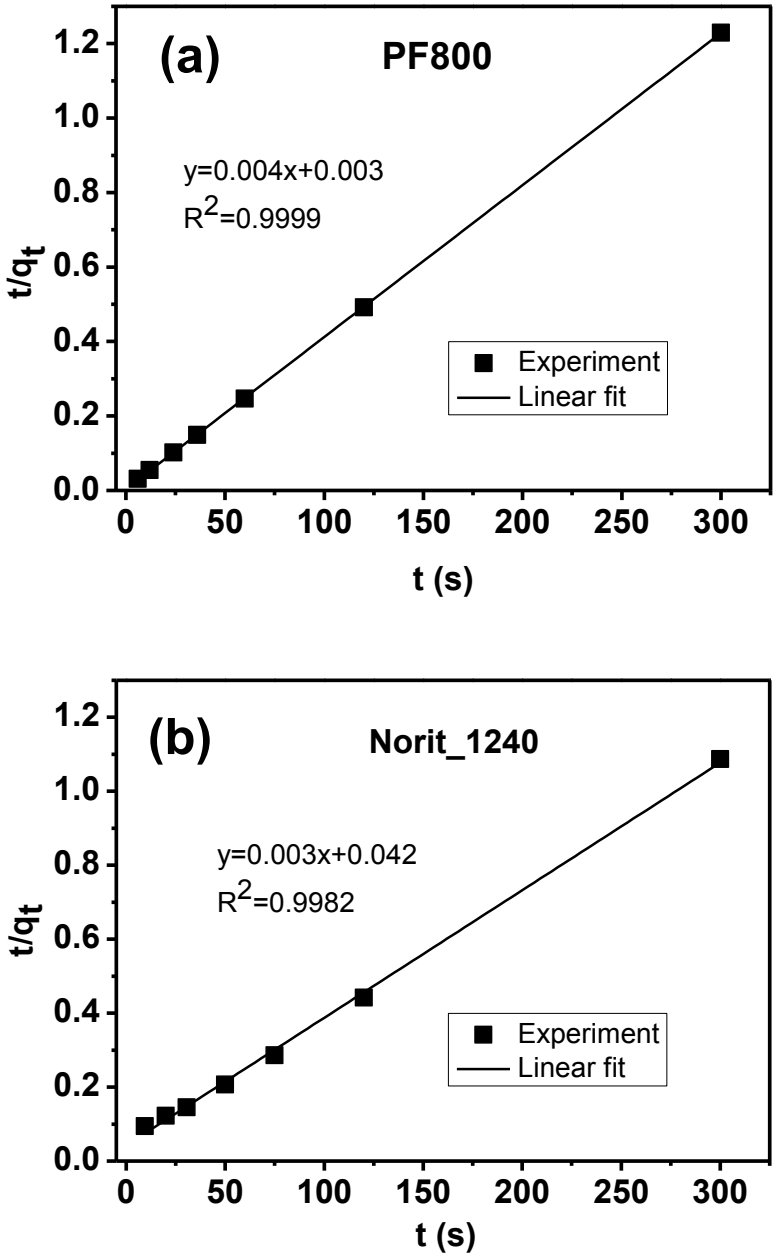

Figure 4.14 Pseudo-second-order kinetics for adsorption of furfural by activated carbons: (a) PF800; (b) Norit_1240 (at 25 ℃).

To determine the diffusivity in the adsorption process, Kinetic data could be treated by models given by Boyd et al. [11], which is valid under the experimental conditions used. With diffusion rate controlling in the adsorption on particles of spherical shape, Vermeulen's approximation [12] was applied and lead to calculation of effective particle diffusivity by the following equation:

$$\ln[\frac{1}{(1-F^2(t))}] = \frac{\pi^2 D_e t}{R_a^2} \qquad (4\text{-}7)$$

where $F(t) = q_t/q_e$ is the fractional attainment of equilibrium at time t, De is the effective diffusion coefficient of adsorbates in the adsorbent phase (m^2/s), Ra is radius of the adsorbent particle assumed to be spherical (m), and t is the time (s).

De was determined from the slope of the plot of $ln\ [1/(1-F^2(t))]$ versus t, as shown in Fig. 4.15. Value of De is 0.824×10^{-11} and 1.19×10^{-10} m^2/s, respectively, for furfural adsorption on PF800 and Norit_1240. The higher pore diffusion rate of Norit_1240 is due to the larger pore size; however, since the particle size of PF800 is much smaller than Norit_1240, the equilibrium time of PF800 is still faster than Norit_1240.

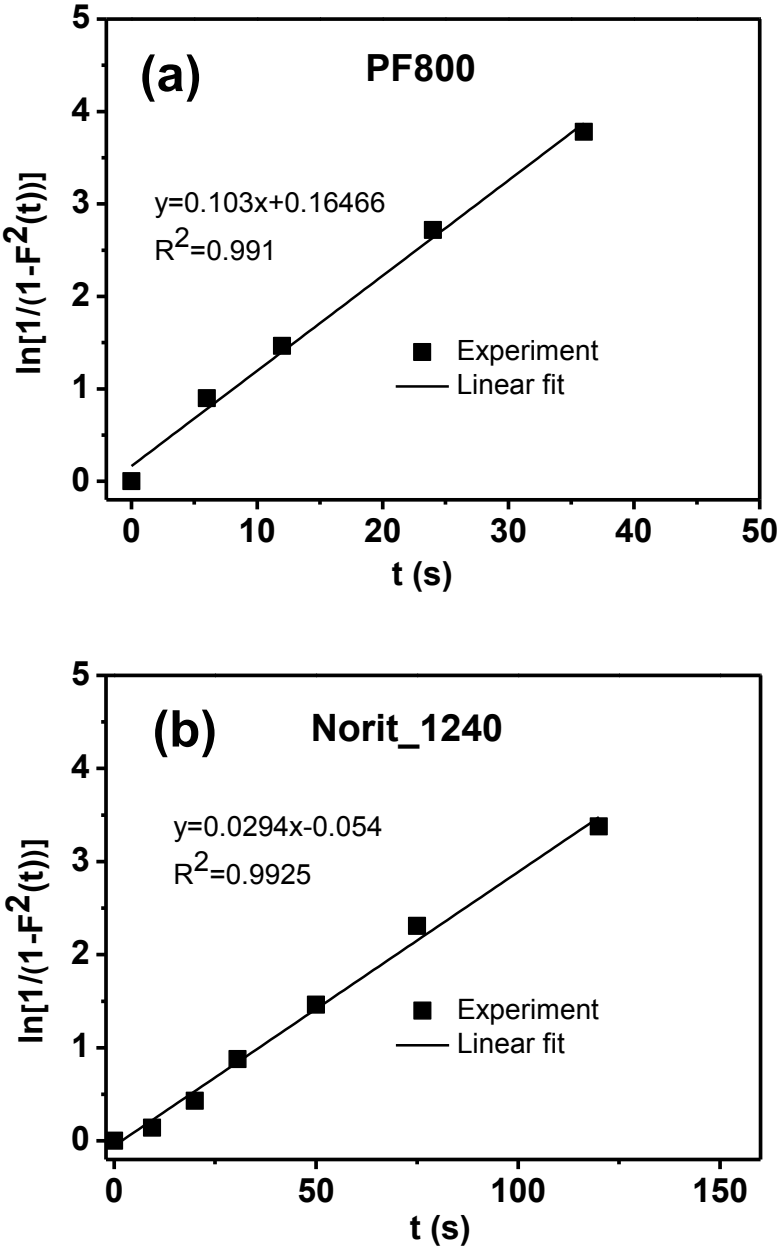

Figure 4.15 Determination of the diffusivity of furfural in the adsorption process: (a) PF800; (b) Norit_1240.

4.4.4 The Effect of Particle Size

The effect of the particle size on adsorption kinetics of furfural on activated carbon was investigated at room temperature, as it is directly connected with intra-particle diffusion. Norit_1240_G is granular with about 1 millimeter radius. Norit_1240 was crushed from Norit_1240_G and screened to particle size of 200 micrometers radius. The effect of the adsorbent particle size on the adsorption of furfural onto Norit carbons are shown in Fig. 4.16 .

Fig. 4.16 reveals that the adsorption rate (dq_t/dt) decreases with time until it gradually approaches the equilibrium state due to the continuous decease in the driving force $(q_e - q_t)$. It also demonstrates that the adsorbate uptake q_t decreases with increasing adsorbent. The equilibrium time is 2 min and 30 min for Norit_1240 and Norit_1240_G, respectively.

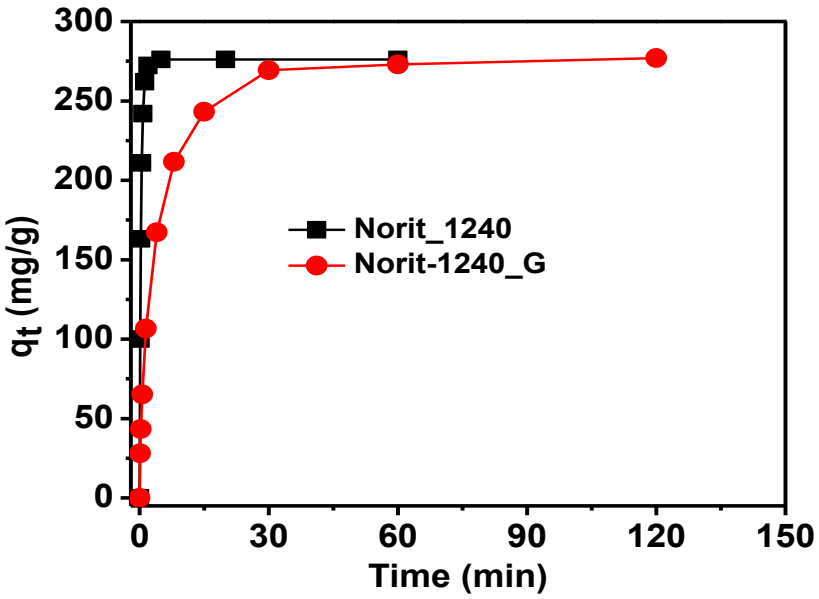

Figure 4.16 The effect of particle size on the equilibrium time of adsorption of furfural on activated carbons at room temperature.

Even though the effect of the particle size on adsorption kinetics is obvious, the effect of the particle size on adsorption isotherm is negligible, as shown in Fig. 4.17. The adsorption isotherm is strongly influenced by the porous structure and chemical structure of the adsorbent. Norit_1240 and Norit_1240_G have the same porous structure and chemical structure. Therefore they exhibit similar isotherms.

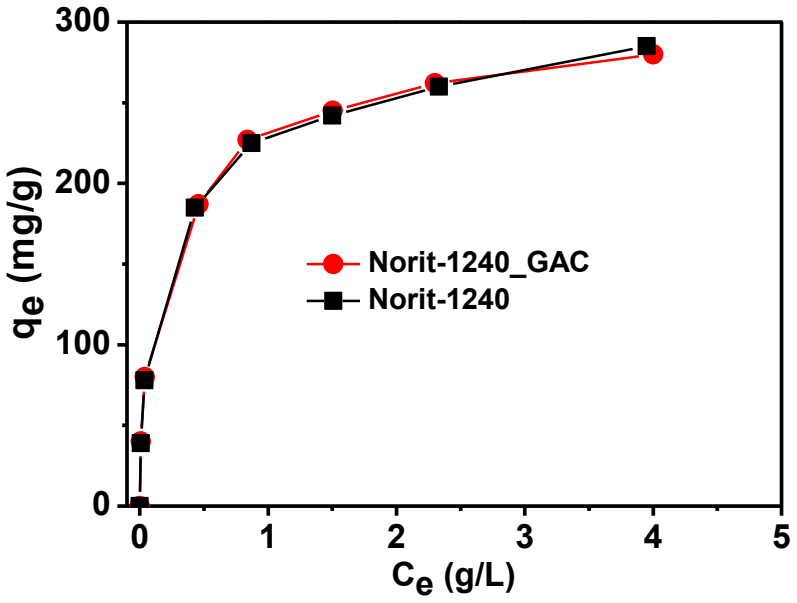

Figure 4.17 The effect of the particle size on adsorption isotherm of furfural on activated carbons at room temperature.

4.4.5 Selectivity of the Adsorption

4.4.5.1 Selectivity between Furfural and Monosaccharides

The separation of furfural from sugar containing liquid by activated carbon involves a competitive adsorption process between furfural and sugars. Selectivity ($\alpha_{f/s}$) between furfural and sugar is an important factor in the performance of adsorbents. The equilibrium selectivity ($\alpha_{f/s}$) is defined as the ratio of the distribution coefficient of furfural and sugar, as expressed in the following equation:

$$\alpha_{f/s} = \frac{K_f}{K_s} = \frac{C_{fc} / C_{fs}}{C_{sc} / C_{ss}} \qquad (4\text{-}8)$$

Where and C_{fc} and C_{fs} are the equilibrium concentration of furfural in the carbon and in the solution, respectively. C_{sc} and C_{ss} are the the equilibrium concentration of sugar in the carbon and in the solution, respectively.

Higher $\alpha_{f/s}$ indicates higher priority of adsorption of furfural over sugar. The oxygen functional groups on the carbon surface, such as carbonyls and carboxyls, exercise a profound influence on the surface chemistry and surface properties of activated carbon. Oxygen groups tend to increase hydrophilicity of carbon surface, making the carbon adsorb more hydrophilic sugar, rather than hydrophobic furfural, in the aqueous solution. Therefore, a low $\alpha_{f/s}$ is observed with increasing surface oxygen content. Accordingly, Norit_1240 with 5% oxygen on the surface exhibits lower $\alpha_{f/s}$ (646), compared to PF800 with 1% oxygen and higher $\alpha_{f/s}$ (7321).

PF800: $$\alpha_{f/s} = \frac{K_f}{K_s} = \frac{C_{fc} / C_{fs}}{C_{sc} / C_{ss}} = \frac{4100}{0.56} = 7321$$

Norit-1240: $$\alpha_{f/s} = \frac{K_f}{K_s} = \frac{C_{fc} / C_{fs}}{C_{sc} / C_{ss}} = \frac{4200}{6.5} = 646$$

To investigate the adsorption of monosaccharides on activated carbons, adsorption tests were conducted when the solution contains only glucose and xylose. Fig. 4.18 reveals change of the monosaccharide content in the solution before and after the adsorption tests of activated carbons. For PF800, the overlapping of two peaks in Fig. 4.18a indicates the adsorption of sugars on PF800 is negligible. But a clear adsorption of sugars on Norit_1240 was observed, as shown in Fig. 4.18b. The adsorption capacity of

Norit_1240 for monosaccharides can reach 125 mg/g. This implies the commercial carbon could adsorb sugars when the furfural content is reduced to a low level. The preliminary results of adsorption of oligosaccharides on activated carbon can be found in Appendix A.

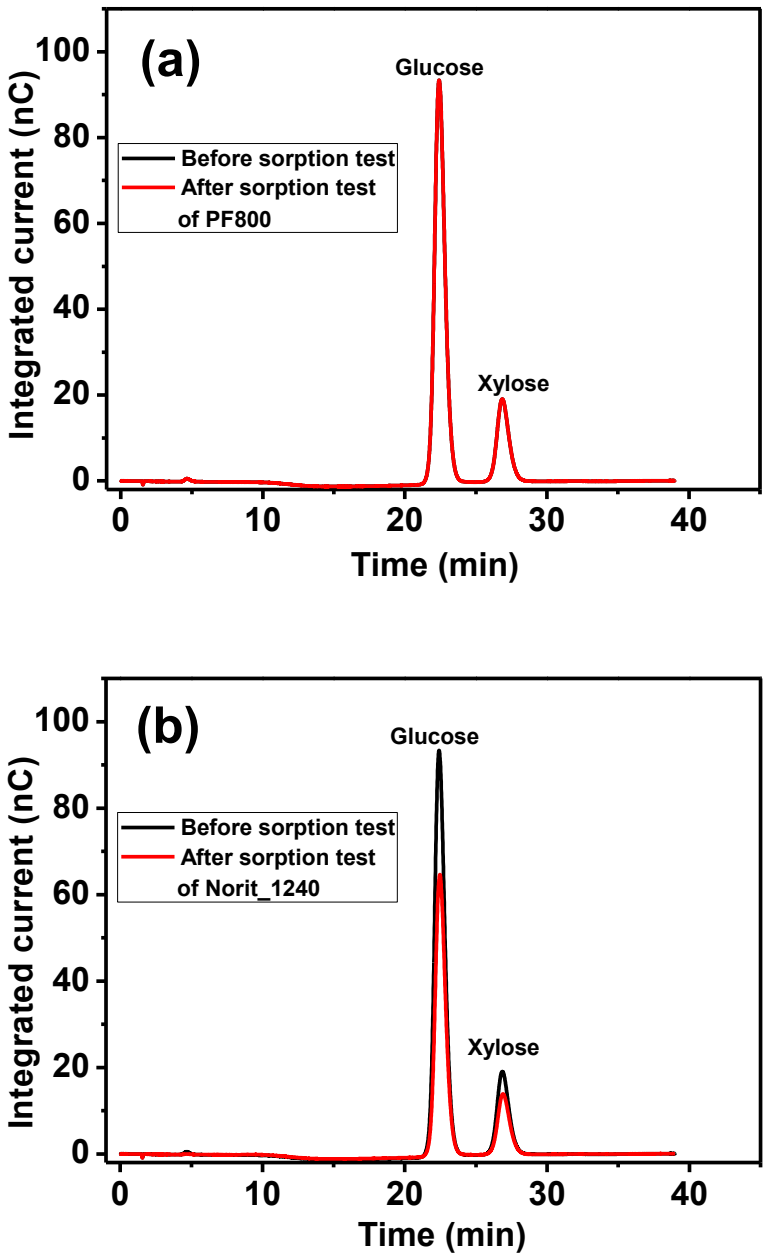

Figure 4.18 Monosaccharide analysis by HPAEC before and after adsorption tests on the solution containing only glucose and xylose: (a) PF800; (b) Norit_1240.

4.4.5.2 The Effect of Chemical Structure of Carbon Surface on Selectivity

To further investigate the effect of carbon surface oxygen groups on the adsorption process, a known amount of commercial carbon (Norit-1240) and polymer-derived carbon (PF800) were oxidized using 60 wt% nitric acid [13, 14]. After oxidation with nitric acid, the oxygen content increased clearly as expected on both modified carbon samples, PF800_HNO_3 and Norit_1240_HNO_3, respectively. No presence of peaks in the Nls regions (395-405ev) on the modified carbon indicates that the carbon samples were washed thoroughly after modification and no nitric acid remained on the samples, as shown in Fig. 4.19. The selectivity between furfural and sugars on other different commercial carbons are shown in Appendix B.

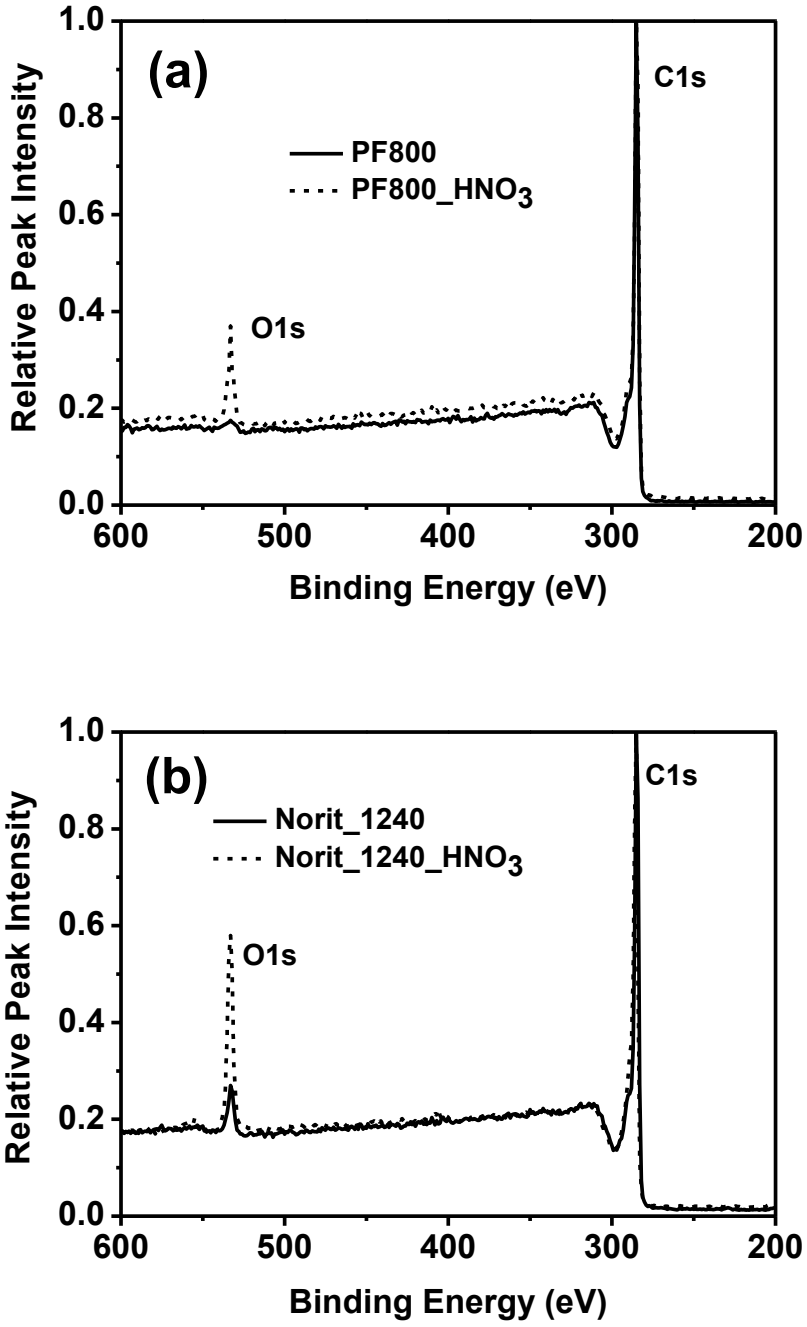

Figure 4.19 Chemical composition of activated carbon surface by XPS after oxidization using 60 wt% nitric acid: (a) PF800; (b) Norit_1240.

Table 4.3 Change of oxygen amount on the carbon surface after oxidization using 60 wt% nitric acid, and the consequent change of selectivity of activated carbons between furfural and sugars.

Carbon Sample	**Oxygen, wt%**	**$\alpha_{f/s}$**
Norit_1240	5%	646
Norit_1240_HNO_3	18%	120
PF800	0.5%	7321
PF800_HNO_3	8%	510

Table 4.3 shows that the total oxygen amount on the carbon surface increased clearly after oxidation for both carbons. A consequent change of selectivity of activated carbons between furfural and sugars was observed after oxidation. An increase of oxygen amount on the carbon surface results in a decrease of selectivity. Therefore, the chemical structure of carbon surface, oxygen functional groups in particular, can strongly affect the selectivity between the furfural and sugars.

Even though the $\alpha_{f/s}$ of Norit_1240 is not as high as PF800, it is still much higher than 1, which indicates Norit_1240 adsorbs furfural preferentially to sugar at the beginning. Only when furfural concentration drops to a low level, Norit_1240 starts to adsorb sugar as well. A further experiment showed that Norit_1240 did not adsorb sugar when there was 1 g/l furfural (and above) existing in the solution. But when the furfural concentration falls below 1 g/l, Norit_1240 started to adsorb sugars. In comparison, PF800 does not adsorb sugar because of much higher $\alpha_{f/s}$, even when there is only 0.1

g/L furfural remaining in the liquid. Thus, due to the difference of selectivity between Norit_1240 and PF800, the two sorbents can be used in two steps to optimally remove furfural from the water solution. The first step is to reduce furfural content from about 4 g/l, the original concentration after biomass pretreatment, to about 1g/l by using Norit_1240, because the commercial carbon does not adsorb sugar in this range of furfural concentration. The second step is to use PF800 to decrease the furfural content from about 1 g/l to about 0.1 g/L. As a consequence, the majority of furfural (about 75%) could be removed by the commercial carbon, thereby potentially reducing the cost of adsorbent in whole and increasing the efficiency, which would be a benefit in the industrial application.

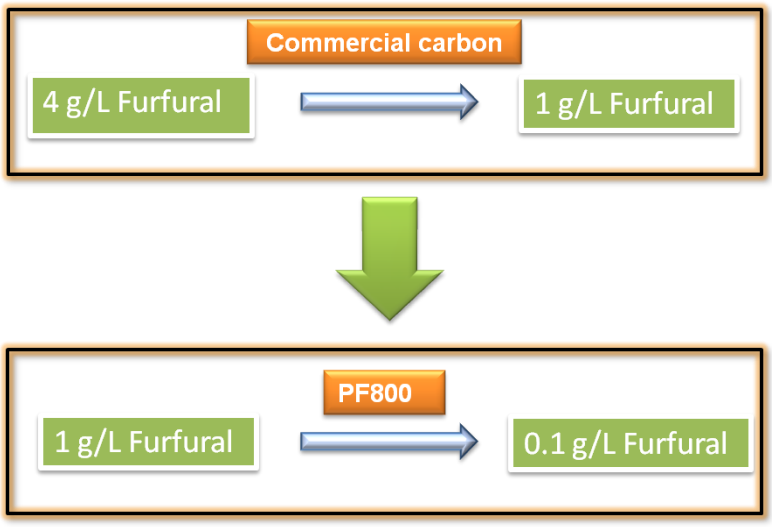

Figure 4.20 Economical and selective removal of furfural by two steps with less hydrophobic commercial carbon in the first step and highly hydrophobic polymer-derived carbon in the second step.

4.5 The Effect of Acetic Acid on the Adsorption of Furfural

After biomass pretreatment, there are components existing in the solution other than furfural compounds. Acetic acid is a common organic acid in the solution and its

concentration can be 5 wt% [15]. To investigate the effect of acetic acid on the adsorption of furfural on activated carbons, adsorption tests were performed with different chemical composition in the solution: (a) Furfural & HMF/glucose & xylose/H_2O; (b) Furfural & HMF/glucose & xylose/acetic acid/H_2O; and (c) solution (b) neutralized by aqueous ammonia.

Fig. 4.21 shows the UV-spectrum of furfural in the adsorption tests. In Fig. 4.21a, almost all furfural was removed after adsorption test with PF800. After adding 50 g/l acetic acid in the solution, the removal of furfural was clearly affected and part of furfural still remained in the solution after the test, as shown in Fig. 4.21b. This implies the acetic acid molecules could compete with furfural for the adsorption on the activated carbon, especially when the concentration of acetic acid is much higher than furfural. However, this negative effect of acetic acid on the adsorption of furfural could be eliminated by neutralizing the acid, which is indicated by the dashed line in Fig. 4.21c. After neutralization with aqueous ammonia, acetic acid became acetate, which is highly soluble in water solution. As a result, the interaction between water and acetate is much stronger than the interaction between activated carbon and acetate. Therefore acetate does not compete with furfural for the adsorption on the activated carbon. Ammonia was used to neutralize the acetic acid for the following two reasons: weak basicity and the potential nitrogen source for the microbes in the latter fermentation.

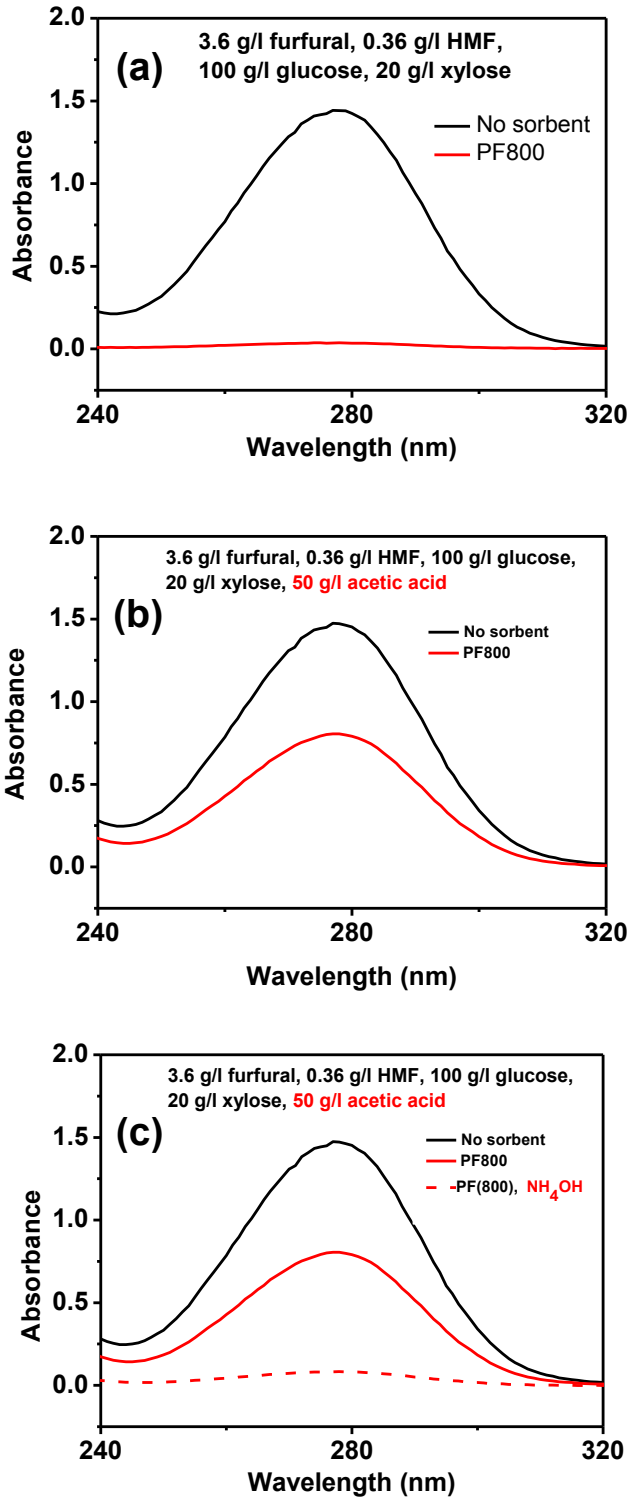

Figure 4.21 UV-spectrum of furfural in the adsorption tests with different chemical composition in the solution: (a) no acetic acid; (b) with 50 g/l acetic acid; and (c) neutralization of acetic acid with ammonia.

4.6 Adsorption Tests with True Biomass Hydrolytes

After the preliminary adsorption tests with model solutions mentioned above, adsorption tests with real feed after biomass pretreatment were performed. The feed was provided by Teresita from Dr. Jones group. Switchgrass was hydrolyzed by 8 wt% formic acid at 150 ^{o}C to produce monosaccharides [16]. After the pretreatment, 3.6 g/l furfrual & 0.36 g/l HMF were co-produced. After neutralizing the formic acid with aqueous ammonia, adsorption tests with this real feed were conducted using PF800 in the same condition as mentioned in Chapter 3.2.2. The concentrations of furfural & HMF in the solution were analyzed by UV method (Fig. 4.22), and by HPLC (Fig. 4.23). The results of two methods are consistent: after the neutralization of formic acid, most of furfural & HMF were removed from the solution after adsorption tests with PF800.

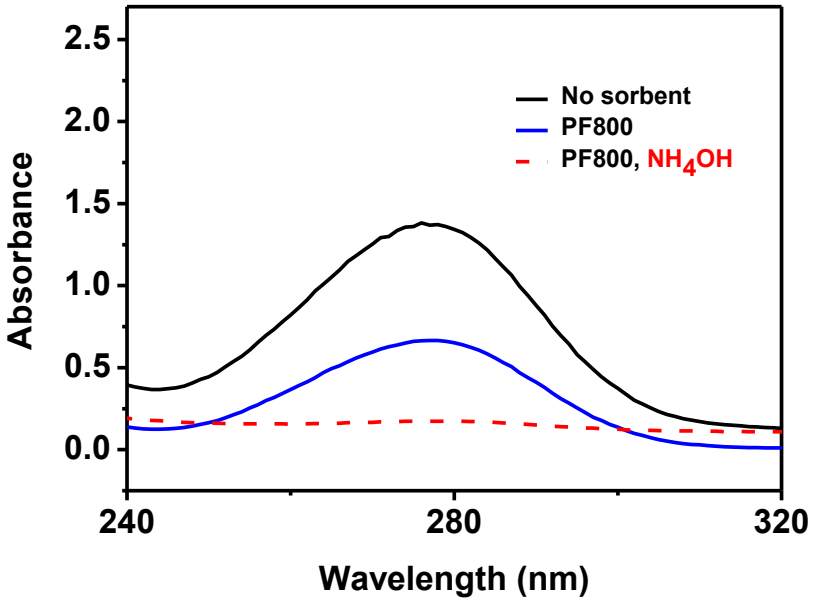

Figure 4.22 UV-spectrum of furfural and HMF on true biomass hydrolyte before and after the adsorption tests with PF800.

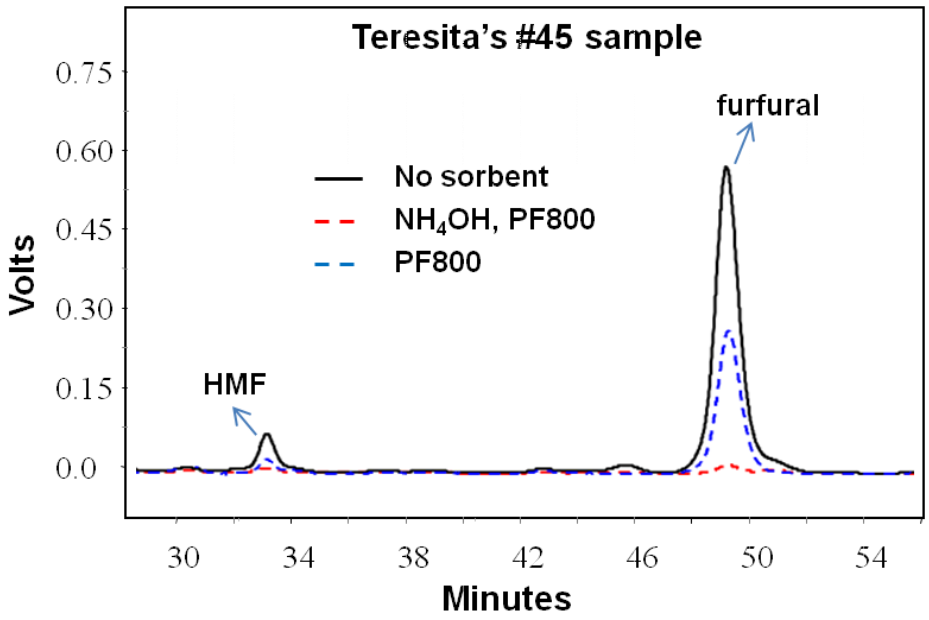

Figure 4.23 HPLC analysis of furfural and HMF on true biomass hydrolyte before and after the adsorption tests with PF800.

4.7 Conclusions

The previous section summarized the separation of furfural and HMF from the aqueous solution with commercial activated carbon and newly polymer-derived carbon. The adsorbents were characterized in terms of morphology, pore structure and surface chemistry. Langmuir isotherm is the suitable isotherm model for the adsorption of furfural on PF800. Conformation of the experimental data into Langmuir isotherm model indicates the homogeneous nature of PF800 surface. For Norit_1240, Freudlich isotherm is the suitable isotherm equation for the adsorption of furfural, which indicates the heterogeneous surfaces of Norit_1240. Two kinetic models, pseudo-first-order and pseudo-second-order models, were used to investigate the adsorption process of furfural on activated carbons. Pseudo-second-order model fits both PF800 and Norit_1240. Even though the effect of the particle size on adsorption kinetics is obvious, the effect of the

particle size on adsorption isotherm is negligible. The chemical structure of carbon surface, oxygen functional groups in particular, can strongly affect the selectivity of activated carbon between the furfural and sugars. An increase of oxygen amount on the carbon surface results in a decrease of selectivity. A two-step method was proposed to utilize the commercial carbon when the furfural concentration is above 1 g/l, followed by using polymer-derived carbon when furfural concentration is below 1 g/l, thereby potentially reducing the cost of adsorbent in whole and increasing the efficiency. The negative effect of acetic acid on the separation of furfural can be eliminated by neutralization with aqueous ammonia. Furfural and HMF can be successfully removed in the adsorption tests with true biomass hydrolytes

4.8 References

[1] El-Merraoui M, Aoshima M, Kaneko K. Micropore Size Distribution of Activated Carbon Fiber Using the Density Functional Theory and Other Methods. Langmuir 2000;16:4300-4304.

[2] Lastoskie C, Gubbins KE, Quirke N. Pore size distribution analysis of microporous carbons: a density functional theory approach. The Journal of Physical Chemistry 1993;97:4786-4796.

[3] Biniak S, Szymański G, Siedlewski J, Świątkowski A. The characterization of activated carbons with oxygen and nitrogen surface groups. Carbon 1997;35:1799-1810.

[4] Kozlowski C, Sherwood PMA. X-ray photoelectron spectroscopic studies of carbon fibre surfaces vii-electrochemical treatment in ammonium salt electrolytes. Carbon 1986;24:357-363.

[5] Freundlich H. Over the adsorption in solution. J Phys Chem 1906:385-471.

[6] Langmuir I. The adsorption of gases on plane surfaces of glass, mica and platinum. J Am Chem Soc 1918:1361–1403.

[7] Srivastava VC, Swamy MM, Mall ID, Prasad B, Mishra IM. Adsorptive removal of phenol by bagasse fly ash and activated carbon: Equilibrium, kinetics and thermodynamics. Colloids and Surfaces A: Physicochemical and Engineering Aspects 2006;272:89-104.

[8] Hameed BH, Din ATM, Ahmad AL. Adsorption of methylene blue onto bamboo-based activated carbon: Kinetics and equilibrium studies. Journal of Hazardous Materials 2007;141:819-825.

[9] Skelland AHP. Diffusional Mass Transfer. Wiley: NY 1974.

[10] Ho YS, McKay G. Sorption of dye from aqueous solution by peat. Chemical Engineering Journal 1998;70:115-124.

[11] Boyd GE, Schubert J, Adamson AW. The Exchange Adsorption of Ions from Aqueous Solutions by Organic Zeolites. I. Ion-exchange Equilibria1. Journal of the American Chemical Society 1947;69:2818-2829.

[12] Hall KR, Eagleton LC, Acrivos A, Vermeulen T. Pore- and Solid-Diffusion Kinetics in Fixed-Bed Adsorption under Constant-Pattern Conditions. Industrial & Engineering Chemistry Fundamentals 1966;5:212-223.

[13] Li L, Quinlivan PA, Knappe DRU. Effects of activated carbon surface chemistry and pore structure on the adsorption of organic contaminants from aqueous solution. Carbon 2002;40:2085-2100.

[14] Chingombe P, Saha B, Wakeman RJ. Surface modification and characterisation of a coal-based activated carbon. Carbon 2005;43:3132-3143.

[15] Gray KA, Zhao L, Emptage M. Bioethanol. Current Opinion in Chemical Biology 2006;10:141-146.

[16] Marzialetti T, Miller SJ, Jones CW, Agrawal PK. Switchgrass pretreatment and hydrolysis using low concentrations of formic acid. Journal of Chemical Technology & Biotechnology 2011;86:706-713.

CHAPTER 5: FERMENTATION WITH ACTIVATED CARBON TREATMENT

5.1 Overview

As presented in the preceding chapter, furfural & HMF could be removed from water solution by activated carbon treatment. In this chapter, the toxic effect of furfural & HMF on the fermentation of glucose and xylose by *Zymomonas mobilis* will be presented.

Wild type *Zymomonas mobilis* ZM4 and recombinant stain *Zymomonas mobilis* A3 were used in this study. Bacterial cell growth, sugar consumption and ethanol yield were investigated during the fermentation. When there were 4 g/L furfural and HMF in the fermentation broth, cells of ZM4 and A3 stopped growing during the fermentation and zero sugar consumption and ethanol yield occurred correspondingly. The complete elimination of inhibition effect of furfural & HMF was observed after PF800 treatment of the solution with residual 0.1g/l furfural & HMF. The value of specific growth rate of ZM4 and A3 in the control (no furfural & HMF) and PF800-treated fermentations was about 0.32 h^{-1}. Ethanol yield reached 0.46 g ethanol/g sugar consumed, about 90% of the theoretical ethanol yield (0.51 g/g).

5.2 Analytical Methods for Monosaccharides and Ethanol

5.2.1 Calibration Curves for Glucose and Xylose

In the fermentation experiments, glucose and xylose were measured by Agilent 1100 HPLC equipped with an Aminex HPX-87H column (Bio-Rad) with 5 mM H_2SO_4 at 0.4 ml/min as mobile phase. The calibration curve between sugar concentration and the area (nRIU*s) was then plotted [1]. Calibration curves with good linearity are shown in Fig. 5.1 and Fig. 5.2. Concentrations of glucose and xylose in the fermentation experiments were calculated from calibration curves.

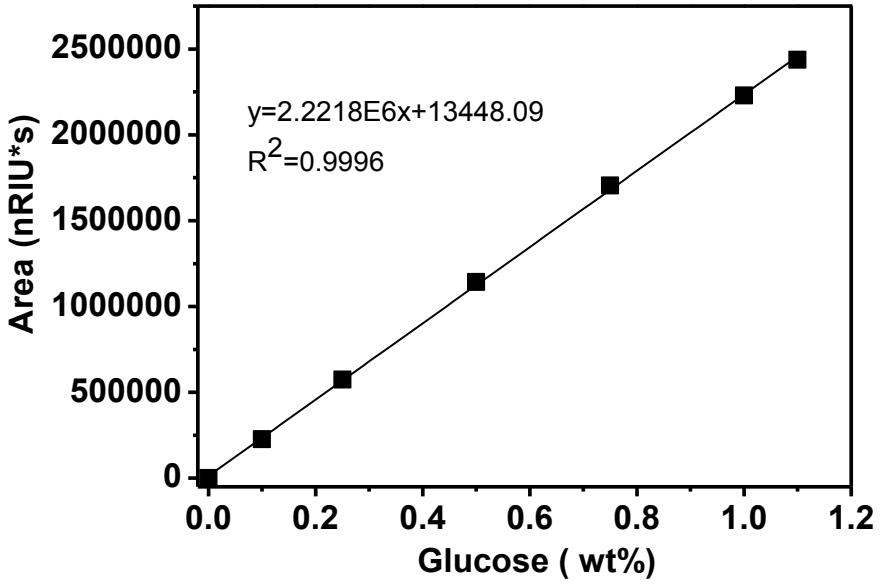

Figure 5.1 Calibration curve of glucose by HPLC in the fermentation experiments.

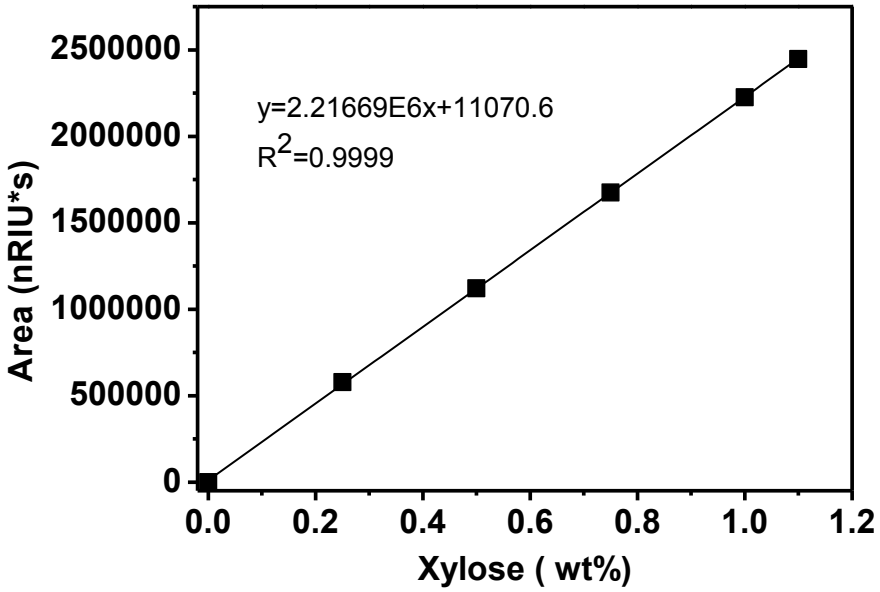

Figure 5.2 Calibration curve for xylose by HPLC in the fermentation experiments.

5.2.2 Calibration Curve for Ethanol

In the fermentation experiments, ethanol was measured by Agilent 1100 HPLC equipped with an Aminex HPX-87H column (Bio-Rad) with 5 mM H_2SO_4 at 0.4 ml/min as mobile phase. Good linearity was also observed between ethanol concentration and the area (nRIU*s), shown in Fig. 5.3. This calibration curve was used to calculate the concentration of ethanol in the fermentation experiments.

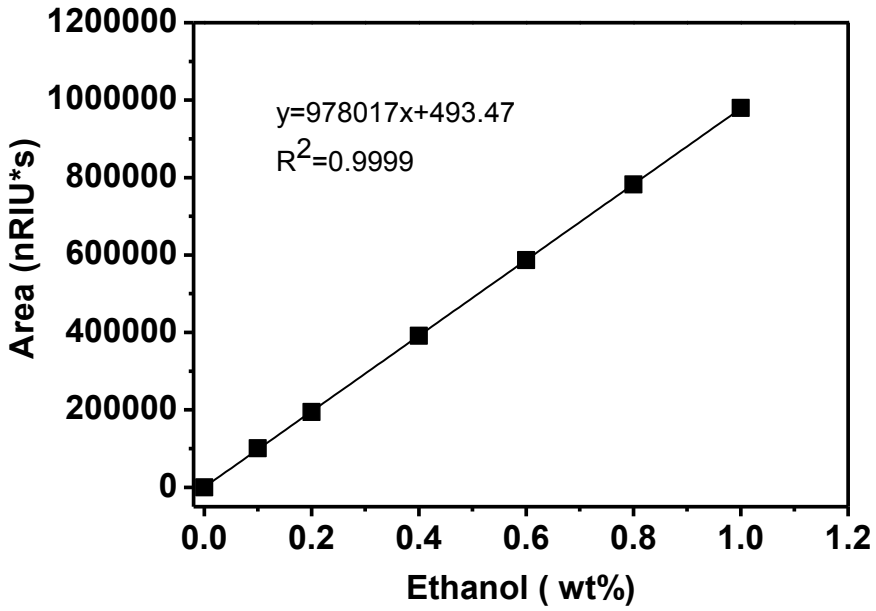

Figure 5.3 Calibration curve for ethanol by HPLC in fermentation experiments.

5.3 Fermentation Experiments

5.3.1 Microorganism

Wild type *Zymomonas mobilis* ZM4 (ATCC31821) was obtained from ATCC (American Type Culture Collection) [2]. *Zymomonas mobilis* A3 is a recombinant stain from wild-type *Zymomonas mobilis* ZM4. A3 was engineered to decompose both glucose and xylose, while ZM4 is able to utilize only glucose [3, 4]. Both ZM4 and A3 were used in this study.

For long-term storage, all strains were kept at -80 ^{o}C in 30% (v/v) glycerol solution by mixing 500μl sterile medium with culture (overnight cultured) with 500μl 60% (v/v) glycerol solution in a 1 ml vial [5]. Glycerol solution was prepared by mixing glycerol and deionized water. The 60% glycerol solution was autoclaved at 120 ^{o}C for 20 minutes.

5.3.2 Medium

Different mediums were needed for different experiments. Pre-seed medium was used in pre-seed culture for adaption of ZM4 and A3 to high glucose and xylose concentration in seed medium and main fermentation medium. Therefore, the glucose and xylose concentration in pre-seed medium are usually half of those in seed medium and main fermentation medium. Seed medium was used in seed culture, which helps to further prepare the cells for main fermentation. Main fermentation medium was needed for bacterial characterization in different conditions.

5.3.2.1 Pre-seed Medium

Pre-seed medium contained 5 g/l glucose, 1 g/l xylose, 10 g/l yeast extract, 2 g/l KH_2PO_4. This medium is similar to rich medium (RM medium) except sugar concentrations are different [6]. H_3PO_4 or NH_4OH was used to adjust the pH to 6, if necessary. This medium was then sterilized by filtration using a 0.22 μm filter.

5.3.2.2 Seed Medium

Seed medium contained 10 g/l glucose, 2 g/l xylose, 10 g/l yeast extract, 2 g/l KH_2PO_4. H_3PO_4 or NH_4OH was used to adjust the pH to 6, if necessary. This medium was then sterilized by filtration using a 0.22 μm filter.

5.3.2.3 Main Fermentation Medium

Main fermentation medium contained basic components including 10 g/l glucose, 2 g/l xylose, 10 g/l yeast extract, 2 g/l KH_2PO_4. Other than these basic components, different samples contained different amounts of furfural & HMF. Sample 1 was the control fermentation and did not contain furfural & HMF. Sample 2 contained 4 g/l furfural & HMF (3.6 g/l furfural & 0.36 g/l HMF). Sample 3 was the PF800-treated sample 2 and contained 0.1 g/l furfural & HMF after PF800 treatment. The media were sterilized by filtration using a 0.22 μm filter.

5.3.3 Culture Conditions

Pre-seed culture (PSC) and seed culture (SC) of ZM4 (or A3) were cultivated at 30 ^{o}C in 15 ml centrifuge tube and 50 ml centrifuge tube, respectively, filled to 60% volume and shaken at 250 rpm. PSC was prepared by inoculating a single colony from agar plate into the liquid medium. For 10 g/l glucose & 2g/l xylose fermentation, PSC contained 5 g/l glucose & 1g/l xylose. PSC was grown to the stationary phase. SC was prepared by inoculating it to an optical density (OD) of 0.1 using the stationary phase PSC. SC contained the same amount of sugars as the fermentation media. Appropriate amount of cells were harvested from SC at exponential phase, resuspended in fresh medium and were used to inoculate the main fermentation to get a starting OD of 0.05 [4]. Sample 1, 2, and 3 were utilized in the main fermentation individually. The culture procedure was shown in Fig. 5.4.

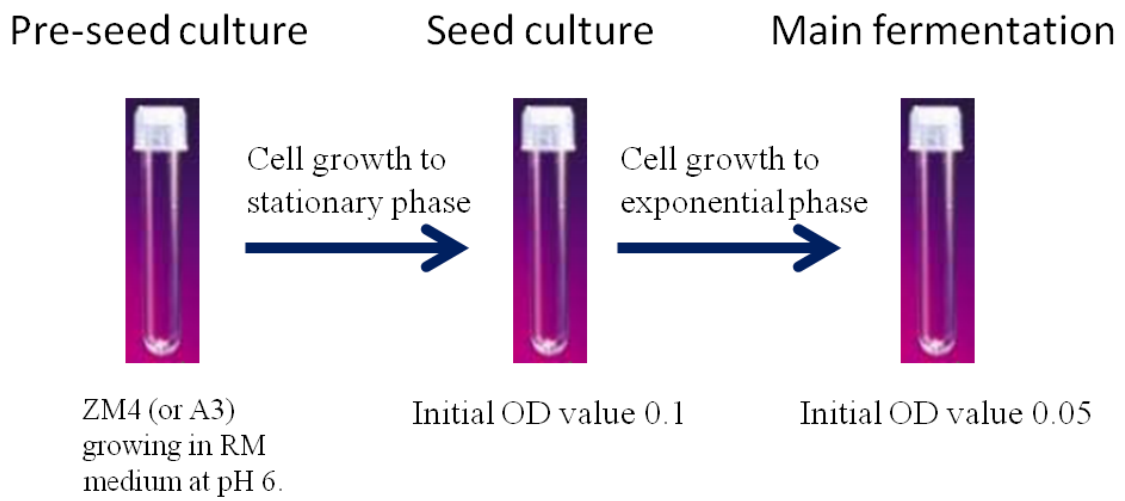

Figure 5.4 Culture procedure of fermentation of ZM4 (or A3).

5.3.4 Fermentation Results

5.3.4.1 Bacterial Growth

Since optical density was directly proportional to the dry cell mass concentration and easy to measure, it was routinely used to investigate cell growth [7]. Fig.5.5 presents the growth of ZM4 and A3 in the fermentation with different conditions. For both ZM4 and A3, an exponential growth was observed in the control fermentation (without furfural and HMF). Cell density quickly reached maximum after 16 h of fermentation and entered the stationary phase when net growth was zero. As a comparison, when there were 4 g/L furfural and HMF in the broth, cells of ZM4 and A3 stopped growing during the fermentation. Therefore, furfural and HMF are strong inhibitors at the level of 4 g/L during the bio-ethanol fermentation of *Z. mobilis*. Franden also investigated the toxic effect of furfural on *Z.mobilis* 8b (a recombinant strain from ZM4) and reported that furfural caused reduction in growth rate of 8b at 66 h of incubation up to 5 g/1 at which point growth was completely inhibited [8].

The overlapping of black and blue lines in Fig 5.5 indicates that cell growth completely recover after PF800 treatment with residual 0.1 g/L furfural & HMF in the solution. Therefore, the inhibition effect of furfural & HMF on ZM4 and A3 could be eliminated by separating inhibitors from the water solution.

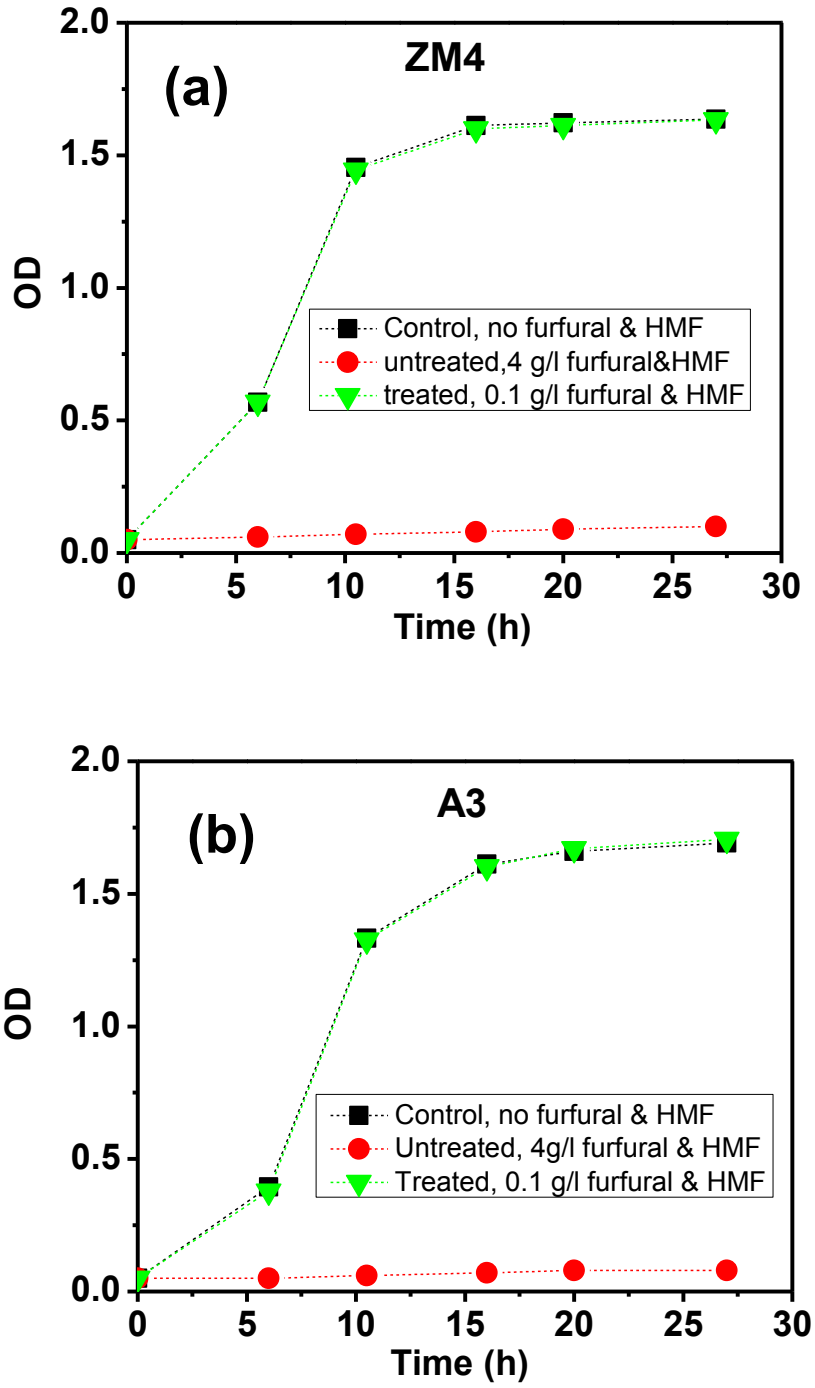

Figure 5.5 Optical density of bacterial growth in the fermentation at different conditions: (a) ZM4; (b) A3.

Fig. 5.6 shows the pictures of growth results observed for *Z. mobilis* ZM4 at different conditions. At 0 h of control fermentation in the absence of furfural & HMF, the fermentation broth was clear enough to see the lines on the back of the tube, as shown in Fig. 5.6a. This is because the cell density at the beginning of the fermentation is very small due to the low initial OD (0.05) from the seed culture. After 24 h, the control fermentation broth was highly turbid, which was caused by the high cell density in the broth (Fig. 5.6b). For the fermentation with 4 g/l furfural & HMF, the fermentation broth was still clear even after 24 h (Fig. 5.6c). This proves the strong inhibition effect of furfural on the ZM4 growth. Fig. 5.6d shows the result of PF800-treated sample. After treatment, only 0.1 g/l furfural and HMF remained in the solution. The high turbidity of the fermentation broth after 24 h implied ZM4 grew normally at the level of 0.1 g/l furfural and HMF. The similar results were observed in the fermentation experiments of A3.

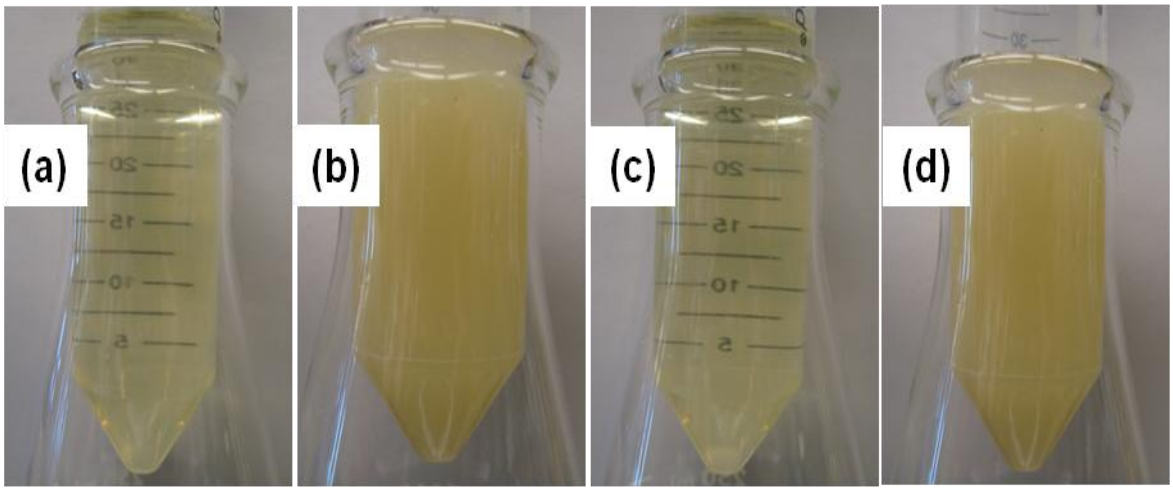

Figure 5.6 Growth results observed for *Z. mobilis* ZM4 at different conditions: (a) control fermentation (without furfural & HMF) at 0 h; (b) control fermentation (without furfural & HMF) at 24 h; (c) fermentation with 4 g/l furfural & HMF at 24 hr; (d) fermentation with 0.1 g/l furfural & HMF at 24 h.

The specific growth rate of a bacterial population is a measure of the increase in biomass over time and it is determined from the exponential phase. The specific growth rate can be calculated by the following equations [9]:

$$Y = ae^{\mu t} \qquad (5\text{-}1)$$

a is the original OD value 0.05. μ is defined as the specific growth rate (h^{-1}). Y is the OD value and t is time (h). The equation 5-1 can be written as:

$$\ln(Y / 0.05) = \mu t \qquad (5\text{-}2)$$

When ln (Y/0.05) is plotted with growth time, a linear line should result, and the slope is μ.

The results of specific growth rate of ZM4 and A3 are shown in Fig. 5.7. The value of specific growth rate of ZM4 in the control fermentation is 0.325 h^{-1}. The specific growth rate dropped to almost zero in the fermentation when 4g/l furfural & HMF existed in the solution. For the PF800-treated sample with 0.1 g/l furfural & HMF, the specific growth rate recovered to 0.325 h^{-1}. The similar results were obtained for the fermentation of A3. The value of specific growth rate of A3 in the control and PF800-treated fermentations were 0.315 h^{-1}, slightly smaller than ZM4. This could be caused by the slower consumption of xylose by A3. But the effect of xylose consumption is limited due to the low initial xylose concentration. The effect of high initial xylose concentration on the fermentation will be studied in the latter part of this chapter.

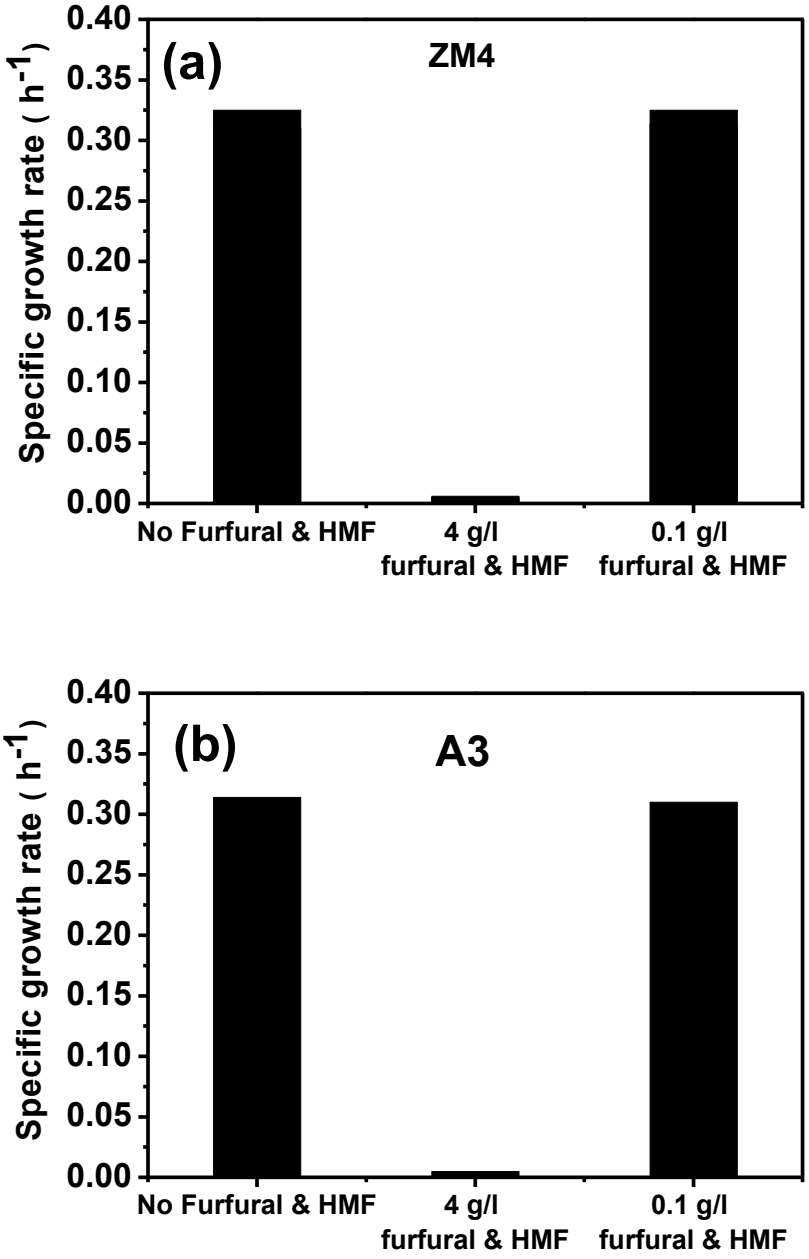

Figure 5.7 Specific growth rate of bacteria in the fermentation with different conditions: (a) ZM4; (b) A3.

5.3.4.3 Sugar Consumption

Sugar consumption in the batch fermentation of ZM4 and A3 were studied and the results were highly related to cell growth. Fig. 5.8 presents the results of sugar concentrations in the batch fermentation of ZM4. In the control fermentation, only glucose could be utilized by ZM4 with 2 g/l xylose still remaining after glucose depletion. Glucose exhaustion occurred after 12 h of fermentation. Consequently, the cell growth of ZM4 reached stationary phase after 12h. No glucose and xylose were utilized by ZM4 in the fermentation with 4 g/l furfural & HMF, as a result of the zero cell growth of ZM4 caused by the complete inhibition. In the PF800-treated fermentation, similar results were observed as in the control fermentation. This again demonstrates that the inhibition effect of furfural & HMF on the fermentation could be eliminated after removing the inhibitors. In addition, no sugar loss was observed after PF800 treatment, implying the good selectivity of PF800 between furfural and sugars.

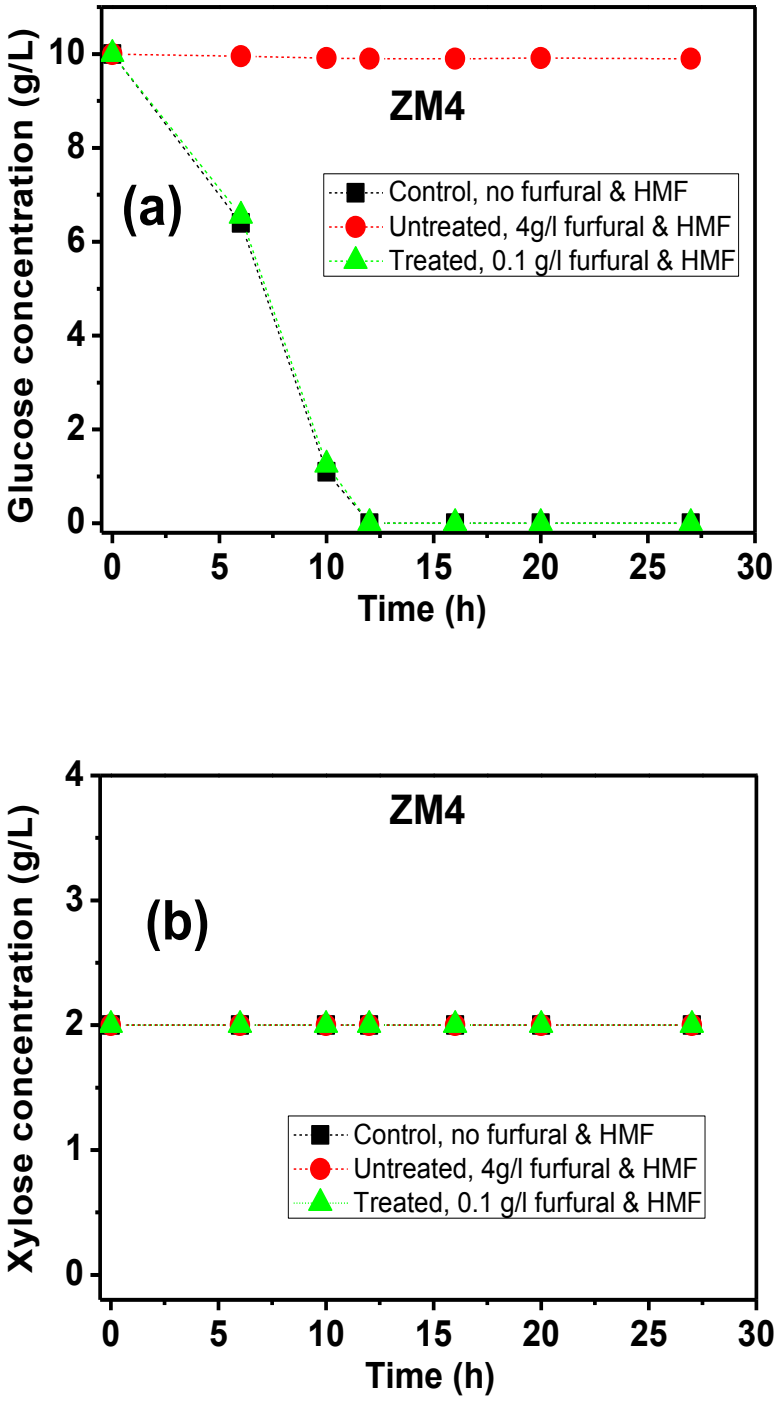

Figure 5.8 Sugar concentrations in the batch fermentation of ZM4: (a) glucose concentration; (b) xylose concentration.

The results of sugar concentrations in the batch fermentation of A3 are shown in Fig. 5.9. In the control fermentation, glucose was first utilized by A3 and uptake of xylose occurred after glucose exhaustion at 12 h of fermentation. All sugars were consumed after 20 hr of fermentation. This means although A3 was engineered from wild type ZM4 to utilize xylose, it still utilized glucose prior to xylose. In the fermentation with 4 g/l furfural & HMF, no glucose and xylose was consumed by A3, same as ZM4. The elimination of inhibition effect of furfural & HMF on A3 was also observed after PF800 treatment.

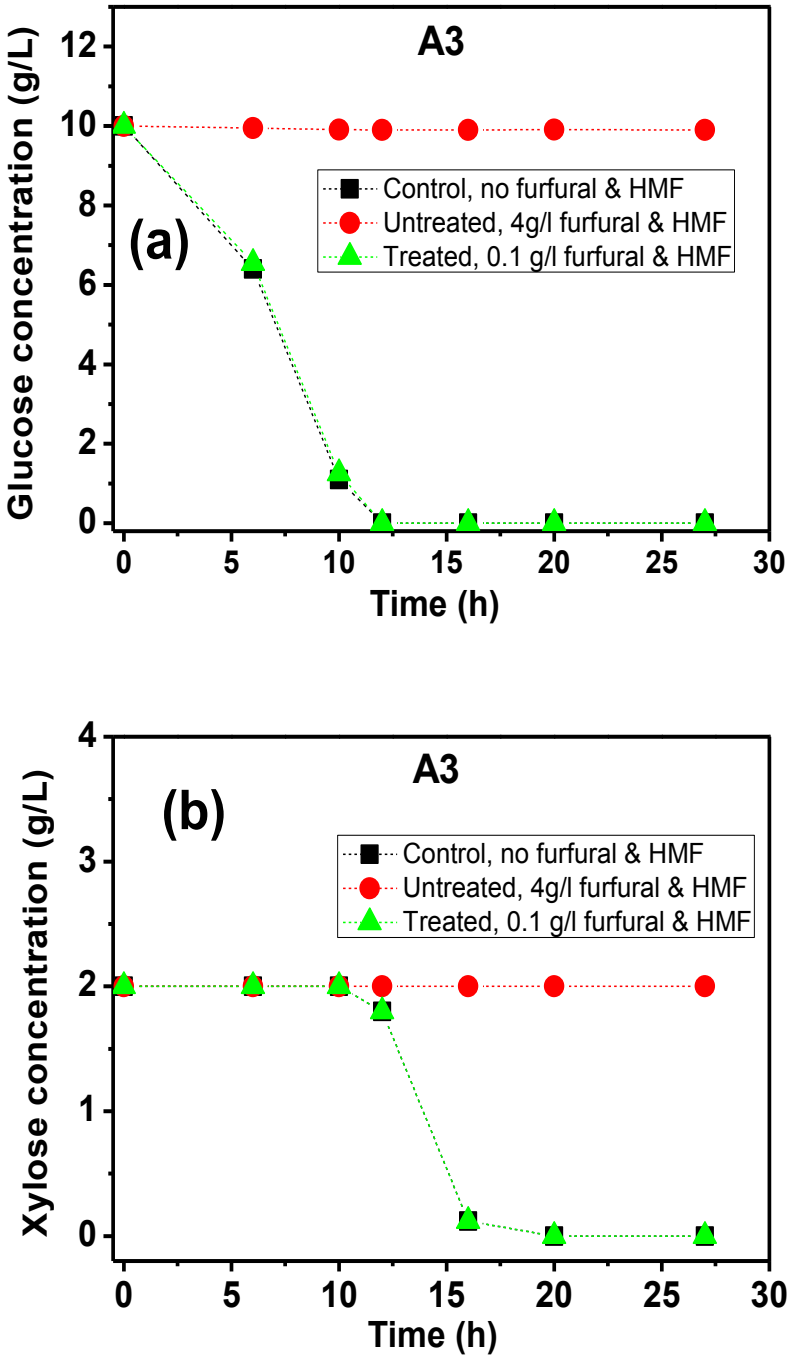

Figure 5.9 Sugar concentrations in the batch fermentation of A3: (a) glucose concentration; (b) xylose concentration.

5.3.4.4 Ethanol Production

The ethanol concentrations in the batch fermentation of ZM4 and A3 are shown in Fig. 5.10. A3 produced higher ethanol concentration than ZM4. This is because A3 can utilize both glucose and xylose while ZM4 only utilized glucose. For both ZM4 and A3, no ethanol was produced in the fermentation with 4 g/l furfural & HMF, as a result of zero sugar consumption. After PF800 treatment, the ethanol production recovered in both ZM4 and A3 fermentation.

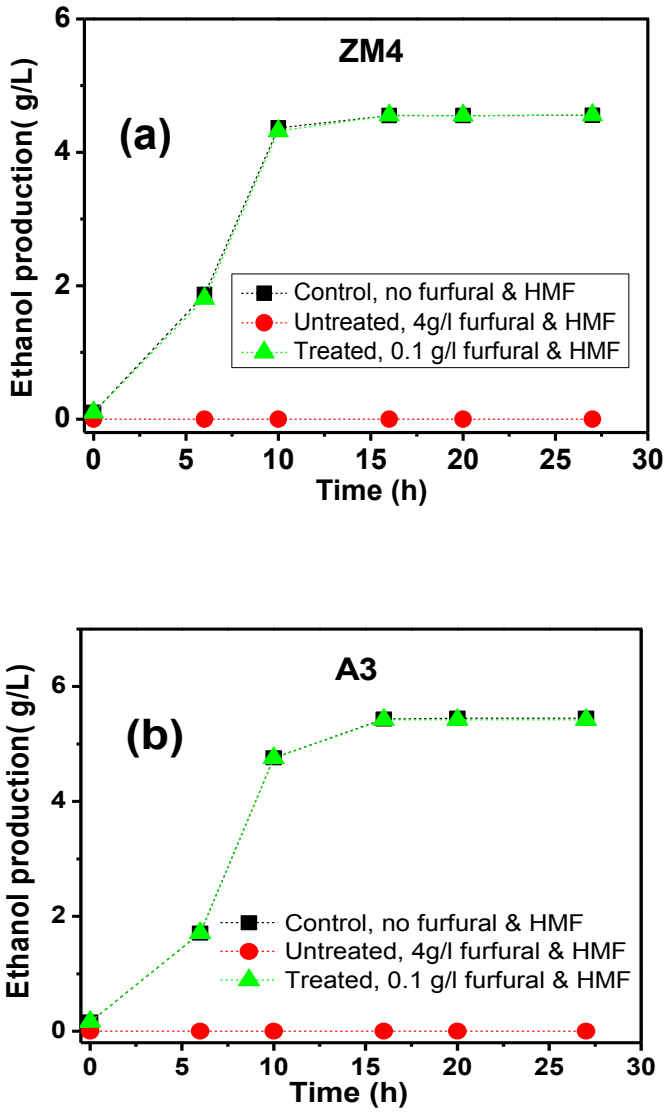

Figure 5.10 Ethanol concentration in the batch fermentation: (a) ZM4; (b) A3.

Ethanol fermentation results in three major products: additional cells (cell division), ethanol, carbon dioxide. One molecule of glucose yields, stoichiometrically, 2 molecules of ethanol plus 2 molecules of carbon dioxide. On a mass basis, one gram of glucose will theoretically produce 0.51 gram of ethanol and 0.49 gram of carbon dioxide [10].

$$C_6H_{12}O_6 \rightarrow 2C_2H_5OH + 2CO_2$$

Glucose Ethanol Carbon dioxide

Similarly, the theoretical ethanol yield from xylose is 0.51 g/g based on the following mechanism [11]:

$$C_5H_{10}O_5 \rightarrow \frac{5}{3}C_2H_5OH + \frac{5}{3}CO_2$$

D-xylose Ethanol Carbon dioxide

Table 5.1 Ethanol yield in the batch fermentation of ZM4 and A3 with initial 10 g/l glucose and 2 g/l xylose.

Strain	**Ethanol yield (g/g)** [a]	**Ethanol yield (%)** [b]
ZM4	**0.461**	**90.3**
A3	**0.457**	**89.4**

[a] Calculated based on consumed sugar.

[b] Calculated as a percentage of theoretical ethanol yield (0.51 g/g).

Table 5.1 shows the ethanol yield in the batch fermentation of ZM4 and A3. During the fermentation of ZM4, the ethanol yield was 0.461 g ethanol/g glucose consumed. Overall ethanol yield was equated with the ratio of final ethanol concentration to initial glucose concentration, since initial ethanol and final glucose concentrations were zero. For A3, the ethanol yield was 0.457 g ethanol/g glucose & xylose consumed. The overall ethanol yield was equated with the ratio of final ethanol concentration to initial glucose

and xylose concentration, since A3 utilized both glucose and xylose. For both ZM4 and A3, the ethanol yield is about 90% of the theoretical ethanol yield (0.51 g/g). This means that a part of sugars were consumed to generate bacterial cells and did not result in the production of ethanol. Most industrial fermentation processes operate at 90–95% of the theoretical yield of ethanol from sugars fed to the microbes [12].

5.3.4.5 Fermentations with High Initial Glucose and Xylose Concentration

Fermentations of A3 with high initial sugar concentration (50 g/L glucose and 50 g/l xylose) were also investigated in terms of cell growth, sugar consumption, and ethanol yield. In this study, only sugar concentration was different from the previous research, while other conditions were identical.

Cell growth of A3 in the fermentation is shown in Fig. 5.11. The specific growth rate of A3 is about 0.26 h^{-1} in the control fermentation, slower than that of previous fermentation with low initial sugar concentration (0.315 h^{-1}). This is because the xylose consumption rate by A3 is slower than glucose consumption rate. Therefore, when the sugar concentrations were changed from 10 g/l glucose & 2 g/l xylose in the previous fermentation to 50 g/L glucose & 50 g/l xylose in this study, the overall specific growth rate dropped to a certain degree. It should be noted that the inhibition effect of furfural & HMF on the cell growth of A3 was still very strong even when the initial sugar concentrations were high. And this inhibition effect could be eliminated by PF800 treatment.

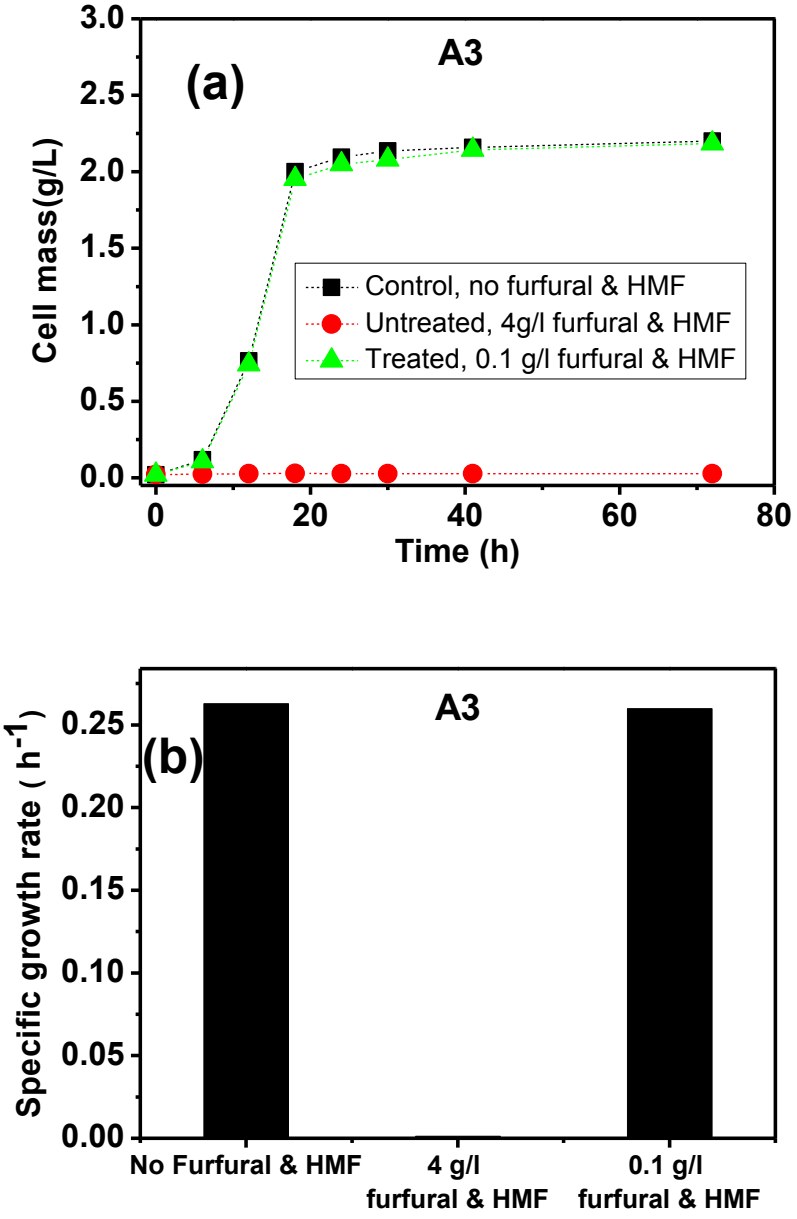

Figure 5.11 Cell growth of A3 in the fermentation with high initial sugar concentration: (a) cell mass; (b) specific growth rate.

A3 unitized glucose prior to and fully consumed glucose at 18 h in the control and PF800-treated fermentation, as shown in Fig. 5.12. The xylose uptake occurred after glucose depletion. The uptake of xylose was incomplete at 40 h with residual xylose of 16 g/L. Even after 72 h, residual 16 g/L xylose was measured. At 72 h of fermentation, a

pH drop from 6.0 to 4.0 was observed. This phenomenon could have been attributed to the formation of carbonic acid. Even though pH was not measured at 40 h, it is highly believed that pH has already declined to a low level so that A3 stopped growing and utilizing xylose. Nevertheless, full xylose consumption can be achieved with a timely pH adjustment during the fermentation. The Chen group has reported the full utilization of sugars (initial 50 g/L glucose & 50 g/l xylose) by A3 in the fermenter (500ml) with minimum pH maintained at 5.75 [4].

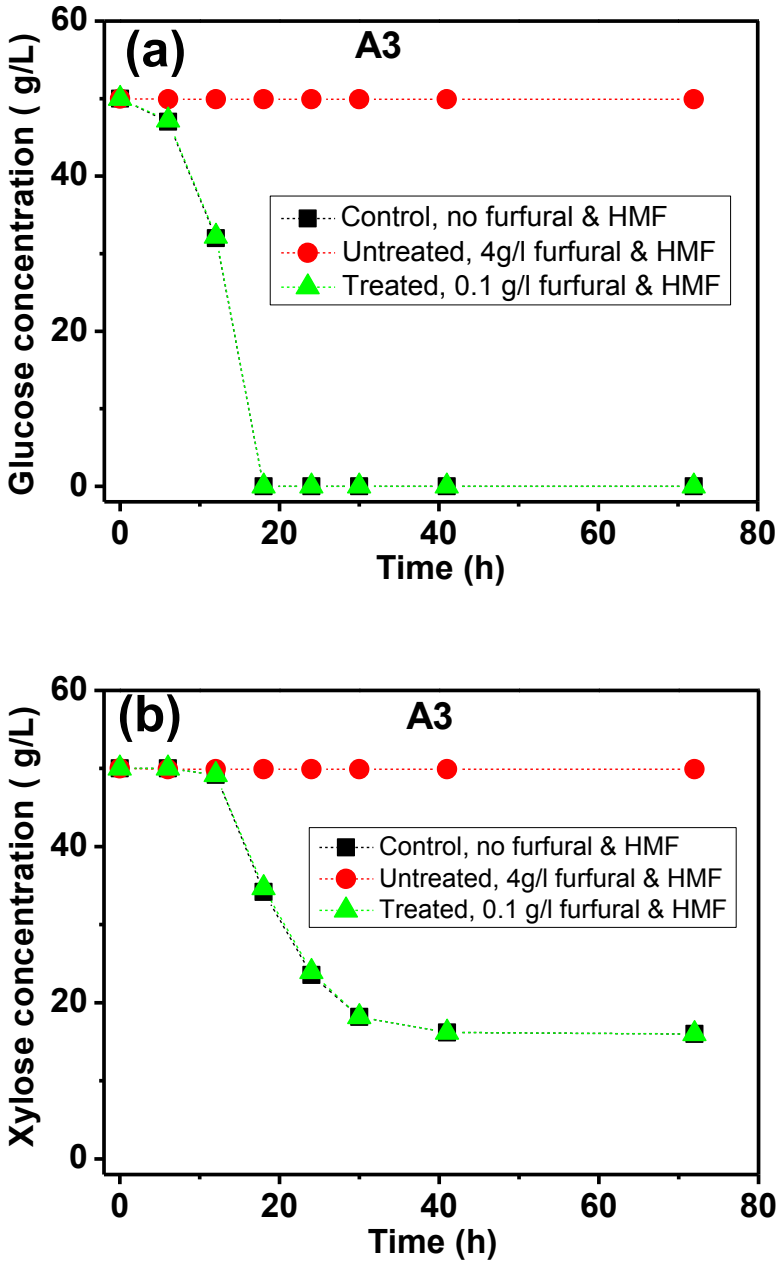

Figure 5.12 Sugar concentrations in the batch fermentation of A3: (a) glucose concentration; (b) xylose concentration.

Fig. 5.13 presents 39.8 g/l ethanol was produced in the control and PF800-treated fermentation. The ethanol yield was 0.47 g/g based on 84 g/l consumed sugars, including 50 g/l glucose and 34 g/l xylose, and this ethanol yield is about 92% of the theoretical ethanol yield (0.51 g/g). Zero ethanol yield was observed in the fermentation with 4 g/l furfural & HMF, as a result of zero cell growth of A3 an sugar consumption.

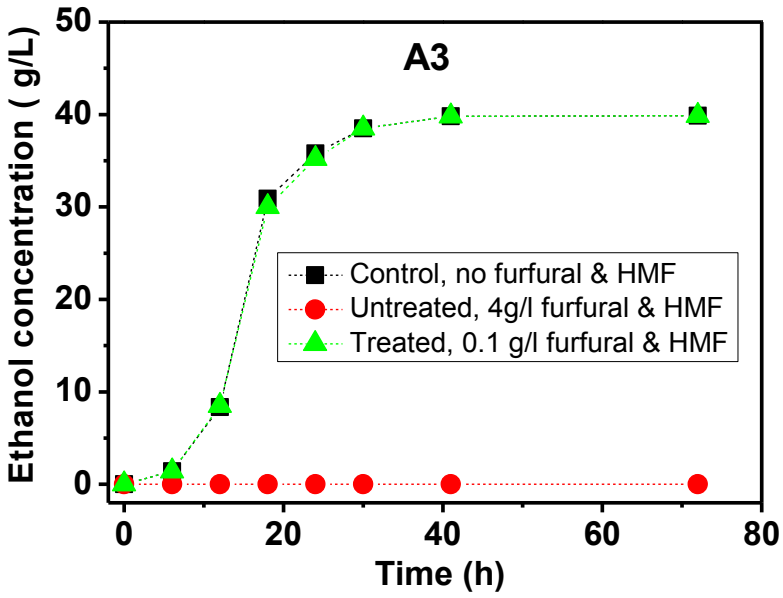

Figure 5.13 Ethanol concentration in the batch fermentation of A3 with high initial sugar concentration

5.4 Conclusions

This chapter is devoted to exploit the elimination of toxic effect of furfural & HMF in the bio-ethanol fermentation by *Zymomonas mobilis* ZM4 and *Zymomonas mobilis* A3 after PF800 treatment of the fermentation broth. Bacterial cell growth, sugar concentrations, and ethanol concentrations were monitored throughout the course of each fermentation experiment.

For both ZM4 and A3, inhibition of cell growth has been shown to be very strong in the fermentation with 4 g/l furfural & HMF. Cell growth is closely associated with sugar consumption and ethanol production. Zero sugar consumption and ethanol yield were observed as a result of complete inhibition of cell growth. The inhibition effect could be eliminated by PF800 treatment of the solution to selectively remove furfural & HMF. After PF800 treatment, the residual 0.1 g/l furfural & HMF did not exhibit inhibition effect on the fermentation. The specific growth rate, sugar consumption and ethanol yield recovered completely, as compared with the control fermentation without furfural & HMF.

Strong inhibition effect of 4g/l furfural & HMF still existed in the fermentation with high initial sugar concentrations (50 g/L glucose and 50 g/l xylose). The toxic effect could also be eliminated by PF800 treatment. A drop of pH owing to the formation of carbonic acid resulted in incomplete xylose utilization after 40 h of fermentation. pH adjustment will be necessary in the fermentation with high initial sugar concentrations.

5.5 References

[1] Wentz FE, Marcy AD, Gray MJ. Analysis of Wood Sugars in Pulp and Paper Industry Samples by HPLC. Journal of Chromatographic Science 1982;20:349-352.

[2] Doelle HW, Kirk L, Crittenden R, Toh H, Doelle MB. Zymomonas Mobilis—Science and Industrial Application. Critical Reviews in Biotechnology 1993;13:57-98.

[3] Agrawal M, Chen R. Discovery and characterization of a xylose reductase from Zymomonas mobilis ZM4. Biotechnology Letters 2011:1-7.

[4] Agrawal M, Mao Z, Chen RR. Adaptation yields a highly efficient xylose-fermenting Zymomonas mobilis strain. Biotechnology and Bioengineering 2011;108:777-785.

[5] Fieschko J, Humphrey RE. Effects of temperature and ethanol concentration on the maintenance and yield coefficient of Zymomonas mobilis. Biotechnology and Bioengineering 1983;25:1655-1660.

[6] Yanase H, Nozaki K, Okamoto K. Ethanol production from cellulosic materials by genetically engineered <i>Zymomonas mobilis</i&gt. Biotechnology Letters 2005;27:259-263.

[7] Lee C, Lim H. New device for continuously monitoring the optical density of concentrated microbial cultures. Biotechnology and Bioengineering 1980;22:639-642.

[8] Franden MA, Pienkos PT, Zhang M. Development of a high-throughput method to evaluate the impact of inhibitory compounds from lignocellulosic hydrolysates on the growth of Zymomonas mobilis. Journal of Biotechnology 2009;144:259-267.

[9] Exponential growth, http://en.wikipedia.org/wiki/Exponential_growth. Wikipedia March 2008.

[10] Alterthum F, Ingram LO. Efficient ethanol production from glucose, lactose, and xylose by recombinant Escherichia coli. Appl Environ Microbiol 1989;55:1943-1948.

[11] Slininger PJ, Bothast RJ, Van Cauwenberge JE, Kurtzman CP. Conversion of D-xylose to ethanol by the yeast Pachysolen tannophilus. Biotechnology and Bioengineering 1982;24:371-384.

[12] Dien BS, Cotta MA, Jeffries TW. Bacteria engineered for fuel ethanol production: current status. Applied Microbiology and Biotechnology 2003;63:258-266.

CHAPTER 6: REGENERATION OF ACTIVATED CARBON

6.1 Summary

For economic concerns, adsorbents should be regenerated efficiently. Thus, different methods to regenerate the spent adsorbents were studied, including:

(1) Thermal regeneration by calcining the spent adsorbents at high temperature.

(2) pH adjustment by leaching the spent sorbents with acidic or basic water solution.

(3) Organic solvent stripping by contacting the spent sorbents with different organic solvents.

To evaluate the regeneration efficiency, adsorption batch tests were performed with regenerated adsorbents after regeneration, and the adsorption capacity of regenerated adsorbents was compared with the fresh adsorbents.

Batch tests were first conducted in the desorption tests of the adsorbent. An adsorption/desorption cycle method was designed based on the results of desorption batch tests. Granular Norit_1240 was utilized in column tests to investigate the adsorption/desorption approach. Dynamic mass balance was obtained after running four or five cycles and regeneration results were stable even after twenty cycles. These results paved the way to the potential integration of ethanol production during fermentation into the adsorption/desorption regeneration approach.

6.2 Thermal Regeneration

The first method investigated to expel furfural from adsorbents is thermal regeneration. The spent PF800 (saturated with furfural) were calcined at high temperature under nitrogen atmosphere. The weight of spent adsorbents was monitored by TGA

(Thermo gravimetric analysis). The effect of regeneration temperature on the furfural removal of regenerated carbon is demonstrated in Fig. 6.1. The weight loss of spent PF800 at high temperature should be the weight of desorbed furfural, and the weight began to decrease when the temperature was above 120 ℃ and the furfural removal increased with an increase in the regeneration temperature. Little weight loss was observed when the temperature was above 300 ℃, which indicated most furfural was expelled from the carbon. The remaining 82 wt% was the weight of residual carbon.

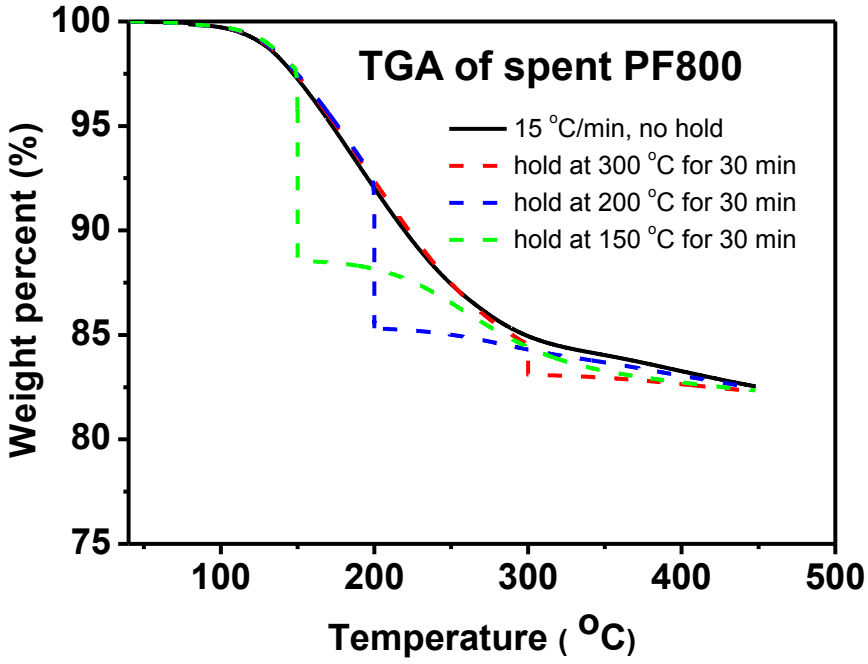

Figure 6.1 TGA of spent PF800 (saturated with furfural) under nitrogen atmosphere.

Based on the result of TGA, spent PF800 (saturated with furfural) was calcined in the furnace at 300 °C for 2 h with heating rate 15 °C/min, purging nitrogen. Furthermore, to evaluate the regeneration efficiency, the regenerated PF800 were employed to perform the adsorption tests again after regeneration, and its adsorption capacity was compared with the fresh PF800:

$$\frac{\text{Sorption capacity of regenerated PF800}}{\text{Sorption capacity of fresh PF800}} = \frac{183\ \text{mg/g}}{245\ \text{mg/g}} = 75\%$$

Although most furfural was expelled from PF800 at 300 ^{o}C, the adsorption capacity of regenerated PF800 regeneration was not completely recovered. Some small organic molecules might be generated by furfural decomposition at high temperature and could be attached on the surfaces of regenerated PF800, leading to a loss of the adsorption capacity of the regenerated PF800.

To expel all the attached chemicals from adsorbents, thermal regeneration tests were carried out at 800 ^{o}C for 2 h with heating rate 15 ^{o}C/min, purging nitrogen. This is the same condition as in the pyrolysis of poly-furfural. Regeneration efficiency was evaluated by comparing the adsorption capacity of regenerated PF800 with the fresh PF800. After thermal regeneration at 800 ^{o}C, the adsorption capacity of regenerated PF800 recovered completely, shown below:

$$\frac{\text{Sorption capacity of regenerated PF800}}{\text{Sorption capacity of fresh PF800}} = \frac{246\ \text{mg/g}}{245\ \text{mg/g}} = 100.4\%$$

Although the regeneration efficiency is very high, there are some drawbacks of regeneration of activated carbon at such high temperature. The main drawback is that this is a highly energy-consuming process due to the high temperature required, making it both an energetically and commercially expensive method [1]. Some activated carbon companies can provide a service to ship the used activated carbon to a specialized facility for regeneration. In this situation, thermal regeneration involves not only thermal desorption; several different processes and chemical reactions also occur. The spent

activated carbon could also pass through carbonization and gasification at high temperature in the presence of limited amounts of oxidant such as water vapour, oxygen, etc. Loss of carbon may reach 5-10% in the gasification stage and could be increased by particle attrition [2, 3]. Gasification in industry could also cause oxygen groups on the carbon surface and lead to a decrease in the selectivity of regenerated activated carbon between furfural and sugars.

6.3 Chemical Regeneration in Batch Tests

Chemical regeneration is an alternative to thermal regeneration. It has a number of significant advantages: (1) It can be done *in situ*, thus unloading, transporting, and repacking of the adsorbent are eliminated. (2) The loss of carbon resulting from thermal desorption is eliminated. (3) Recovery of valuable adsorbates is possible [4]. The most commonly used regenerants can be categorized into two groups: organic solvents or inorganic chemicals, such as acidic solution and basic solution.

6.3.1 Condition of Desorption Tests

Fig. 6.2 presents the condition of the desorption tests, in which spent PF800 was contacted with pure water, inorganic eluents with different pH, and organic solvents, respectively. Spent PF800 refers to the PF800 already used in the adsorption tests and saturated with furfural. The content of furfural desorbed into the regenerants was analyzed by UV-Vis spectrophotometer after desorption tests. Furthermore, the regenerated PF800 was employed to perform the adsorption tests again after regeneration, and its sorption capacity was compared with that of the fresh PF800 to evaluate the regeneration efficiency.

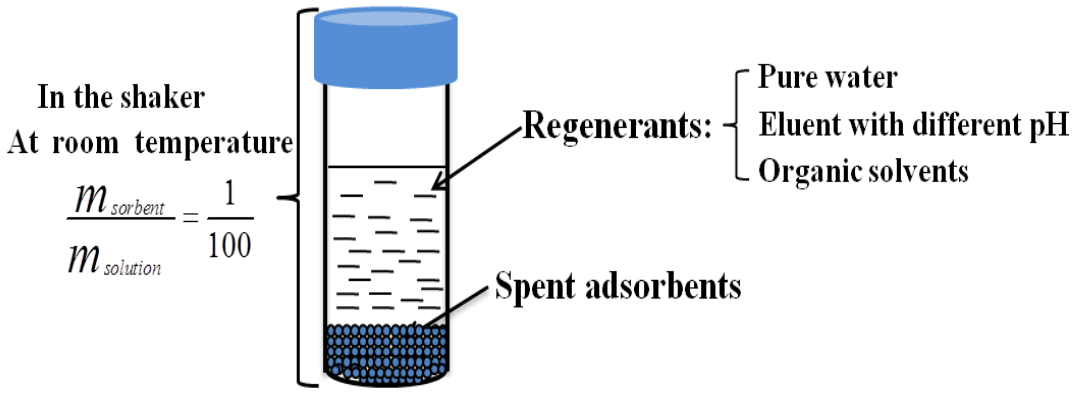

Figure 6.2 Condition of desorption tests using spent PF800 saturated with furfural.

6.3.2 Desorption by Pure Water

DI water was first utilized in the desorption tests to desorb furfural from the spent PF800 at 25 ^{o}C (room temperature) and 95 ^{o}C (in hot water bath), respectively. Fig. 6.3 presents the results of UV spectra of furfural desorbed from spent PF800 into water. The peak in the wavelength of 278 nm is corresponding to the content of desorbed furfural in water. Even though furfural was detected in the water after desorption tests at 25 ^{o}C, this amount of desorbed furfural was only 5% of furfural on the spent PF800 before regeneration. In chapter 4, we have discussed the distribution coefficient of furfural K_f, i.e., the ratio of the concentration of furfural in carbon to the equilibrium concentration of furfural in the solution.

$$K_f = C_{fc} / C_{fs} \qquad (6\text{-}1)$$

Where and C_{fc} and C_{fs} are the equilibrium concentration of furfural in the carbon and in the solution, respectively.

For PF800 at room temperature, K_f is about 4100 in the adsorption tests in chapter 4. In the desorption tests, an equilibrium was also reached between the concentration of furfural in regenerated PF800 and concentration of desorbed furfural in pure water. The distribution coefficient of furfural in the desorption tests is still 4100 at room temperature. Therefore, most of furfural remained in the carbon while only a small amount of furfural was desorbed into water. When desorption tests were performed at 95 ^{o}C, more furfural was desorbed into pure water than at 25 ^{o}C. This is due to higher solubility of furfural in water at high temperature than at room temperature. Nevertheless, only 12% furfural was desorbed from the spent PF800 by pure water at 95 ^{o}C, indicating the regeneration was not complete by pure water at 95 ^{o}C.

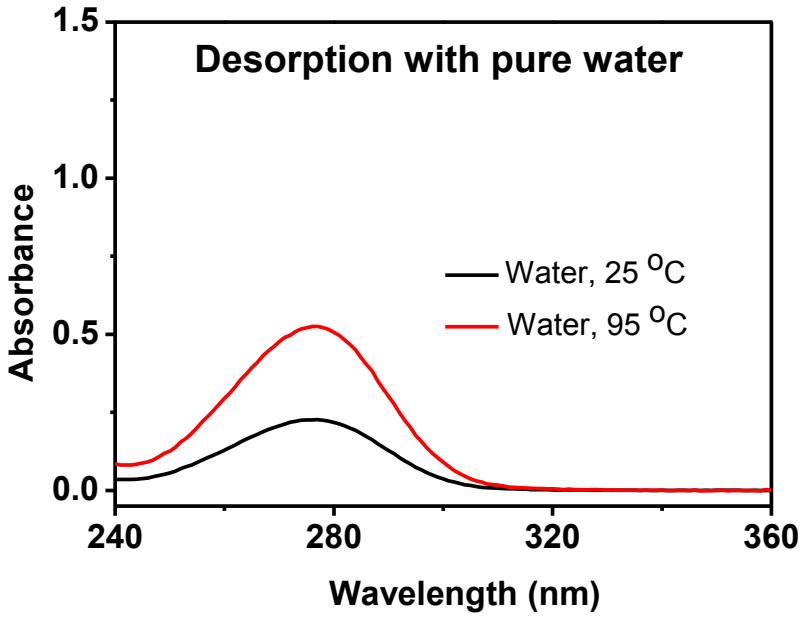

Figure 6.3 UV spectra of furfural desorbed from the spent PF800 with pure water at different temperature.

For PF800 regenerated by pure water at 25 ^{o}C, the regeneration efficiency was evaluated and shown in the following:

$$\frac{\text{Sorption capacity of regenerated PF800}}{\text{Sorption capacity of fresh PF800}} = \frac{12\ \text{mg/g}}{245\text{mg/g}} = 4.9\%$$

For PF800 regenerated by pure water at 95 ^{o}C, the regeneration efficiency was:

$$\frac{\text{Sorption capacity of regenerated PF800}}{\text{Sorption capacity of fresh PF800}} = \frac{29\ \text{mg/g}}{245\text{mg/g}} = 11.8\%$$

The results presented in this research showed that regeneration of activated carbons used as furfural adsorbents by pure water is not feasible at room temperature or 95 ^{o}C. Salvado reported desorption of phenols from activated carbon with liquid water under subcritical conditions (300℃ and 120 atm) [5]. Although high regeneration efficiency was achieved, this process was high energy consuming and not attractive in industry.

6.3.3 Desorption by pH Adjustment

Desorption tests of spent PF800 were performed by using water solution with different pH: (a) 5 wt% H_2SO_4/H_2O, and (b) 5 wt% $NaOH/H_2O$, respectively, to desorb furfural from spent PF800.

Fig. 6.4 presents the results of UV spectra of furfural desorbed from spent PF800 into water solution. Neither acidic solution nor basic one improved the desorption of furfural from spent PF800. The amount of furfural desorbed by acidic solution or basic solution was almost the same as by pure water.

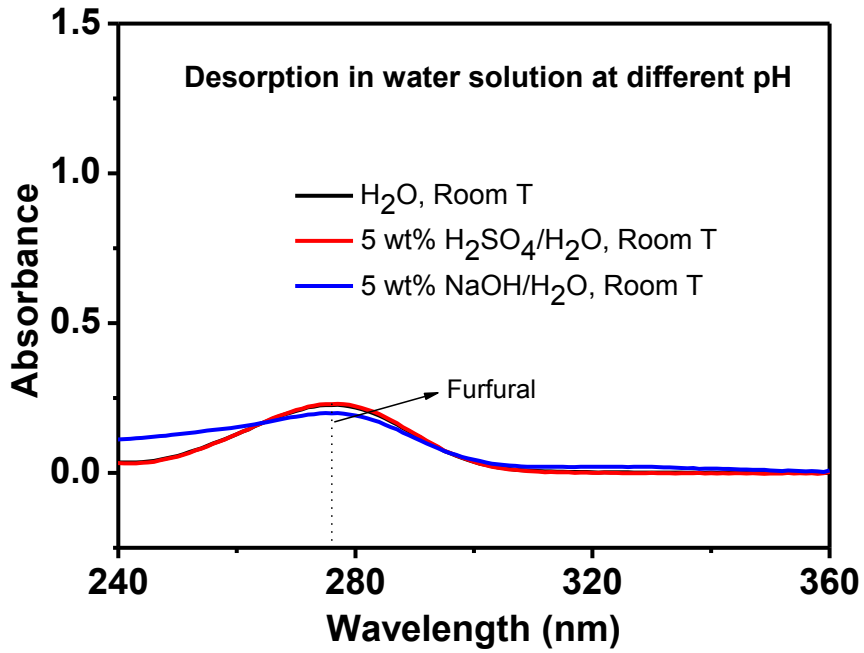

Figure 6.4 UV spectra of furfural desorbed from the spent PF800 with water solution at different pH.

Accordingly, adsorption capacity of the regenerated PF800 by acidic or basic solution was only 4.9 % of that of fresh PF800, shown in the following:

$$\frac{\text{Sorption capacity of regenerated PF800}}{\text{Sorption capacity of fresh PF800}} = \frac{12\ \text{mg/g}}{245\text{mg/g}} = 4.9\%$$

Acidic or basic solution is commonly used in the recovery of ionized chemicals [6], which could be exchanged with H^+ or OH^-. Furfural, however, is in the form of a non-ionized molecule in both solution and sorbent, thereby H^+ or OH^- is ineffective. The failure of the attempt to regenerate sorbent by pH adjustment in aqueous phase lead us to employ different organic solvents to regenerate the sorbent.

6.3.4 Desorption by Organic Solvent

Solvent regeneration is an alternative to thermal regeneration[7, 8]. The desorption of adsorbate from the carbon surface by solvent extraction is a partitioning process. When the solubility of adsorbate is higher in a solvent than in water, the presence of the solvent in the sorption system can reduce the solid-to-liquid equilibrium concentration ratio of the adsorbate; thus desorption takes place as the solvent is displacing or mixing with the water.

6.3.4.1 Effect of Organic Solvent

The desorption condition used herein was the same as in the case of pH adjustment, except that organic solvent was utilized, rather than water solution with different pH. Five organic solvents were utilized in the desorption tests, including DMSO (Dimethyl sulfoxide), DCM (Dichloromethane), THF (Tetrahydrofuran), ethanol and butanol, with the first three solvents found to be employed to extract furfural from some sorbents in the references [9, 10]. Fig. 6.5 presents the UV spectra of furfural desorbed from the spent PF800 by organic solvent at room temperature. The results show that DMSO and DCM are better than other solvents, especially compared with DI water, to strip furfural from spent PF800.

It should be noted that UV spectrometer is very sensitive to furfural in the water solution. A linear relationship between furfural concentration and absorbance by UV spectrometer at 278 nm was observed only when furfural concentration is below 10 ppm. Therefore, the samples with higher concentration of furfural (10 ppm) were diluted with distilled water to make the concentration less than 10 ppm, for the accurate determination of the furfural concentration. The dilution of samples was 6 times higher than in the

desorption tests by pure water (Fig. 6.3) or pH adjustment (Fig. 6.4). But the results of DI water in Fig. 6.5 were of the same dilution as other organic solvents. Since furfural is miscible or highly soluble in these organic solvents, the distribution coefficient of furfural (K_f) is much lower in carbon-organic solvent system than in carbon-water solution system, which leads to the desorption of furfural from spent PF800.

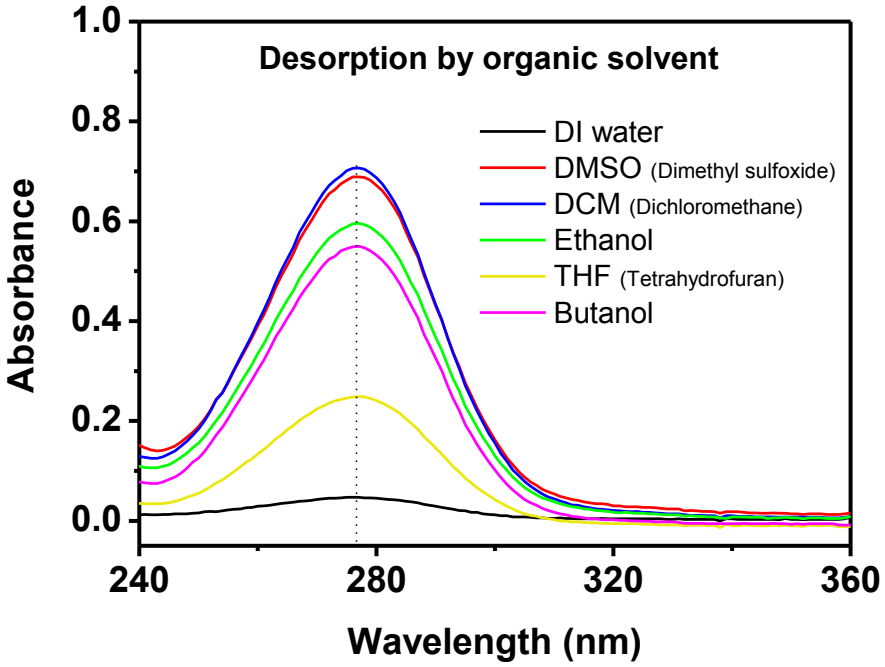

Figure 6.5 UV spectra of furfural desorbed from the spent PF800 by organic solvent at room temperature.

Table 6.1 Regeneration efficiency of different organic solvents to desorb furfural from spent PF800 at room temperature.

	DMSO	**DCM**	**Ethanol**	**Butanol**	**THF**
Regeneration Efficiency (%)	**85**	**83**	**74**	**70**	**37**

After air-drying the regenerated PF800 at room temperature for 24 h, the adsorbents were employed to perform adsorptions tests to evaluate the regeneration efficiency. The results are shown in Table 6.1. Although DMSO and DCM present high regeneration efficiency, ethanol has advantages in industry application due to its lower cost and relative eco-friendliness.

6.3.4.2 Effect of Ethanol-containing Water Solution

Ethanol water solution was further investigated to desorb furfural form Spent PF800 at room temperature. Ethanol water solutions with different ethanol concentration were utilized in the desorption tests, and the results are shown in Fig.6.6. The desorption of furfural from spent PF800 increased with an increase of ethanol concentration up to 50 wt%. The overlapping of black, red and blue lines indicates that 100% ethtanol, 80 wt% ethanol/H_2O and 50 wt% ethanol/H_2O have the same ability to strip furfural from adsorbent.

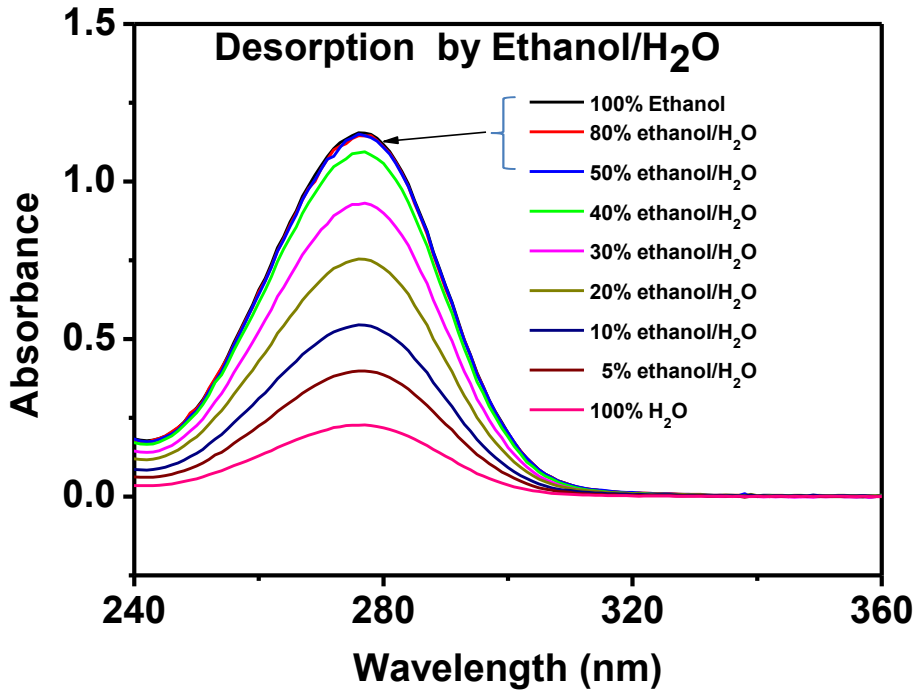

Figure 6.6 UV spectra of furfural desorbed from the spent PF800 by ethanol water solution at room temperature.

For 100% ethanol, 80 wt% and 50 wt% ethanol/H_2O, the regeneration efficiency is shown below:

$$\frac{\text{Sorption capacity of the regenerated PF800}}{\text{Sorption capacity of fresh PF800}} = \frac{181\ \text{mg/g}}{213\ \text{mg/g}} = 74\%$$

For 10 wt% ethanol/H_2O, the regeneration efficiency is:

$$\frac{\text{Sorption capacity of the regenerated PF800}}{\text{Sorption capacity of fresh PF800}} = \frac{61\ \text{mg/g}}{245\ \text{mg/g}} = 30\%$$

6.3.4.3 Effect of Temperature

Desorption tests with ethanol water solution were also investigated at high temperature (90 ^{o}C, in hot water bath). It is found in the figure 5 that the difference of UV result between room temperature and 90 ^{o}C is not very obvious. A slight more amount of furfural was desorbed into 50 wt% ethanol water solution at 90 ^{o}C than at room temperature (25 ^{o}C). This means temperature is not a significant factor in this regeneration process. Temperature swing regeneration is not a feasible approach to desorb furfural from spent activated carbon in the liquid phase.

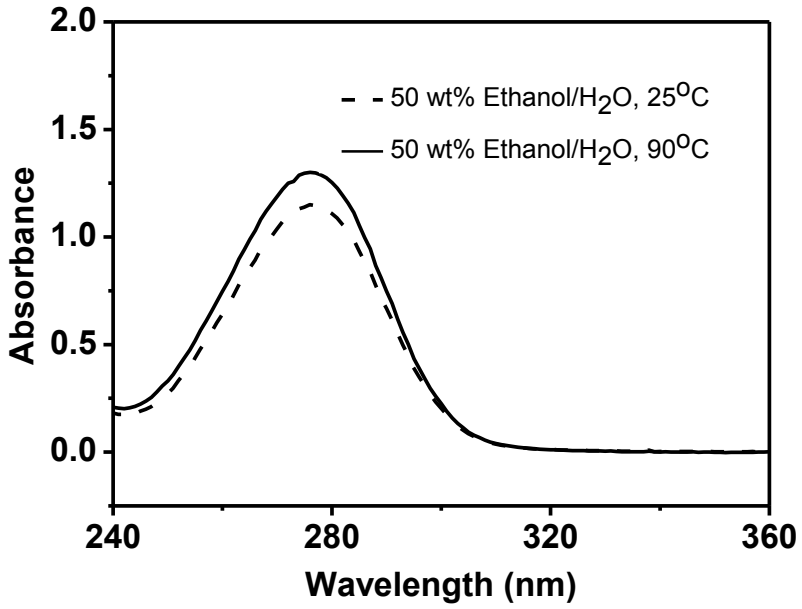

Figure 6.7 UV spectra of furfural desorbed from the spent PF800 by ethanol water solution at different temperature.

6.4 Adsorption/Desorption Regeneration in Column System

6.4.1 Design of Adsorption/Desorption Cycle

Based on the results of desorption tests with ethanol water solution, a sorption-desorption cycle method was designed, as shown in Fig. 6.8. After biomass pretreatment, the furfural-rich feed passes through adsorption column for furfural removal, followed by the flow of low furfural-containing feed goes to fermentation for ethanol production. After fermentation, the ethanol-containing liquid flows back into the column to desorb the furfural from adsorbents. After desorption, furfural enriched liquid goes to distillation to purify ethanol from the solution. Then, the regenerated adsorbents are ready for the next cycle of sorption-desorption. The efficiency of adsorbent use could be greatly improved by integrating ethanol production during fermentation in this regeneration approach.

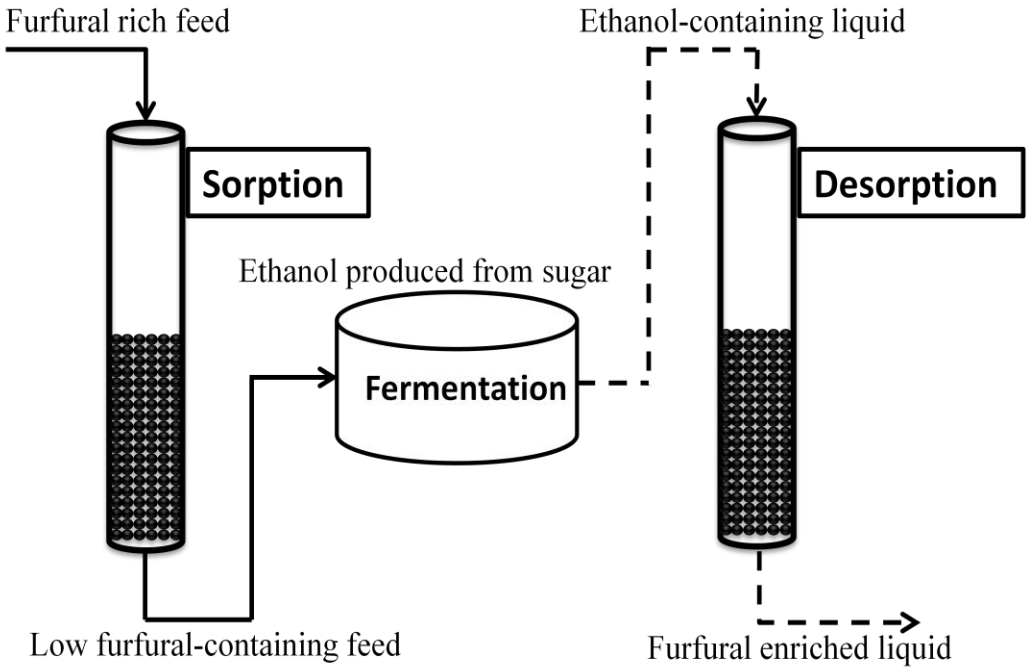

Figure 6.8 Sorption/desorption cycle of adsorbents during cellulosic-ethanol production.

6.4.2 Determination of Working Adsorption Capacity in Adsorption/Desorption cycle

It should be noted that a certain amount of furfural would still remain on adsorbents after desorption during the adsorption/desorption cycle. Therefore, the adsorption capacity of activated carbon in the adsorption batch tests in chapter 4 would not be the working adsorption capacity in this adsorption/desorption cycle. To evaluate the working adsorption capacity of activated carbon, adsorption batch tests were performed with and without 7.5 wt% ethanol in the liquid. The results are shown in Fig. 6.9. For both PF800 and Norit_1240, a difference of adsorption capacity for furfural was observed in the adsorption batch tests with and without 7.5 wt% ethanol in the liquid. This difference of sorption capacity would be the working sorption capacity in the sorption/desorption cycle test in the column system. The working sorption capacity of PF800 and Norit_1240 for furfural is about 50-60 mg/g, about one fifth of the adsorption capacity in the batch tests without ethanol.

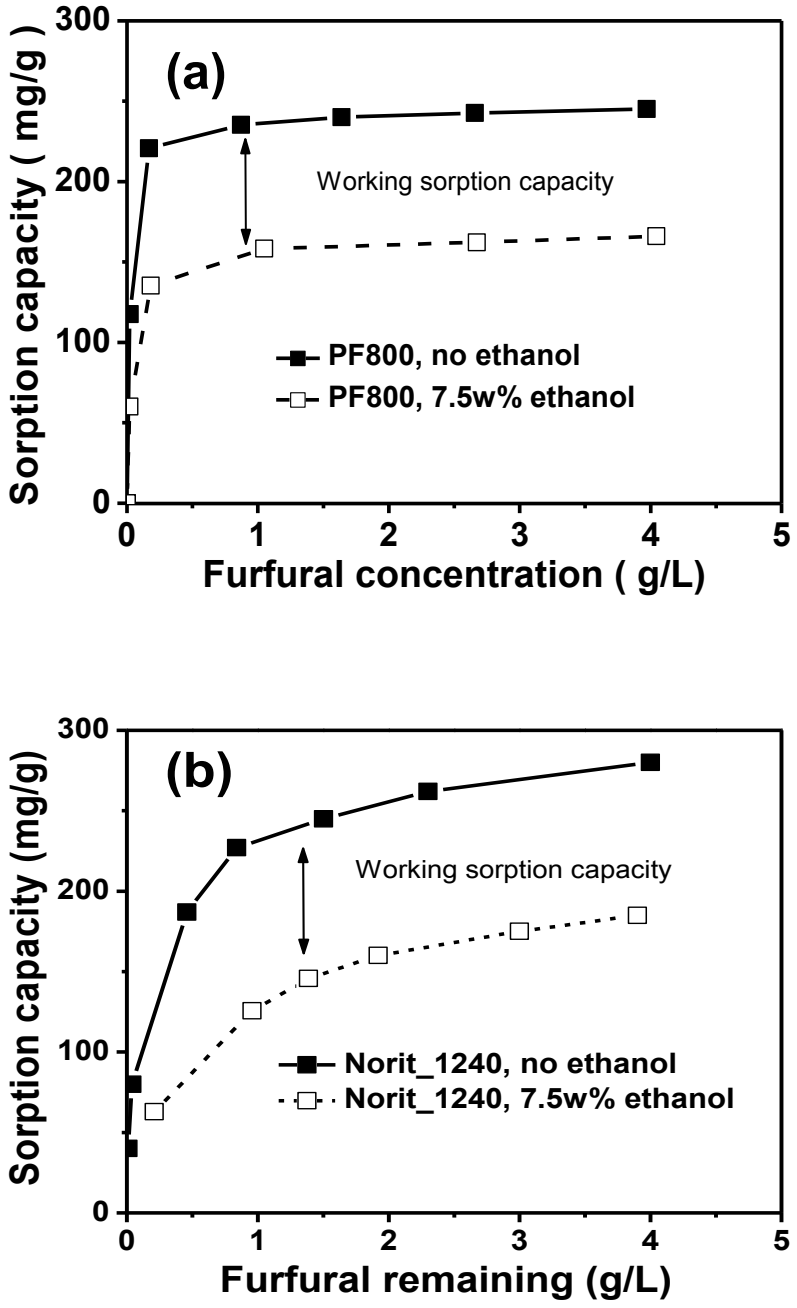

Figure 6.9 Working sorption capacity of (a) PF800; and (b) Norit_1240 in sorption/desorption cycle.

6.4.3 Adsorption/Desorption Tests in Column System

Norit_1240 was first studied in the column system, because it is granular (8-20 mesh, about 1.5 to 2.5 micrometers in diameter), which is suitable in the column system. Water pressure drop in the column study did not occur with size of 8×20 mesh. The glass column used in the test is 6 cm in inner diameter and 50 cm in length. By maintaining a column inner diameter to carbon particle diameter ratio greater than 25, wall effects on adsorbate diffusion in the bulk solution were minimized. 100 g Norit_1240 were utilized in the column tests. And 2 liters of water solution with 4 g/L furfural, 20 g/l glucose and 10 g/l xylose was utilized to simulate biomass-pretreated liquid. The flow rate was controlled at 50 ml/min by peristaltic pump, thus the residence time was 40 min. As was discussed in Chapter 4, the equilibrium time is 30 min for granular Norit_1240 in the batch tests. 40 min of residence time would allow the activated carbon fully contact with the furfural solution. In addition, a small amount of ethanol was added into the liquid after adsorption process to simulate 7.5 wt% ethanol was produced in fermentation.

The procedure and results of column test are shown in Fig. 6.11. After sorption, the furfural concentration was reduced from 4 g/L to 1 g/L. Since 200 ml ethanol was added into the liquid to simulate 7.5 wt% ethanol produced during fermentation, the furfural concentration became 0.9 g/L before the liquid flew back to the column to desorb furfural from the adsorbents. After desorption using 7.5 wt%-ethanol-containing liquid, furfural concentration was enriched to 3.6 g/L, which was less than 4 g/L in the liquid flowing during the sorption process. Although the addition of ethanol lead to a change of furfural concentration, the mass of furfural flowing out the desorption process was still 8g. Moreover, four or five sorption/desorption cycles are needed before reaching this

dynamic mass balance. The results were still stable after running the sorption-desorption cycle 20 times. Meanwhile, the sugars were not removed indicated by the overlapping of black and red curves in the HPAEC (High Performance Anion Exchange Chromatography) results in Fig. 6.11.

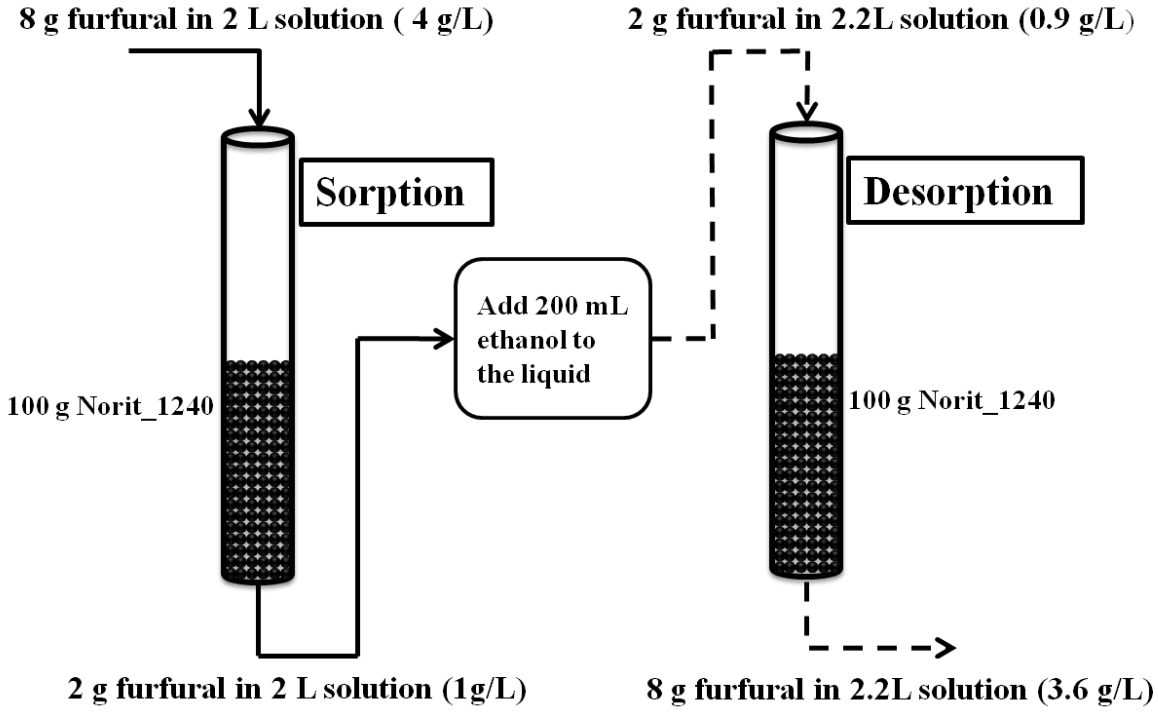

Figure 6.10 Sorption/desorption cycle test with Norit_1240 at room temperature.

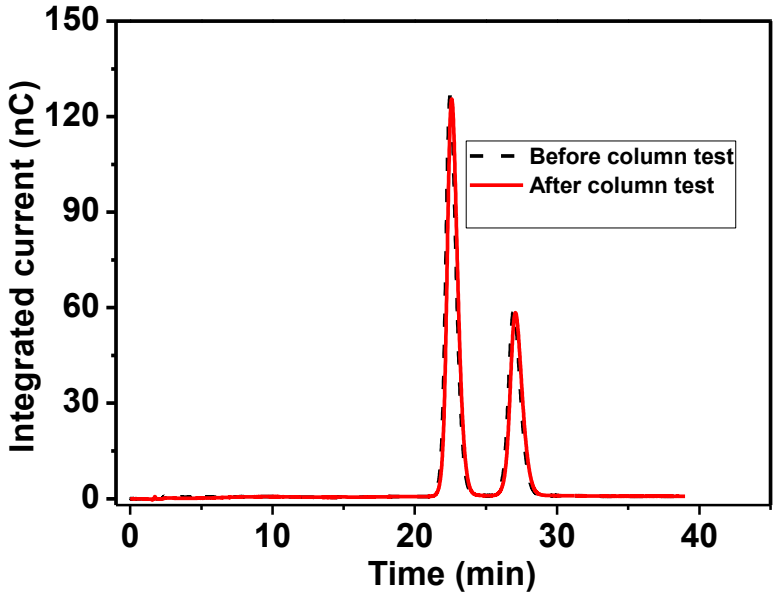

Figure 6.11 Monosaccharide analysis by HPAEC before and after column tests with granular Norit_1240.

Although the working sorption capacity of PF800 is similar to granular Norit_1240, the small size of powder PF800 caused a water pressure drop in the column system. This problem could be solved by pelletizing PF800. Furthermore, 0.1 g/L furfural could be reached with pelletized PF800 while not losing sugars.

The efficiency of sorbent use could be greatly improved by this regeneration method. Additionally, the presence of furfural in the liquid has no effect on the purification of ethanol by distillation, due to the high boiling point of furfural (161.7 ℃). In this research, the ethanol-containing standard solution utilized in the regeneration did not contain acetic acid and other components that could exist in the real fermentation broth. The effect of these components on the regeneration is recommended to be investigated in the future research.

6.5 Conclusions

In the present work, experimental tests were conducted to evaluate the regeneration process for spent activated carbon. Different methods of regenerating the spent adsorbents were studied, including (1) calcination at different high temperature; (2) pH adjustment; (3) organic solvent stripping.

Although the spent PF800 was completely regenerated by thermal regeneration at 800 ^{o}C, the requirement of high energy consumption makes this approach unattractive in industry. Desorption with pure water, acidic solution, and basic solution are not feasible due to the extreme low regeneration efficiency. Several organic solvents present high regeneration efficiency to desorb furfural from spent PF800. Ethanol has advantages over other organic solvents in industry application due to its lower cost and relative eco-friendliness.

Based on the results of desorption batch tests, an adsorption/desorption cycle method was designed and tested with granular Norit_1240 in a column system. Furfural was successfully desorbed from activated carbon and regeneration results were stable even after twenty cycles. These results laid the foundation to potentially integrate the ethanol production during fermentation into the adsorption/desorption regeneration method.

6.6 References

[1] Moreno-Castilla C, Rivera-Utrilla J, Joly JP, López-Ramón MV, Ferro-García MA, Carrasco-Marín F. Thermal regeneration of an activated carbon exhausted with different substituted phenols. Carbon 1995;33:1417-1423.

[2] Bagreev A, Rahman H, Bandosz TJ. Thermal regeneration of a spent activated carbon previously used as hydrogen sulfide adsorbent. Carbon 2001;39:1319-1326.

[3] Sabio E, González E, González JF, González-García CM, Ramiro A, Gañan J. Thermal regeneration of activated carbon saturated with p-nitrophenol. Carbon 2004;42:2285-2293.

[4] Leng C-C, Pinto NG. An Investigation of the Mechanisms of Chemical Regeneration of Activated Carbon. Industrial & Engineering Chemistry Research 1996;35:2024-2031.

[5] Salvador F, Jiménez CS. A new method for regenerating activated carbon by thermal desorption with liquid water under subcritical conditions. Carbon 1996;34:511-516.

[6] Michard P, Guibal E, Vincent T, Le Cloirec P. Sorption and desorption of uranyl ions by silica gel: pH, particle size and porosity effects. Microporous Materials 1996;5:309-324.

[7] Cooney DO, Nagerl A, Hines AL. Solvent regeneration of activated carbon. Water Research 1983;17:403-410.

[8] Sutikno T, Himmelstein KJ. Desorption of phenol from activated carbon by solvent regeneration. Industrial & Engineering Chemistry Fundamentals 1983;22:420-425.

[9] Coca J, Diaz R. Extraction of furfural from aqueous solutions with chlorinated hydrocarbons. Journal of Chemical & Engineering Data 1980;25:80-83.

[10] Croker JR, Bowrey RG. Liquid extraction of furfural from aqueous solution. Industrial & Engineering Chemistry Fundamentals 1984;23:480-484.

CHAPTER 7: CONCLUSIONS AND RECOMMENDATIONS

7.1 Summary and Conclusions

Interest in the use of bio-ethanol worldwide has grown strongly in recent years due to limited oil reserves, concerns about climate change from greenhouse gas emissions and the desire to promote domestic rural economies. Even though the cellulosic ethanol can be produced by fermentation, the fermentation efficiency can be substantially impeded by toxic substances present in pretreated hydrolyzates. Furfural, a pentose degradation product, is highly toxic to *Z. mobilis* during the cellulosic fermentation. Therefore the overarching goal of this four year project was to selectively separate the model fermentation inhibitor, furfural, from water solution, and to use the adsorbents efficiently.

7.1.1 Selective Adsorption of Furfural

Commercial activated carbon (Norit_1240) and newly polymer-derived carbon (PF800) were utilized to separate furfural from aqueous solution. The adsorbents were characterized in terms of morphology, pore structure and surface chemistry. Through analysis of nitrogen adsorption-desorption isotherms on adsorbent at 77k, Norit_1240 presented heterogeneous surface and broad pore size distribution while PF800 showed homogeneous surface and narrow pore size distribution. XPS revealed the presence of oxygen functional groups on the commercial carbon surface, while PF800 only contains trivial oxygen groups.

The oxygen groups on the carbon surface were believed to have contributed to the decrease on the selectivity of activated carbon between furfural and monosaccharides, which are the valuable source of bio-ethanol production and should not be separated from

solution. Oxidization of activated carbons by nitric acid generated more information which supports the above assumption. The selectivity of polymer-derived carbon between furfural and sugars was ten times higher than the commercial carbon. A two-step method was proposed to utilize the commercial carbon in the first step, followed by using polymer-derived carbon in the second step, thereby potentially reducing the cost of adsorbents in whole and increasing the efficiency.

Different isotherm models were used to investigate the adsorption of furfural on activated carbons. The Langmuir isotherm was the suitable isotherm model for the adsorption of furfural on PF800. Conformation of the experimental data into Langmuir isotherm model also indicated the homogeneous nature of PF800 surface. For Norit_1240, the Freudlich isotherm was the suitable isotherm equation for the adsorption of furfural, which indicated the heterogeneous surfaces of Norit_1240. Two kinetic models, pseudo-first-order and pseudo-second-order models, were used to investigate the adsorption process of furfural on carbons. Pseudo-second-order model fitted both PF800 and Norit_1240. Even though the effect of the particle size on adsorption kinetics was obvious, the effect of the particle size on adsorption isotherm was negligible.

The negative effect of acetic acid, another component present in the true biomass hydrolytes, on the adsorption of furfural on activated carbons was observed. This negative effect was eliminated by neutralization with aqueous ammonia. Furfural and HMF were successfully removed in the adsorption tests with true biomass hydrolytes.

7.1.2 Fermentation with Activated Carbon Treatment

The toxic effect of furfural & HMF on the fermentation of glucose and xylose by *Zymomonas mobilis* was investigated. Wild type *Zymomonas mobilis* ZM4 and recombinant stain *Zymomonas mobilis* A3 were used in this study. For both ZM4 and A3, when there were 4 g/L furfural and HMF in the fermentation broth, cells stopped growing during the fermentation. Cell growth was closely associated with sugar consumption and ethanol production. Zero sugar consumption and ethanol yield were observed as a result of complete inhibition of cell growth.

The complete elimination of inhibition effect of furfural & HMF was achieved after PF800 treatment of the solution with residual 0.1g/l furfural & HMF. The value of specific growth rate of ZM4 and A3 in the control (no furfural & HMF) and PF800-treated fermentations was about 0.32 h^{-1}. Ethanol yield reached 0.46 g ethanol/g sugar consumed, about 90% of the theoretical ethanol yield (0.51 g/g). Strong inhibition effect of 4g/l furfural & HMF still existed in the fermentation with high initial sugar concentrations (50 g/L glucose and 50 g/l xylose). The toxic effect could also be eliminated by PF800 treatment.

7.1.3 Regeneration of Activated Carbon

For the economic concerns, the used adsorbents should be regenerated efficiently. Thus, different methods to regenerate the spent PF800 (saturated with furfural) were studied, including (1) thermal regeneration at different high temperature; (2) pH adjustment by contacting the spent sorbents with acidic or basic water solution; (3) organic solvent stripping. Regeneration efficiency was evaluated by comparing the adsorption capacity of regenerated adsorbents with the fresh adsorbents.

Thermal regeneration was unattractive in industry due to requirement of high energy consumption, even though the spent PF800 can be completely regenerated by thermal regeneration at 800 ^{o}C. Extremely low regeneration efficiency was observed when the spent PF800 was desorbed by pure water, acidic solution, and basic solution. Organic solvents demonstrated high regeneration efficiency to desorb furfural from spent PF800. Ethanol has advantages over other organic solvents in industry application due to its low cost and relative eco-friendliness. Moreover, as a component in the product stream from fermentation, a simple recycling scheme can be implemented.

Based on the results of desorption batch tests, an adsorption/desorption cycle method was designed and tested with granular Norit_1240 in a column system. Furfural was successfully desorbed from activated carbon and regeneration results were stable even after twenty cycles. These results laid the foundation to potentially integrate the ethanol production during fermentation into the adsorption/desorption regeneration method.

7.2 Recommendations for Future Work

While this research was successful in selectively separating furfural from aqueous solution with activated carbons, to improve the industrial viability some of the areas still need to be explored and developed. Several of these potential research areas are listed below.

7.2.1 Investigation on Other Potential Fermentation Inhibitors

The present work was focused on the separation of furfural compounds; however, there are other potential inhibitors that are released during the processing of lignocellulosic biomass. These include acetic acid, as well as phenolic compounds and

oligosaccharides all of which can prove to be inhibitory during the bio-ethanol fermentation [1].

Acetic acid is a common organic acid in the solution during the pretreatment process and its concentration can be 5 wt% [2]. Acetate-resistant strains have been developped to be capable of produce ethanol at high acetate concentration [3]. Phenolic compounds are also formed during hydrolysis. Activated carbons were reported to separate phenolic compounds from water solution in different industrial areas [4, 5]. Adsorption tests of activated carbon are necessary when both furfural compounds and phenolic compounds are present in the solution. Competitive adsorption of furfural and phenolic compounds onto activated carbon should be further investigated. Even though PF800 showed high selectivity between furfural and monosaccharides, the adsorption tests of oligosaccharides on activated carbon will be required in the future work due to the presence of large quantity of oligosaccharides in the solution after biomass pretreatment.

7.2.2 Integration of Ethanol Fermentation in Adsorption-desorption Regeneration of Activated Carbon

In our research, the step of fermentation between sorption and desorption was simulated by adding a certain amount of ethanol into the liquid after sorption process to simulate 7.5wt% ethanol was produced in the fermentation.

Realistic cellulosic fermentations have a complex mixture of other components including cells, organic acids derived from the fermentation, and proteins that might released from cells. Therefore, it is expected that the effect of these components on the regeneration of the activated carbon should be further investigated. The amount of organic acids produced during fermentation could be minimized by optimizing the

fermentation conditions. In addition, organic acid can be neutralized and the resulting organic salt is expected to be highly soluble in water, thus showing little effect on the desorption of furfural from activated carbon. The cells and proteins might block the pores between (or inside) activated carbons. If cells and proteins demonstrate negative effect on the desorption of furfural from spent activated carbon, separation of cells and proteins from fermentation broth by filtration as the first step in the desorption will be necessary. Then, integration of ethanol production during fermentation into adsorption-desorption regeneration approach will be feasible in industry, which could greatly improve the efficiency of adsorbent.

7.2.3 Pelletize PF800

In the present work, granular commercial carbon was utilized in the adsorption-desorption column tests. The drawback of commercial carbon is its low selectivity between furfural and sugars. Therefore, the minimum furfural level was reduced to 1 g/l in the regeneration column tests without losing sugars. Even though PF800 demonstrated high selectivity between furfural and sugars, the small size of its particles could cause water pressure drop in the column tests. Thus, it is desirable to pelletize PF800 in the future work.

Conventional preparation methods of pelletizing activated carbon consist of (1) mixing the activated carbon with a binder, (2) compression and molding using a hydraulic press, (3) pyrolysis to improve the binder properties and decrease the weight of binder. The binder must possess certain properties: (i) it must have good mechanical properties using the lowest binder / activated carbon ratio to achieve the maximum

amount of activated carbon; (ii) its pyrolysis must not produce pore blocking of the activated carbon [6].

Different binders could been used for pelletizing PF800: (1) a humic acid-derived sodium salt (HAS) from Acros organics, (2) polyvinyl alcohol (PVA), a novolac phenolic resin (PR) (Georgia Pacific 5506), and (3) Teflon (TF) from Du Pont. Humic acid is a good binder for making activated carbon pellets in the previous research [7]. PVA gave good results with as little as 4 wt% binder content. Teflon has the advantages of not needing the pyrolysis step for improving the binder properties. The selection of a better binder is to achieve the best equilibrium between adsorption capacity and bulk density of the carbon pellet.

After obtaining the PF800 pellets, the adsorption-desorption column tests could be performed with these pellets. With high selectivity of PF800 between furfural and sugars, it will be able to reach 0.1 g/l furfural in the column test while not losing sugars.

7.2.4 Fiber Sorbents with PF800

Hollow fiber sorbents are monolithic materials with polymer as 'binder', impregnated with high loadings of powdered sorbents as 'fillers'. Such organic – inorganic hybrid materials are planned to be created with relative ease by modifying the hollow fiber membrane spinning technology [8]. Fiber sorbents have to be created with high sorbent loadings (> 50 wt. %), to achieve sorption capacities comparable to the conventional packed bed technology. Fiber sorbents have an advantage of fast adsorption rate and low pressure drop when compared with granular adsorbents and powdered adsorbents. Composite fiber sorbents were developed for gas separation and water treatment, such as the recovery of uranium from seawater [9].

Polyethylene or a copolymer of ethylene and vinyl acetate can be used as a matrix polymer to entrap powdered PF800. Powdered PF800 and polymer should have intentionally bad adhesion with a sieve-in–a-cage morphology desired. The water solution travels through the voids/pores to reach the carbon particles improving the kinetics and hence separation performance.

7.3 References

[1] Ranatunga T, Jervis J, Helm R, McMillan J, Hatzis C. Identification of inhibitory components toxic toward zymomonas mobilis CP4(pZB5) xylose fermentation. Applied Biochemistry and Biotechnology 1997;67:185-198.

[2] Gray KA, Zhao L, Emptage M. Bioethanol. Current Opinion in Chemical Biology 2006;10:141-146.

[3] Wang Y. Development of acetic-acid tolerant Zymomonas mobilis strains through adaptation. PhD Thesis 2008.

[4] Hameed BH, Rahman AA. Removal of phenol from aqueous solutions by adsorption onto activated carbon prepared from biomass material. Journal of Hazardous Materials 2008;160:576-581.

[5] Mukherjee S, Kumar S, Misra AK, Fan M. Removal of phenols from water environment by activated carbon, bagasse ash and wood charcoal. Chemical Engineering Journal 2007;129:133-142.

[6] Lozano-Castelló D, Cazorla-Amorós D, Linares-Solano A, Quinn DF. Activated carbon monoliths for methane storage: influence of binder. Carbon 2002;40:2817-2825.

[7] Avelina G-G. Ph.D. Thesis. Universidad de Alicante 1997.

[8] Wallace DW, Staudt-Bickel C, Koros WJ. Efficient development of effective hollow fiber membranes for gas separations from novel polymers. Journal of Membrane Science 2006;278:92-104.

[9] Kobuke Y, Tabushi I, Aoki T, Kamaishi T, Hagiwara I. Composite fiber adsorbent for rapid uptake of uranyl from seawater. Industrial & Engineering Chemistry Research 1988;27:1461-1466.

APPENDIX A: ADSORPTION OF OLIGOSACCHARIDES ON ACTIVATED CARBON

To investigate the adsorption of oligosaccharides on activated carbon, adsorption tests were conducted when the solution contains only cellobiose or melezitose. Cellobiose is a disaccharide with two glucose molecules linked in a β(1→4) bond. Melezitose is a nonreducing trisaccharide. The chemical structure of cellobiose and melezitose are shown in Fig. A.1.

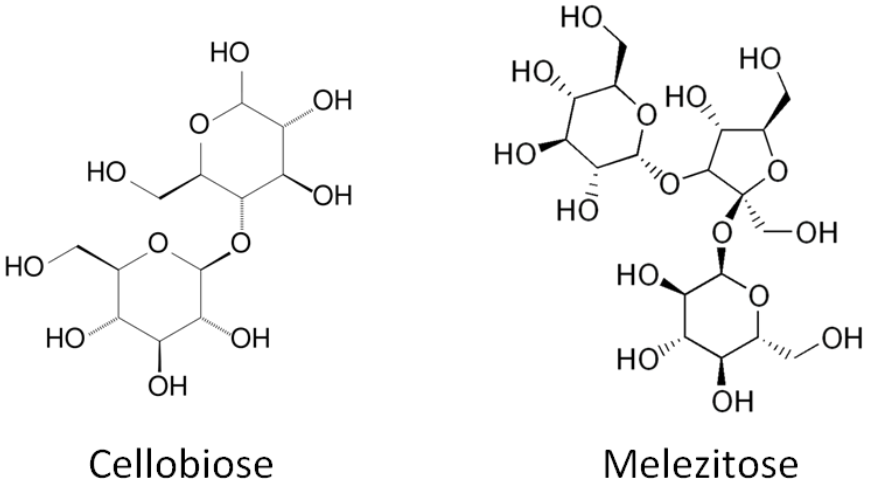

Figure A.1 Chemical structure of cellobiose and melezitose.

The content of cellobiose or melezitose in water solution was analyzed by UV-Vis spectrophotometer. Even though this method did not provide accurate estimate of content of cellobiose or melezitose, it gave qualitative information about adsorption tests. Fig. A.2 reveals change of the cellobiose content in the solution before and after the adsorption tests of activated carbons. For PF800, the overlapping of blue curve and black curve indicates the adsorption of cellobiose on PF800 is negligible. But a clear adsorption of cellobiose on Norit_1240 was observed. Similar results were observed in adsorption

tests with melezitose, shown in Fig. A.3. These results imply that the commercial carbon adsorbs oligosaccharides while PF800 dose not. Other analysis methods are required in future work for accurate quantitative analysis of oligosaccharides in water solution.

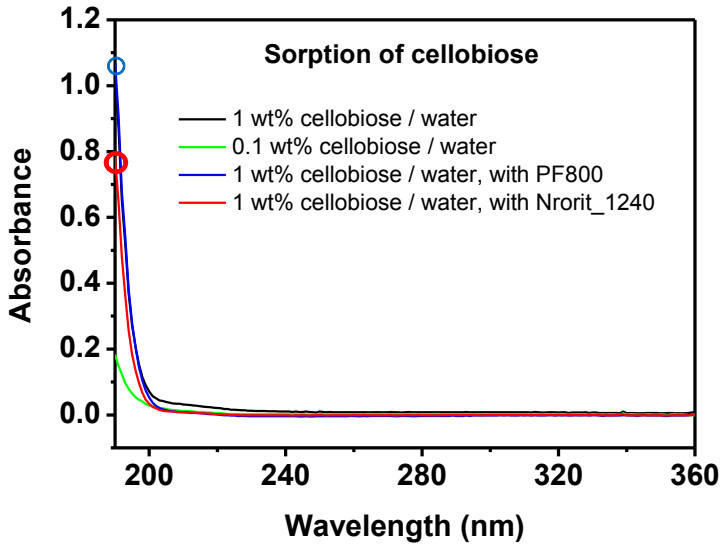

Figure A.2 UV-spectrum of cellobiose in the adsorption tests with activated carbon.

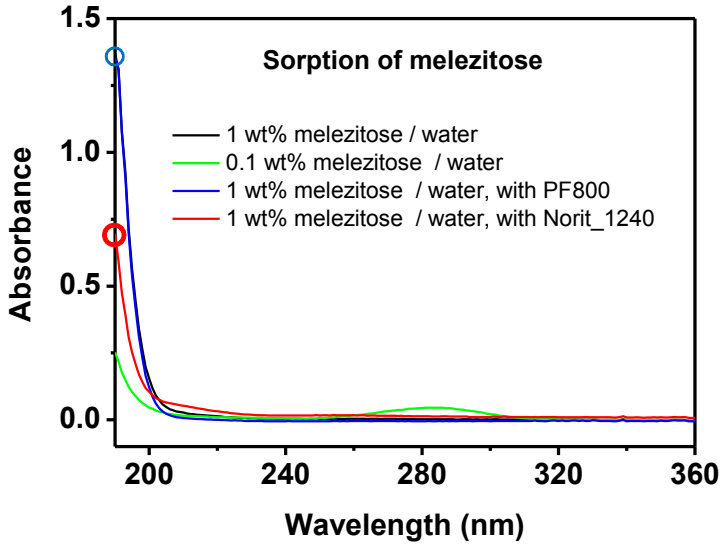

Figure A.3 UV-spectrum of melezitose in the adsorption tests with activated carbon.

APPENDIX B: ADSORPTION TESTS ON FURFURAL WITH DIFFERENT COMMERCIAL CARBONS

Other than Norit_1240, different commercial carbons were investigated in the adsorption tests of furfural. Three varieties of commercially available activated carbon were used as adsorbents in this study. The first carbon is designated as Norit_3777 (Norit Americas Incorporated, Marshall, TX). Norit_3777 is wood-based and is chemically activated using KOH. A coconut-based carbon was also studied and is designated as Calgon (Calgon Carbon Corporation, Pittsburgh, PA). The final carbon was peat-based and steam activated, referred to as Darco (Darco®, Norit Americas Incorporated, Marshall, TX).

The condition of adsorption tests was the same as in Chapter 3.2.1. The oxygen amount on carbon surface was analyzed by XPS. Most commercial carbon contains 5-6 wt% oxygen on the surface, therefore the selectivity between furfural and monosaccharides is about 600, lower than PF800, as shown in Table B.1.

Table B.1 Oxygen amount on different commercial carbon surface, and their selectivity between furfural and monosaccharides.

Carbon Sample	Oxygen, wt%	$\alpha_{f/s}$
Norit_3777	6	606
Calgon	5.5	621
Darco	6	600
Norit_1240	5	646
PF800	0.5	7321